Investigation of Spine Loading to Understand Vertebral Fractures

by

Alexander G. Bruno

B.E. Biomedical Engineering
Stony Brook University, 2009

SUBMITTED TO THE HARVARD-MIT PROGRAM IN HEALTH SCIENCES AND TECHNOLOGY IN PARTIAL FUFILLMENT OF THE REQUIREMENTS FOR THE DEGREE OF

DOCTOR OF PHILOSOPHY IN MEDICAL ENGINEERING AND BIOASTRONAUTICS
AT THE
MASSACHUSETTS INSTITUTE OF TECHNOLOGY

June 2015

Signature of Author: Signature redacted
Harvard-MIT Program in Health Sciences and Technology
May 4, 2015

Certified by: Signature redacted
Mary L. Bouxsein, PhD
Director, Center for Advanced Orthopaedic Studies, Beth Israel Deaconess Medical Center
Associate Professor of Orthopedic Surgery, Harvard Medical School
Thesis Supervisor

Accepted by: Signature redacted
Emery N. Brown, MD, PhD
Director, Harvard-MIT Program in Health Sciences and Technology
Professor of Computational Neuroscience and Health Sciences and Technology

Investigation of Spine Loading to Understand Vertebral Fractures

by
Alexander G. Bruno

Submitted to the Harvard-MIT Program in Health Sciences and Technology on May 4, 2015 in partial fulfillment of the requirements for the degree of Doctor of Philosophy in Medical Engineering and Bioastronautics

ABSTRACT

Vertebral fractures are the most common complication of osteoporosis and are associated with significant pain, height loss, disfigurement, respiratory impairment, depression, and decreased life span. Despite the high personal and societal costs of vertebral fractures, little is known regarding their biomechanical etiology. In particular, whereas much is known about the determinants of vertebral strength, little is known about the *in vivo* loading of the spine that may contribute to vertebral fracture. Prior efforts to understand the possible contribution of spine mechanics to vertebral fractures have been limited by the inability to accurately assess *in vivo* spinal loading, especially in the thoracic region. Thus, the overall goal of this work was to improve the understanding of vertebral fractures through detailed analysis of spinal loading.

We first developed and validated a novel musculoskeletal model capable of predicting forces in the thoracolumbar spine during daily activities. Model-derived predictions of vertebral compressive loading and trunk muscle activity were highly correlated with previously collected *in vivo* measurements of intradiscal pressure, vertebral compression from telemeterized implants, and trunk muscle myoelectric activity from electromyography. To gain insights into how individual variation in trunk anatomy influences vertebral loading, we developed a robust set of methods for rapid, automated generation of subject-specific musculoskeletal models of the thoracolumbar spine using computed tomography based measurements of spine curvature and trunk muscle morphology. Using these subject-specific models, we found that normal variations in spine curvature and muscle morphology in the adult population have a large effect on vertebral loading predictions. Specifically, we found that increasing thoracic kyphosis and reducing lumbar lordosis, changes that commonly occur with age, were both associated with higher spinal loads. Lastly, we used our musculoskeletal model to describe how vertebral loading and the factor-of-risk (load-to-strength ratio) vary along the spine for a large number of activities. For a majority of activities, the highest loads and factor-of-risk were in the thoracolumbar region, which is the spine region with the highest incidence of vertebral fracture. Further, we identified a unique biomechanical mechanism responsible for the high loads in this region.

Thesis Supervisor: Mary L. Bouxsein, PhD
Director, Center for Advanced Orthopaedic Studies, Beth Israel Deaconess Medical Center
Associate Professor of Orthopedic Surgery, Harvard Medical School

ACKNOWLEDGMENTS

I have immensely enjoyed my academic journey, and there are many individuals who have contributed to my success and happiness during this period. Firstly, I would like to thank Professor Helmut Strey of Stony Brook University for starting me on my research journey. Helmut welcomed me into his lab as a college sophomore and introduced me to the worlds of scientific research and technology development. The wonderful experience of working in Helmut's lab was a key factor in my decision to pursue a PhD degree and continue my scientific journey. Other Stony Brook faculty that stimulated my curiosity and passion for learning include professors Daniel Davis, Richard Larson, Mark Aronoff, Gene Sprouse, Eriko Sato, and Mario Mignone. I would also like to thank my college roommates Michael Small, Tomasz Bakowski, Andrew McGowan, Michael Budassi, Cory Clifton, and Aleksey Shtivelman. I learned so much from this great group of guys, and could not have survived college without them.

During my graduate studies at MIT, I was fortunate to have the best PhD advisor a student could hope for, Professor Mary Bouxsein. Under Mary's guidance, I had the opportunity to work on a project that was interesting, challenging, and clinically relevant. Mary helped me mature into a confident scientist and engineer, and most importantly, I always knew that she had my back. Another important mentor during my PhD studies was Dr. Dennis Anderson, who taught me everything I know about musculoskeletal modeling. Dennis was always happy to answer my questions, and I very much enjoyed our many brainstorming sessions over the years. Other individuals at the Center for Advanced Orthopaedic Studies that helped me successfully complete my PhD project include Brett Allaire, John D'Agostino, Kelsey Velie, Clara De Paolis Kaluza, and Paula Cohen. I would also like to thank my thesis committee members Dava Newman, Elise Morgan, and Jonathan Bean for their insightful guidance and feedback.

There are many other members of the MIT community that contributed to my success and enjoyment of graduate school. The Man Vehicle Laboratory at MIT was always a second home to me, and I learned everything I know about Bioastronautics and human spaceflight from Laurence Young, Charles Oman, Dava Newman, Andrew Liu, Jeffrey Hoffman, and Alan Natapoff. Bioastronautics journal club was by far my favorite MIT class, and I always looked forward to our stimulating and entertaining discussions about human spaceflight and countless other topics. I would also like to thank Elizabeth Zotos for being so welcoming and always making me feel like part of the MVL.

My other home away from lab was of course HST, and I would like to thank Julie Greenberg, Laurie Ward, Traci Anderson, Patty Cunningham, and Joseph Stein for all of their help and advice during the PhD journey, as well as for making HST the best and most welcoming department on campus. I would also like to thank Roger Mark, who was a great mentor, qualifying exam chairmen, and housemaster at Sidney and Pacific, where I was fortunate enough to live for three years. Bruce Rosen was a great academic advisor and an invaluable source of guidance on classes, research, and life in general. I also had many memorable HST professors that introduced me to the world of medicine, including Jeffrey Drazen, David Housman, Trudy Van Houten, and Richard Mitchell.

My graduate school journey would not have been complete without my good friends Ronn Friedlander and Alex German. They were my HST comrades, and we shared many great

times together, including many trivia nights, many pitchers of beer, and many great hikes and trips together.

I of course have to thank my parents, Anthony and Debra Bruno, for all of their encouragement and advice throughout the years. I could never have made it to MIT without them. Lastly, I would like to thank my fiancée and soon to be wife Connie Kim for all of her support and encouragement. Despite the fact that Connie was pursuing her medical degree in New York while I worked on my PhD in Boston, she was always my base of support, and I could never have completed my degree without her. Thank you Connie, for always having my back.

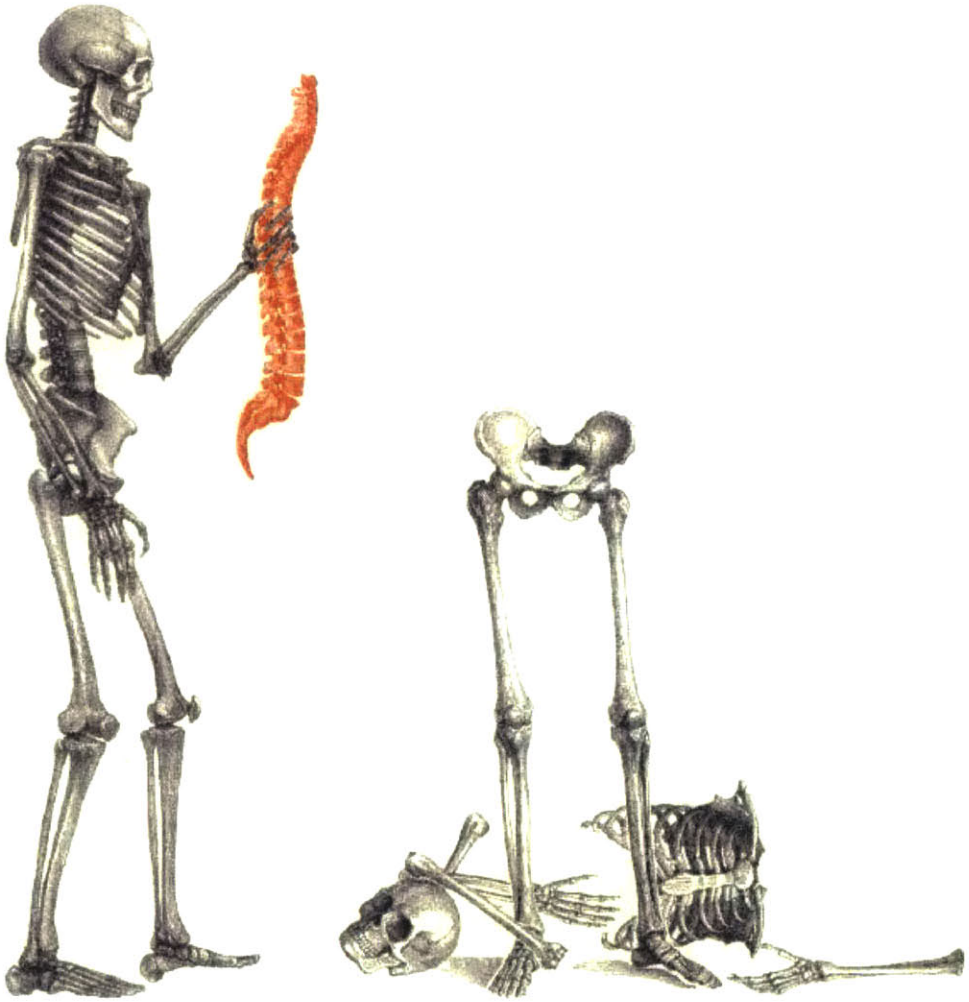

I GOT YOUR BACK

TABLE OF CONTENTS

Chapter 1: Background and Thesis Outline

1.1 Clinical Significance of Vertebral Fractures

Vertebral fractures pose a significant threat to individual and public health [1]. They are the most common fracture associated with osteoporosis and are associated with significant morbidity and increased mortality [1]. In the United States there are approximately 1.2 million osteoporosis-related fractures a year, 700,000 of which are vertebral fractures [2]. Approximately 10% of women and 30% of men in their fifties have a vertebral fracture; this proportion increases each decade such that by the eighth decade of life, 40 to 50% of women and men have had at least one vertebral fracture [3-6]. These fractures cause acute and chronic back pain, height loss, physical deformity, reduced lung function, and increased difficulty performing various activities of daily living [7-9]. In addition to these physical impairments, vertebral fractures negatively affect mood, self-esteem, and body image [10] and it is common for individuals with fractures to suffer from depression and anxiety [10]. The economic burden associated with vertebral fractures is significant as well, with direct health care costs of approximately $750 million annually in the US, in addition to indirect costs associated with lost work days and decreased productivity [1]. With an ever-growing elderly population, the incidence of vertebral fractures and the associated clinical and economic burden are expected to increase dramatically. From 2000 to 2025, the number of individuals over the age of 50 will increase by 60% in the US [11, 12], which is of particular concern because this is the age group in which vertebral fractures are most common.

1.2 Gaps in Current Knowledge

1.2.1 The Activities Associated with Vertebral Fracture

Most vertebral fractures occur during activities of daily living without specific trauma [13], making it difficult for individuals who have been diagnosed with a fracture to identify the causative event. A population-based study by Cooper et. al. showed that 83% of vertebral fractures followed moderate to no trauma, 14% followed severe trauma, and 3% were pathologic (malignancies spreading to the bone and weakening it) [13]. Of the fractures that followed moderate to no trauma, in 59% no specific traumatic episode could be identified. It is also important to note that the majority of the severe fractures reported in this study occurred

in younger men, whereas the elderly typically suffered fractures following minimal to no trauma [13]. Another study by Patel et al. found that in a group of 30 subjects between 60 and 80 years of age who suffered an acute, painful vertebral fracture, 50% of fractures occurred spontaneously, 37% during trivial strain (housework), and 17% during moderate to severe injury (stumble, falling off a ladder) [14]. These data indicate that most vertebral fractures occur during the minimal trauma activities of daily life and are of unknown etiology. Thus the activities that are most strongly associated with vertebral fracture remain unclear.

1.2.2 *The Distribution of Fractures Within the Spine*

Vertebral fractures occur most frequently in the mid-thoracic (T7-T8) and thoracolumbar (T12-L1) regions of the spine (Fig. 1.1), but the biomechanical mechanisms underlying this site-specific distribution of fractures along the spine remains unexplained. This issue is further complicated by the fact that we don't know which activities are most likely to result in vertebral fracture, and it is therefore unclear if there are different activities/mechanical mechanisms responsible for mid-thoracic versus thoracolumbar vertebral fractures.

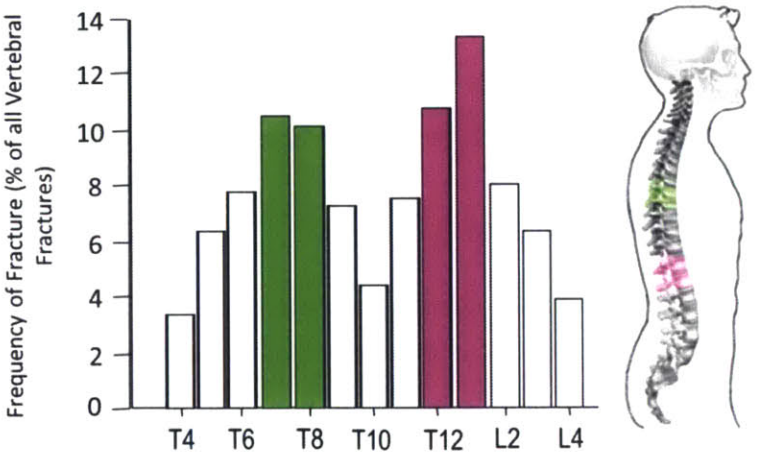

Figure 1.1: Percentage of vertebral fractures at each level of the spine in 3600 European women over age 50. Vertebral fractures occur most frequently in the mid-thoracic (T7/T8) and the thoracolumbar (T12/L1) regions of the spine. Data adapted from Ismail and colleagues [15].

1.2.3 *The Vertebral Fracture Cascade*

The presence of a vertebral fracture dramatically increases an individual's risk for sustaining additional vertebral fractures relative to other osteoporotic individuals matched for

age and bone mineral density (BMD), but with no pre-existing fracture. This phenomenon is referred to as the 'vertebral fracture cascade' [16] and has been well documented [17-21]. For example, Ross et al. report that the presence of a vertebral fracture in postmenopausal women increased the risk of future vertebral fractures over a five-year period by 5 to 7.4-fold, and the presence of two fractures increased risk of subsequent fracture by 11.8-fold [20, 21]. Perhaps most alarming of all is that 20% of osteoporotic women with a prevalent vertebral fracture will incur a subsequent fracture within a year [17]. The risk of incurring a subsequent fracture increases dramatically as the number and severity of prior fractures increases [17, 22, 23].

Despite the large negative impact of the vertebral fracture cascade on the health and well-being of the elderly population, the mechanisms underlying this marked increase in fracture risk have not been adequately explored. Ross and colleagues separated individuals into low, middle, and high bone mineral density groups, and found that individuals with high bone mineral density and a prior vertebral fracture had a higher risk of future vertebral fracture than individuals with low bone mineral density but no prior vertebral fracture (Fig. 1.2). Further, while bone mineral density is the primary clinical measure of fracture risk, only about 39% of vertebral fractures are attributable to osteoporosis as defined by low aBMD [24]. Taken together, these data suggest that other factors beyond low bone mineral density may predispose some individuals to their first and subsequent vertebral fractures.

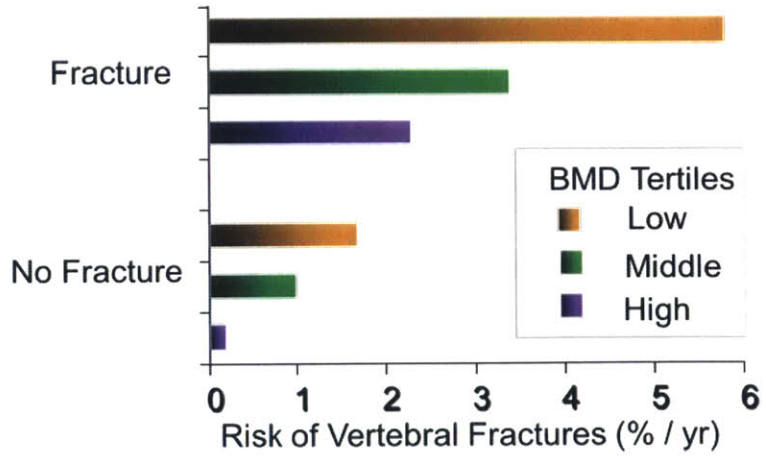

Figure 1.2: History of previous vertebral fracture is a strong risk factor for future vertebral fracture, independent of bone mineral density (BMD). Data adapted from Ross and colleagues [20].

1.3 Investigating Spine Loading To Understand Vertebral Fractures

1.3.1 The Factor-of-risk Concept

A structure will fail when its applied loads exceed its strength. This idea can be formalized mathematically as a load-to-strength ratio, which is referred to as the factor-of-risk [25]. Theoretically, a structure will fail when the factor-of-risk exceeds one. Prior investigations of vertebral fracture etiology have focused almost exclusively on understanding determinants of vertebral strength, such as bone mineral density, and have neglected the study of spine loading. Thus, the overall goal of this thesis was to improve the understanding of vertebral fractures through detailed analysis of spinal loading and its major determinants (Fig. 1.3). Specifically, we wanted to 1) investigate how variations in trunk anatomy influence *in vivo* spinal loads and risk of vertebral fracture, and 2) identify the activities and biomechanical mechanisms responsible for vertebral fractures.

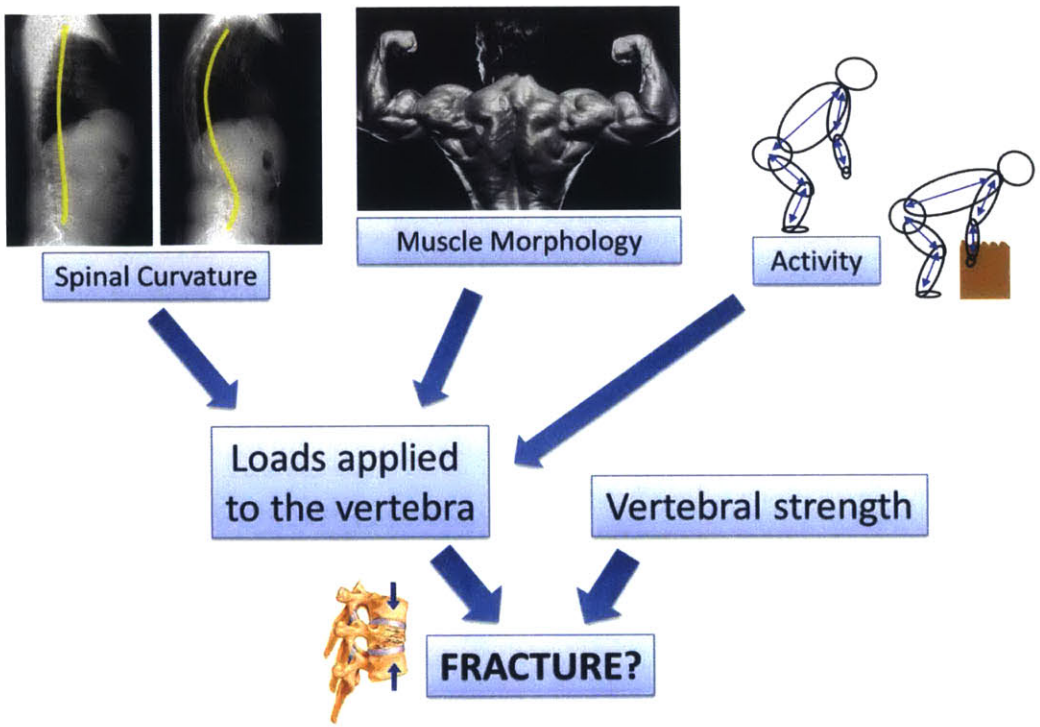

Figure 1.3: Biomechanical view of vertebral fracture etiology. Whereas much is known about the determinants of vertebral strength, little is known about the *in vivo* loading of the spine that may contribute to vertebral fractures. Important determinants of spine loading that are investigated in this thesis include spine curvature and muscle morphology, which vary markedly between individuals, as well as activity and body position.

1.3.2 *Barriers to the Study of Spine Loading*

Prior efforts to understand the possible contribution of spine mechanics to vertebral fractures have been limited by the inability to accurately assess *in vivo* spine loading. Direct measures of spine loading include intradiscal pressure measurements and loads recorded from telemeterized vertebral implants [26-29]. However, these measurements are highly invasive, and there is only limited prior data available from these techniques. Musculoskeletal models can be used to estimate *in vivo* spine loads, and are a convenient alternative to invasive measurements [30]. However, musculoskeletal models of the spine have traditionally focused on the lumbar region, ignoring the thoracic spine because of its anatomic complexity as well as a focus on low-back pain and occupational-related disability [31]. These prior models have incorporated the thorax as a single rigid segment, or have neglected the mechanical contribution of the ribs and sternum in their estimates of vertebral loading [32, 33]. This has impeded efforts to estimate thoracic spinal loads and thus understand the mechanical etiology of fractures in this region.

1.4 Thesis Organization

The overall goal of this work was to improve the understanding of vertebral fractures through detailed analysis of spinal loading. The following is a summary of the research objectives addressed in each thesis chapter.

- Chapter 2: Use the factor-of-risk concept together with estimates of spine loading and vertebral strength to explore possible mechanisms underlying sex-specific differences in skeletal fragility that may be obscured by two-dimensional areal bone mineral density (aBMD) measures, the most commonly used clinical assessment of skeletal fragility and fracture risk.

- Chapter 3: Parametrically investigate how age-related changes in spinal curvature and overall sagittal plane posture influence spinal loading and risk of future vertebral fracture.

- Chapter 4: Use OpenSim to create a novel musculoskeletal model of the full thoracolumbar spine and rib cage that accurately predicts *in vivo* vertebral compressive loading and trunk muscle tension, thereby overcoming the limitations of prior models and allowing us to investigate the biomechanical mechanisms underlying vertebral fracture.

- Chapter 5: Develop a set of methods to rapidly create subject-specific musculoskeletal models of the thoracolumbar spine using measurements of spine curvature and muscle morphology from clinical CT scans, and then use these models to determine how population variability in spine curvature and muscle morphology influences spinal loading.

- Chapter 6: Describe the patterns of spine loading and factor-of-risk across the spine for a large variety of daily activities, and determine if these patterns explain the high incidence of vertebral fractures in the mid-thoracic and thoracolumbar regions of the spine.

- Chapter 7: Investigate the biomechanical mechanisms responsible for high loads predicted by our spine model in the thoracolumbar region of the spine.

1.5 REFERENCES

1. *Bone Health and Osteoporosis: A Report of the Surgeon General.* 2004, US Department of Health and Human Services, Office of the Surgeon General: Rockville, MD, USA.

2. Riggs, B.L. and L.J. Melton, *The worldwide problem of osteoporosis: Insights afforded by epidemiology.* Bone, 1995. **17**(5): p. S505-S511.

3. Davies, K.M., et al., *Prevalence and severity of vertebral fracture: The saunders county bone quality study.* Osteoporosis International, 1996. **6**(2): p. 160-165.

4. Melton, L.J., et al., *Epidemiology of vertebral fractures in women.* American Journal of Epidemiology, 1989. **129**(5): p. 1000-1011.

5. Melton, L.J., et al., *Prevalence and incidence of vertebral deformities.* Osteoporosis International, 1993. **3**(3): p. 113-119.

6. Samelson, E.J., et al., *Incidence and Risk Factors for Vertebral Fracture in Women and Men: 25-Year Follow-Up Results From the Population-Based Framingham Study.* Journal of Bone and Mineral Research, 2006. **21**(8): p. 1207-1214.

7. Nevitt, M.C., et al., *The Association of Radiographically Detected Vertebral Fractures with Back Pain and Function: A Prospective Study.* Annals of Internal Medicine, 1998. **128**(10): p. 793-800.

8. Schlaich, C., et al., *Reduced Pulmonary Function in Patients with Spinal Osteoporotic Fractures.* Osteoporosis International, 1998. **8**(3): p. 261-267.

9. Cook, D.J., et al., *Quality of life issues in women with vertebral fractures due to osteoporosis.* Arthritis & Rheumatism, 1993. **36**(6): p. 750-756.

10. Gold, D.T., *The Nonskeletal Consequences of Osteoporotic Fractures: Psychologic and Social Outcomes.* Rheumatic Disease Clinics of North America, 2001. **27**(1): p. 255-262.

11. Burge, R., et al., *Incidence and Economic Burden of Osteoporosis-Related Fractures in the United States, 2005–2025.* Journal of Bone and Mineral Research, 2007. **22**(3): p. 465-475.

12. Day, J.C., *Population Projections of the United States by Age, Sex, Race, and Hispanic Origin: 1995 to 2050.* 1996, US Government Printing Office: Washington DC.

13. Cooper, C., et al., *Incidence of clinically diagnosed vertebral fractures: A population-based study in rochester, minnesota, 1985-1989.* Journal of Bone and Mineral Research, 1992. **7**(2): p. 221-227.

14. Patel, U., et al., *Clinical Profile of Acute Vertebral Compression Fractures in Osteoporosis.* Rheumatology, 1991. **30**(6): p. 418-421.

15. Ismail, A.A., et al., *Number and Type of Vertebral Deformities: Epidemiological Characteristics and Relation to Back Pain and Height Loss.* Osteoporosis International, 1999. **9**(3): p. 206-213.

16. Briggs, A., A. Greig, and J. Wark, *The vertebral fracture cascade in osteoporosis: a review of aetiopathogenesis.* Osteoporosis International, 2007. **18**(5): p. 575-584.

17. Lindsay, R., et al., *Risk of New Vertebral Fracture in the Year Following a Fracture.* JAMA: The Journal of the American Medical Association, 2001. **285**(3): p. 320-323.

18. Lunt, M., et al., *Characteristics of a prevalent vertebral deformity predict subsequent vertebral fracture: results from the European Prospective Osteoporosis Study (EPOS).* Bone, 2003. **33**(4): p. 505-513.

19. Melton III, L.J., et al., *Vertebral Fractures Predict Subsequent Fractures.* Osteoporosis International, 1999. **10**(3): p. 214-221.

20. Ross, P.D., et al., *Pre-Existing Fractures and Bone Mass Predict Vertebral Fracture Incidence in Women.* Annals of Internal Medicine, 1991. **114**(11): p. 919-923.

21. Ross, P.D., et al., *Predicting vertebral fracture incidence from prevalent fractures and bone density among non-black, osteoporotic women.* Osteoporosis International, 1993. **3**(3): p. 120-126.

22. Delmas, P.D., et al., *Severity of prevalent vertebral fractures and the risk of subsequent vertebral and nonvertebral fractures: results from the MORE trial.* Bone, 2003. **33**(4): p. 522-532.

23. Gallagher, J.C., et al., *Teriparatide Reduces the Fracture Risk Associated with Increasing Number and Severity of Osteoporotic Fractures.* J Clin Endocrinol Metab, 2005. **90**(3): p. 1583-1587.

24. Stone, K.L., et al., *BMD at multiple sites and risk of fracture of multiple types: long-term results from the Study of Osteoporotic Fractures.* J Bone Miner Res, 2003. **18**(11): p. 1947-54.

25. Myers, E.R. and S.E. Wilson, *Biomechanics of Osteoporosis and Vertebral Fracture.* Spine, 1997. **22**(24S): p. 25S-31S.

26. Polga, D.J., et al., *Measurement of In Vivo Intradiscal Pressure in Healthy Thoracic Intervertebral Discs.* Spine, 2004. **29**(12): p. 1320-1324 10.1097/01.BRS.0000127179.13271.78.

27. Rohlmann, A., et al., *Loads on a telemeterized vertebral body replacement measured in two patients.* Spine (Phila Pa 1976), 2008. **33**(11): p. 1170-9.

28. Rohlmann, A., et al., *Activities of everyday life with high spinal loads.* PLoS One, 2014. **9**(5): p. e98510.

29. Wilke, H.-J., et al., *Intradiscal pressure together with anthropometric data - a data set for the validation of models.* Clinical Biomechanics, 2001. **16**(Supplement 1): p. S111-S126.

30. Delp, S.L., et al., *OpenSim: open-source software to create and analyze dynamic simulations of movement.* IEEE Trans Biomed Eng, 2007. **54**(11): p. 1940-50.

31. Iyer, S., et al., *A biomechanical model for estimating loads on thoracic and lumbar vertebrae.* Clin Biomech (Bristol, Avon), 2010. **25**(9): p. 853-8.

32. Christophy, M., et al., *A musculoskeletal model for the lumbar spine.* Biomech Model Mechanobiol, 2012. **11**(1-2): p. 19-34.

33. Han, K.S., et al., *An enhanced and validated generic thoraco-lumbar spine model for prediction of muscle forces.* Med Eng Phys, 2012. **34**(6): p. 709-16.

Chapter 2: VERTEBRAL SIZE, BONE DENSITY, AND STRENGTH IN MEN AND WOMEN MATCHED FOR AGE AND AREAL SPINE BMD

This chapter was previously published in the Journal of Bone and Mineral Research:

Bruno, A.G., et al., *Vertebral size, bone density, and strength in men and women matched for age and areal spine BMD*. J Bone Miner Res, 2014. 29(3): p. 562-9.

2.1 ABSTRACT

To explore the possible mechanisms underlying sex-specific differences in skeletal fragility that may be obscured by two-dimensional aBMD measures we compared QCT-based vertebral bone measures among pairs of men and women from the Framingham Heart Study Multidetector Computed Tomography Study who were matched for age and spine aBMD. Measurements included vertebral body cross sectional area (CSA, cm^2), trabecular volumetric BMD (Tb.vBMD, g/cm^3), integral volumetric BMD (Int.vBMD, g/cm^3), estimated vertebral compressive loading and strength (Newtons) at L3, the factor-of-risk (load-to-strength ratio), and vertebral fracture prevalence. We identified 981 male-female pairs (1:1 matching) matched on age (± 1 yr) and QCT-derived aBMD of L3 (± 1%), with an average age of 51 yrs (range: 34-81 yrs). Matched for aBMD and age, men had 20% larger vertebral CSA, lower Int.vBMD (-8%) and Tb.vBMD (-9%), 10% greater vertebral compressive strength, 24% greater vertebral compressive loading, and 12% greater factor-of-risk than women ($p < 0.0001$ for all), as well as higher prevalence of vertebral fracture. After adjusting for height and weight, the differences in CSA and vBMD between men and women were attenuated but remained significant, whereas compressive strength was no longer different. In conclusion, vertebral size, morphology, and density differ significantly between men and women matched for age and spine aBMD, suggesting that men and women attain the same aBMD by different mechanisms. These results provide novel information regarding sex-specific differences in mechanisms that underlie vertebral fragility.

2.2 INTRODUCTION

Vertebral fractures are the most common clinical manifestation of osteoporosis, with a prevalence of 30-50% in those over age 50 [1-3]. Vertebral fractures result in pain, height loss, disfigurement, reduced pulmonary function, depression, and a five-year mortality equivalent to that seen with hip fractures [4-9]. Despite the tremendous personal and societal costs of vertebral fractures, little is known regarding their biomechanical etiology.

Areal bone mineral density (aBMD) as measured by dual-energy X-ray absorptiometry (DXA) is used to diagnose osteoporosis and estimate fracture risk [10, 11]. However, two-

dimensional aBMD measurements are subject to artifacts caused by aortic calcification and degenerative disease of the spine [12]. Further, since aBMD is measured from a two-dimensional projection of a three-dimensional object, larger bones will have higher aBMD than smaller bones with the same volumetric density [13]. Thus, the relationship between aBMD and bone strength may be different in men and women because of their different body sizes and prevalence of artifacts influencing the aBMD measures. Men on average have larger vertebrae than women, suggesting that when matched by aBMD, men might have larger but less dense (volumetrically) vertebrae than women. However, the extent of these structural differences and how they relate to differences in vertebral strength are not known. Because of the widespread use of aBMD in both clinical practice and research, it is important to determine how vertebral bone structure, strength, and the load-to-strength ratio (factor-of-risk) might differ between men and women with the same spine aBMD.

In this study we determined differences in vertebral structure, spinal loading, and factor-of-risk between men and women of the same age and with the same spine aBMD. Specifically, we examined whether 3D QCT bone measures (vertebral cross-sectional area, volumetric density, and estimated compressive strength), vertebral loading, the factor-of-risk, and vertebral fracture prevalence differed among pairs of men and women matched for age (± 1 year) and for spine aBMD (± 1%, computed from 3D QCT data). We hypothesized that at a given aBMD men would have greater vertebral cross-sectional area, lower volumetric BMD, greater compressive strength, a lower factor-of-risk of fracture, and a lower prevalence of vertebral fracture compared to women. Since men are larger than women, we also examined how bone structure and compressive strength differed between the two sexes after adjusting for height and weight. We hypothesized that sex-specific differences would be reduced when accounting for the larger size of men relative to women.

2.3 Materials and Methods

2.3.1 Participants

Participants included Framingham Heart Study Offspring and Third Generation Cohort members who had QCT scans of the abdomen and thorax for assessment of vascular

calcification, acquired between 2002 and 2005, as part of the community-based Framingham Heart Study Multidetector CT Study [14]. 981 male-female pairs (aged 34-81 years) were selected from 3,312 participants (1,726 men and 1,586 women) with QCT measurements at the third lumbar vertebrae (L3), and no vertebral fracture at L3. For each pair, one man was matched to one woman within 1 year of age and within 1% of QCT-derived L3 aBMD (described below). To maintain the largest number of pairs, all potential pairs were created (with men as the "case") using the above criteria. For cases with more than one matched woman, the pair with the lowest percent difference in aBMD was selected. Age (yrs) was reported at the time of the QCT scan. Height, measured using a stadiometer, and weight, using a balance beam scale, were available from the Framingham exam before the QCT scan or if missing, from the closest previous exam. Current use of osteoporosis medications, including estrogen, was assessed from information gathered at the most recently available Framingham Heart Study clinic visit. The Institutional Review Boards at Boston University, Hebrew SeniorLife, and Beth Israel Deaconess Medical Center approved this study protocol.

2.3.2 QCT DERIVED BONE MEASURES AND ESTIMATED VERTEBRAL COMPRESSIVE STRENGTH

QCT scans were acquired using an 8-slice multidetector CT system (GE Lightspeed Ultra/Plus, General Electric Medical Systems, Milwaukee, WI, USA) with an in-plane pixel size of 0.68 by 0.68 mm, slice thickness of 2.5 mm, tube voltage of 120 kVp, data collection diameter of 500 mm, and a General Electric standard body reconstruction kernel. As described previously, a hydroxy-apatite phantom (Image Analysis, Columbia, KY) was scanned with each patient to allow conversion of CT Hounsfield units to equivalent mineral density [15, 16]. Using custom software [17, 18], individual L3 vertebral levels were identified from abdominal CT scans, in combination with the lateral scout views, and used to estimate aBMD (g/cm^2), determine cross sectional area (CSA, cm^2), trabecular volumetric BMD (Tb.vBMD, g/cm^3), integral volumetric BMD (Int.vBMD, g/cm^3), and to calculate compressive strength (Newtons) at L3. The L3 vertebral level was selected since the largest number of participants had valid measurements at this level.

Although it would have been desirable to match participants by DXA spine aBMD measures, only a small number of individuals had a DXA scan within one year of their QCT exam. Therefore, we estimated L3 aBMD from the QCT scan by projecting the 3D QCT density onto a 2D region in the anterior-posterior plane. In a subset of 402 Framingham Offspring Cohort members who had both a QCT scan and a lumbar spine DXA scan within one year of each other, we found a strong correlation between L3 DXA aBMD and L3 aBMD estimated from QCT: r=0.81 (root mean square error (RMSE) = 0.14, slope = 0.89, and intercept = 0.06) for men (n=180) and r=0.84 (RMSE = 0.12, slope = 0.89, and intercept = -0.01) for women (n=222).

The average CSA of the mid-vertebral body was calculated from a central 10 mm thick slice. The volume of interest for Int.vBMD included the entire vertebral body (both cortical and trabecular compartments), but excluded the transverse and posterior processes [17]. The volume of interest for Tb.vBMD measurements was an elliptical region encompassing the anterior vertebral body, centered at the midvertebral level and encompassing 70% of the volume between vertebral endplates. Vertebral compressive strength was estimated as a linear combination of Int.vBMD and CSA according to engineering beam theory, an approach that assumes the vertebral body is primarily loaded in compression and that the failure load of the vertebra, or its strength, is proportional to its structural rigidity at its weakest cross-section. Structural rigidity depends on bone size and bone elastic modulus. In this case, the elastic modulus of vertebral bone was estimated using a previously published empirical relationship relating Int.vBMD to elastic modulus, which was then used in combination with CSA to estimate vertebral strength according to the following equation: Vertebral Strength = 0.0068 x Elastic Modulus x CSA [19].

2.3.3 Compressive Force and Factor-of-risk

For each subject, a quasi-static musculoskeletal model of the spine was used to estimate compressive force on L3 for two different activities of daily life [20, 21]. The model is similar to previously published musculoskeletal models of the lumbar spine [22, 23]. In brief, the body was modeled as a series of linked-segments, and the weight, length, and center of mass position of each body segment was estimated using each individual's height and weight

together with published anthropometric data. The major trunk muscles present in the model included pectoralis major, rectus abdominus, serratus anterior, trapezius, latissimus dorsi, external oblique, internal oblique, sacrospinalis, transversospinalis, psoas major, and quadratus laborum. Trunk muscle cross-sectional areas and moment arm lengths were estimated using regression equations that derived these properties from each subject's age, sex, height, and weight [24]. The forces and moments applied to L3 due to body mass, as well as any weights or forces applied to the hands, were calculated for each activity. The muscle forces required to maintain static equilibrium were determined using an optimization algorithm that minimized the sum of cubed muscle intensities (equivalent to minimizing muscle fatigue) while limiting the maximum allowable muscle stress to 1 MPa to keep solutions within a physiologically acceptable range [25]. For each activity, compressive force on L3 was calculated as the sum of body weight and muscle loading acting in the axial direction of the vertebral body. The two activities modeled for each subject were lifting (30° of trunk flexion with 10 kg weights in each hand and arms hanging down) and opening a window (bending forward 20° with both arms and shoulders flexed 40°, the elbows flexed 70°, and a 15 N downward force on the hands).

The factor-of-risk for vertebral fracture was computed for each of the activities and calculated as the ratio of the applied compressive force at L3 to the estimated compressive strength of L3 [19]. Theoretically, when the applied force exceeds bone strength a fracture will occur, thus higher values of the factor-of-risk indicate greater risk of fracture.

2.3.4 Vertebral fracture assessment

Two experienced radiologists visually identified prevalent vertebral fractures in all Framingham Heart Study Multidetector CT Study participants with lateral CT scout views (n = 3,469) using Genant's semi-quantitative algorithm [26]. The radiologists were blinded to subject age, and each evaluated approximately half of the study participants. Individual vertebral bodies (T4 through L5) were graded as no fracture (SQ 0), mild (SQ 1), moderate (SQ 2), or severe (SQ 3) fracture. We compared vertebral fracture prevalence in men versus women in the age- and aBMD- matched subjects (n = 981 pairs or 1,962 subjects), as well as in the larger sample of Framingham Heart Study Multidetector CT Study subjects with lateral CT scout

views (n = 3,469), which included the subset of individuals included in the age- and aBMD-matched cohort. We examined prevalent vertebral fracture in four different age groups: <50 years, 50-59 years, 60-69 years, and ≥70 years. Subjects were counted as a fracture case if they had one or more prevalent vertebral fracture of grade SQ 1 or above.

2.3.5 Statistical Analysis

Mixed effect regression models with a random term for matched pairs (SAS, proc mixed) were used to assess differences in QCT bone measures, predicted compressive strength, loading, and factor-of-risk in male-female pairs. These approaches account for the correlation within the pairs of men and women, matched on age and aBMD. In the mixed effect regression models, the QCT measure was the dependent variable and sex and other covariates were the independent variables. Sex-related differences in QCT bone measures and predicted compressive strength were assessed i) with only sex in the model; ii) after adding height and weight to sex as the independent variables; and 3) after adding height, weight, and osteoporosis medication use (including estrogen) to sex in the model. All analyses were performed using SAS software (Windows, 9.2, SAS Institute Inc, Cary, NC, USA).

2.4 Results

A total of 981 male-female pairs were included in this study (Table 2.1). For comparison, descriptive characteristics for all Framingham subjects with lateral CT scout views are also presented in Table 2.1, as well as descriptive characteristics for the Framingham subjects that were not paired during the matching process.

Table 2.1: Descriptive data for all Framingham subjects with lateral CT scout views, subjects matched for age and estimated spine aBMD, and Framingham subjects that were not paired during the matching process. M = Men, W = Women.

	All Subjects		Matched Pairs		Unpaired Subjects	
	M (N=1,726)	W (N=1,586)	M (N=981)	W (N=981)	M (N=745)	W (N=605)
	Mean ± SD	Mean ± SD	Mean ± SD	Mean ± SD	Mean ± SD	Mean ± SD
Age (yrs)	51.24 ± 12.13	53.84 ± 11.20	51.22 ± 10.03	51.24 ± 9.96	51.27 ± 14.44	58.06 ± 11.81
Estimated L3 aBMD (g/cm^2)	1.29 ± 0.22	1.14 ± 0.22	1.23 ± 0.18	1.23 ± 0.18	1.38 ± 0.23	1.01 ± 0.22
Height (cm)	176.86 ± 6.68	162.97 ± 6.40	177.01 ± 6.30	163.75± 6.35	176.68 ± 7.14	161.69 ± 6.28
Weight (kg)	89.03 ± 15.20	71.96 ± 16.05	88.66 ± 15.30	73.36 ± 16.91	89.42 ± 15.06	69.58 ± 14.20

For the matched male-female pairs, the average age of participants was 51 years, ranging from 34 to 81 years. Mean (SD) spine aBMD was 1.23 (0.18) g/cm^2 and ranged from 0.75-1.86 g/cm^2 for both men and women. The men were 21% heavier and 8% taller than the women. 192 women (20%) reported current use of osteoporosis medication, including 180 women who reported current use of estrogen. The estimated spine aBMD of the men in the matched sample was lower than that of all Framingham men together, whereas the average aBMD of the women in the matched sample was higher than the average aBMD of all Framingham women together. The average aBMD of the unpaired men was higher than the average aBMD of all Framingham men together, and the average aBMD of the unpaired women was lower than the average aBMD of all Framingham women together. Average age, height, and weight were similar across the three samples, except that the unpaired women were slightly older compared to the matched women and all Framingham women together.

2.4.1 VOLUMETRIC BONE MEASURES

All QCT-derived bone measures differed significantly ($p < 0.0001$) between men and women matched for age and aBMD (Table 2.2). Thus at the same aBMD, men had on average 8% lower Int.vBMD and 9% lower Tb.vBMD, but had 20% larger vertebral CSA, and 10% higher predicted compressive strength than women. These patterns remained after adjusting for height and weight, although the differences were attenuated, and compressive strength no longer differed significantly between men and women (Table 2.2). Sex-specific differences

were similar after further adjustment for use of osteoporosis medications. Figure 2.1 shows QCT cross-sectional images at L3 for one representative male-female pair matched by age and aBMD to highlight the differences in vertebral CSA and vBMD.

Table 2.2: Comparison of unadjusted and height/weight adjusted bone QCT measures and estimated L3 compressive strength in men and women matched for age and estimated spine aBMD. Least squares means and standard errors (SE) from mixed effect regression analysis are presented. *p < 0.0001 for men vs women.

	N = 981 matched pairs		
	Men	**Women**	
	Mean ± SE	Mean ± SE	% Diff
Unadjusted			
Cross-sectional area (cm^2)	12.39 ± 0.0407	10.33 ± 0.0407	20%*
Trabecular vBMD (g/cm^3)	0.137 ± 0.0011	0.150 ± 0.0011	-9%*
Integral vBMD (g/cm^3)	0.181 ± 0.001	0.196 ± 0.001	-8%*
Compressive Strength (N)	4,623 ± 30	4,217 ± 30	10%*
Height and Weight Adjusted			
Cross-sectional area (cm^2)	11.86 ± 0.0461	10.88 ± 0.0467	9%*
Trabecular vBMD (g/cm^3)	0.138 ± 0.0013	0.148 ± 0.0013	-7%*
Integral vBMD (g/cm^3)	0.182 ± 0.0013	0.195 ± 0.0013	-7%*
Compressive Strength (N)	4,443 ± 37	4,400 ± 37	1%

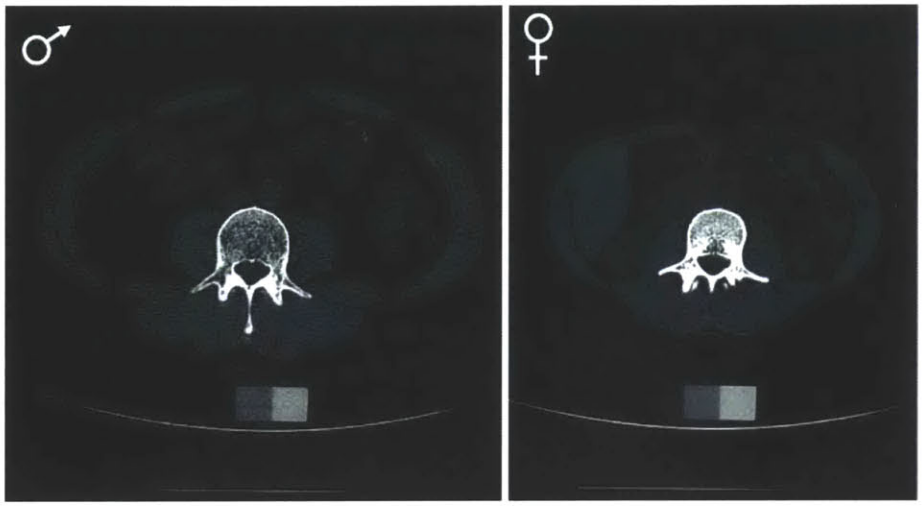

	Sample Male	Sample Female
Age (yrs)	40	40
Estimated L3 aBMD (g/cm^2)	1.25	1.25
Integral vBMD (g/cm^3)	0.156	0.215
Cross-sectional area (cm^2)	13.89	6.68
Compressive Strength (N)	4425	3003

Figure 2.1: QCT cross-sectional image of L3 in a man (left) and woman (right) matched for both age and aBMD. Note the larger CSA in the male vertebra and the higher volumetric density in the female vertebra.

2.4.2 *Biomechanical measures - Compressive Force and Factor-of-risk*

For both lifting and opening a window, L3 compressive loads and L3 factor-of-risk differed significantly between men and women matched for age and aBMD ($p < 0.0001$). L3 compressive loads were 24% higher in the men for lifting, and 24% higher in the men for opening a window (Table 2.3). L3 factor-of-risk was 12% higher in the men for lifting, and 11% higher in the men for opening a window (Table 2.3). For both activities, the values for the factor-of-risk were below one, suggesting low risk of fracture. Results remained the same after adjusting for use of osteoporosis medications.

Table 2.3: Comparison of mean L3 compressive loads and factor-of-risk for two activities of daily living in men and women matched for age and estimated spine aBMD. Least squares means and standard errors (SE) from the mixed effect regression analysis are presented. *p < 0.0001 for men vs women.

	N = 981 matched pairs		
	Men	Women	
	Mean ± SE	Mean ± SE	% Diff
Compressive Force on L3 (N)			
Lifting	2,080 ± 8	1,671 ± 8	24%*
Open window	1,846 ± 8	1,491 ± 8	24%*
Factor of Risk (load to strength ratio)			
Lifting	0.47 ± 0.0036	0.42 ± 0.0036	12%*
Open window	0.42 ± 0.0033	0.38 ± 0.0033	11%*

2.4.3 Vertebral Fracture Status

In the sample of 981 men and women pairs matched for age and spine aBMD, there were 519 pairs <50 years, 255 pairs 50-59 years, 136 pairs 60-69 years, and 71 pairs ≥70 years. In the larger Framingham CT Study cohort, there were 930 men and 720 women <50 years, 395 men and 441 women 50-59 years, 267 men and 304 women 60-69 years, and 203 men and 209 women ≥70 years. In men and women matched for age and aBMD, vertebral fracture prevalence increased with increasing age, and there were more men with vertebral fracture than women in all age groups (men vs women: 13% vs 5% for <50 years, 15% vs 9% for 50-59 years, 16% vs 9% for 60-69 years, and 31% vs 24% for ≥70 years) (Fig. 2.2). In comparison, when examining all Framingham Heart Study Multidetector CT Study subjects with lateral CT scout views (of which the age- and aBMD- matched subjects are a subsample) vertebral fracture prevalence also increased with increasing age. However, whereas more men had prevalent vertebral fracture than women in the younger three age groups, in contrast to the matched aBMD sample women had a higher vertebral fracture prevalence in the oldest age group (men vs women: 13% vs 5% for <50 years, 17% vs 8% for 50-59 years, 21% vs 13% for 60-69 years, and 25% vs 28% for ≥70 years) (Fig. 2.2).

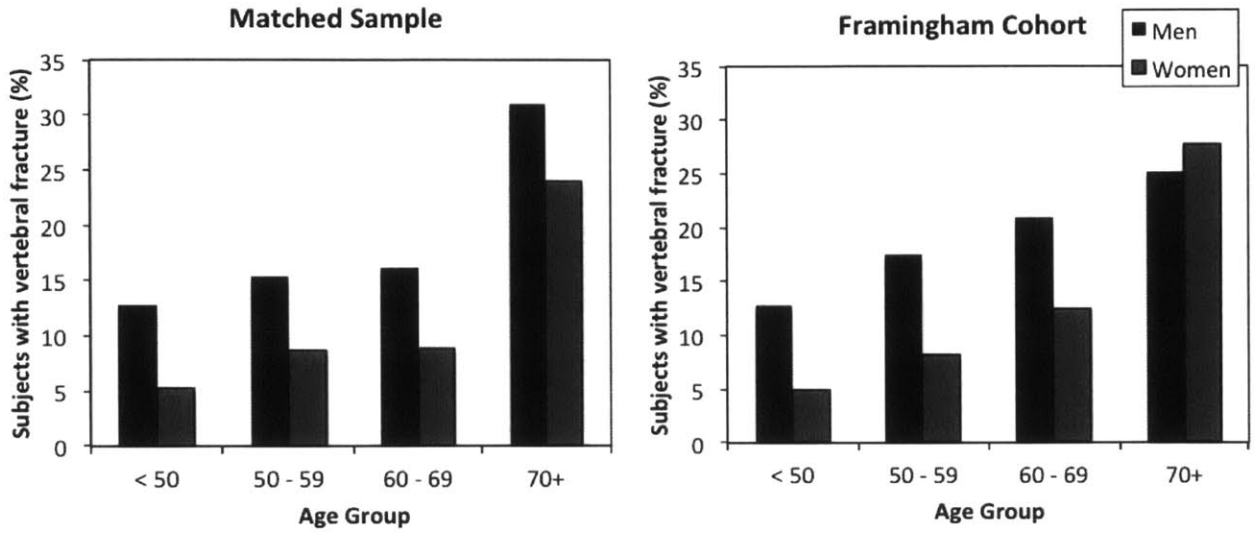

Figure 2.2: Percentage of men and women with one or more prevalent vertebral fracture in the age- and aBMD-matched sample and in the larger Framingham CT study cohort, of which the matched subjects are a subsample. In the matched sample, there were 519 pairs <50 years, 255 pairs 50-59 years, 136 pairs 60-69 years, and 71 pairs ≥70 years. In the larger Framingham CT Study cohort, there were 930 men and 720 women <50 years, 395 men and 441 women 50-59 years, 267 men and 304 women 60-69 years, and 203 men and 209 women ≥70 years.

2.5 Discussion

In this study, we evaluated sex-specific differences in vertebral volumetric bone density measures, cross-sectional area, vertebral fracture prevalence, and biomechanical estimates of vertebral loading and factor-of-risk (ie, load to strength ratio) in pairs of men and women matched closely for age and spine aBMD. We found that when matched for age and aBMD, men have larger vertebral CSA, lower volumetric BMD, and higher vertebral compressive strength compared to women. The larger CSA in men was expected since they were taller and heavier than their female aBMD-matched counterparts, and it would be expected that larger individuals would have bigger vertebrae [27]. The greater CSA of vertebral bodies in men compensated for their lower vBMD, resulting in higher estimated compressive strength in the men than in the women, despite equal aBMD.

Height and weight adjustment attenuated, but did not eliminate, the differences in vertebral size and density, implying that factors other than body size contributed to these findings. However, when adjusted for height and weight, compressive strength no longer differed between men and women matched for aBMD. This finding makes sense from a

biomechanical perspective, since one would expect individuals of the same size to experience similar loads and therefore require similar vertebral strength regardless of gender. However, from a clinical perspective, it is important to note that men and women of the same age and aBMD will typically not have similar vertebral strength unless they are also of similar height and weight. When matched for age and aBMD, men had higher vertebral compressive loads than women for the two activities simulated with our musculoskeletal model. This was expected since the men were taller and heavier than the women, and height and weight are two of the major determinants of vertebral loading for a given activity. Interestingly, the factor-of-risk (ie, load-to-strength ratio) for vertebral fracture was higher (ie, worse) in men despite their greater vertebral compressive strength than women. Therefore, these findings imply that when matched for both age and aBMD, men should have a higher risk of vertebral fracture than women because for a given vertebral strength they experience proportionally greater compressive loads on their vertebrae.

Notably, the patterns we observed for vertebral size and density among men and women matched for aBMD are similar to those previously reported by Srinivasan and colleagues who studied 114 pairs of men and women matched for femoral neck aBMD, and reported that men had 38% greater femoral neck cross-sectional area and 16% lower volumetric BMD compared to women [28]. In a small subset of subjects with QCT-based finite element analysis (n=28 pairs), they found the larger femur size of the men offset their lower vBMD, such that femoral strength estimates were similar between men and women matched for femoral neck aBMD. This contrasts with our finding that men had higher lumbar vertebral compressive strength than women when matched by aBMD. However, after height and weight adjustment, we found no significant compressive strength difference between men and women. Srinivasan et al did not evaluate differences in femoral strength after height and weight adjustment, and given that the men were taller, this type of analysis may have revealed men to have lower femoral strength than women when matched for aBMD. Srinivasan et al also found that men and women who were matched for femoral aBMD had similar femoral loads during a simulated sideways fall, and therefore similar factor-of-risk for hip fracture. However, their estimates of femoral loading did not account for individual differences in

trochanteric soft tissue thickness, which has a large influence on femoral loading [29] and which varies markedly between men and women [30, 31]. Further, men and women in the Srinivasan study were not matched for age, and this resulted in the men being approximately six years older than the women after the aBMD matching, so the observed differences between men and women may not have been solely sex-related.

In the entire Framingham CT Study cohort we found a greater percentage of men had prevalent vertebral fracture than women in the younger three age groups, but that more women had prevalent vertebral fracture in the oldest age group, a pattern consistent with prior studies [32-34]. The greater vertebral fracture prevalence in younger men compared to women may result from more frequent exposure to high load activities and injuries earlier in life, with the women eventually surpassing the men because of accelerated bone loss [16] and a greater incidence of vertebral fracture after age 50 [35]. We observed a similar pattern in the age- and aBMD- matched subset of subjects, except in the oldest age group where the matched men had a greater prevalence of vertebral fracture than their female counterparts, contrasting with the entire Framingham CT cohort where women had higher vertebral fracture prevalence in this age group. Consistent with the patterns we observed in our age- and aBMD- matched sample, Lunt and colleagues [36] reported that after adjusting for body mass index and spine aBMD men had higher prevalence of vertebral deformity than women at all ages. Our observation that men in the age- and aBMD- matched sample had a higher prevalence of vertebral fracture than women in all age groups is consistent with our finding that men in the age- and aBMD-matched cohort had a higher factor-of-risk for vertebral fracture than women, and thus would be predicted to have higher risk for vertebral fracture than women.

At least one prospective study of incident vertebral fracture supports our prediction of higher vertebral fracture risk in men and women matched for age and spine aBMD [37], whereas others conflict with it [38, 39]. Specifically, despite a higher BMD, men in the Canadian Multicenter Osteoporosis Study [37] had a similar incidence of vertebral fracture as women, implying that after adjustment for BMD, men would have had a higher incidence of vertebral fracture than women [37]. In contrast, the European Osteoporosis Study (EPOS) found that whereas the age-adjusted risk of incident vertebral fracture was 2.3 fold greater in women than

men, after adjusting for lumbar spine aBMD there was no longer a sex difference in the age-specific incidence of vertebral fracture [38]. Similarly, the Rotterdam study found that there was no sex difference in the risk of incident vertebral fracture after adjusting for both age and spine aBMD [39].

There are several possible reasons why our predictions differ from these latter two prospective studies. First, it is important to note that while these investigations had a large number of subjects, in fact there were relatively few incident fractures in men: 26 in the EPOS study and 47 in the Rotterdam study. Second, while the current study used specific 1:1 matching of men and women by age and spine aBMD, these other studies used a statistical adjustment to remove the confounding effects of age and aBMD on the association between sex and vertebral fracture. However, if the distribution of aBMD between women and men at the same age was not sufficiently overlapping, statistical adjustment may be inadequate, resulting in residual confounding by age and aBMD. Finally, we did not have DXA-based aBMD, but rather estimated aBMD from 3D-QCT data, and this may have led to errors in the selection of pairs of men and women matched for spine aBMD.

Finally, differences could be the result of the limitations in our factor-of-risk model that might overestimate risk in the men and/or underestimate the risk in the women. For example, we estimated vertebral strength using engineering beam theory and an empirically derived formula relating CSA and Int.vBMD to vertebral compressive strength measured *in vitro* [19]. Although this approach predicts the compressive strength of cadaver vertebrae fairly well (r^2 =0.65) [40], there are additional factors affecting vertebral strength not captured by this approach that might influence the differences in vertebral strength between men and women. Additionally, we only assessed vertebral strength and vertebral loading at L3. However, vertebral fractures occur throughout the spine with peaks in frequency at the mid-thoracic and thoraco-lumbar junction [41]. Despite this, vertebral strength and loading estimates at different spinal levels are typically correlated with each other [42], making it reasonable to look for sex-related differences in loading and factor-of-risk at just one vertebral level.

Further, there may be sex-specific factors that influence vertebral loading that were not accounted for in our musculoskeletal model [42]. For instance, women on average have

greater thoracic kyphosis than men, and previous biomechanical studies have shown that a larger kyphosis angle results in increased compressive loads on both the thoracic and lumbar spine [20, 43-45]. In the current study measurements of spinal curvature were not available, and so our musculoskeletal model used the same spinal curvature for both men and women, and thus would not have captured possible sex-related differences in vertebral loading due to altered spinal curvature. A greater kyphosis angle in women may result in higher compressive loads and thus an increased factor-of-risk in women. Future studies should incorporate individualized spinal curvatures into musculoskeletal models to better delineate sex-specific differences in vertebral loading and factor-of-risk. Finally, it is not clear which activities are most likely to result in vertebral fracture [41, 46], and it is possible that there are sex-specific patterns of loading and factor-of-risk for activities not considered here.

These limitations notwithstanding, major strengths of the current study include the large number of men and women pairs matched closely for aBMD and age, the use of QCT to assess compartment specific differences in volumetric bone density, and the use of the factor-of-risk approach to integrate estimates of vertebral loading and vertebral strength to understand risk of vertebral fracture.

In conclusion, we found that when matched for both age and spine aBMD at L3, men have higher vertebral CSA, lower volumetric density, higher vertebral compressive strength, and higher factor-of-risk for vertebral fracture compared to women. This study provides new insights into the sex-specific structural and biomechanical differences that exist between the vertebra of men and women, and has important clinical implications concerning the use of aBMD to predict vertebral fracture and diagnose osteoporosis in both men and women. Taken together, the results of this study suggest that men and women do not have similar risk of vertebral fracture at the same absolute level of spine aBMD, and that the use of sex-specific spine aBMD reference values to predict fracture risk in men and women deserves further investigation.

2.6 Acknowledgements

This work was supported by grants from the National Institutes of Health (R01AR053986, R01AR/AG041398, T32AG023480, 1F31AG041629-01), and by the National Heart, Lung, and Blood Institute (NHLBI) Framingham Heart Study (NIH/NHLBI Contract N01-HC-25195). The contents are solely the responsibility of the authors, and do not necessarily represent the views of the NIH.

Authors' roles: Study design: MLB. Study conduct: AGB, KEB, XZ, CM, RM, JD, MLB, DPK. Data collection: AGB, KEB, XZ, RM, JD, DPK. Data analysis: KEB, XZ, LAC. Data interpretation: AGB, KEB, EJS, DPK, MLB. Drafting manuscript: AGB, KEB. Revising manuscript content: AGB, KEB, EJS, LAC, DPK, MLB. Approving final version of manuscript: AGB, KEB, XZ, EJS, CM, RM, JD, LAC, DPK, MLB. All authors take responsibility for the integrity of the data analysis.

2.7 REFERENCES

1. Ensrud, K.E. and J.T. Schousboe, *Clinical practice. Vertebral fractures.* N Engl J Med, 2011. **364**(17): p. 1634-42.

2. Melton, L.J., et al., *Epidemiology of vertebral fractures in women.* American Journal of Epidemiology, 1989. **129**(5): p. 1000-1011.

3. Melton, L.J., et al., *Prevalence and incidence of vertebral deformities.* Osteoporosis International, 1993. **3**(3): p. 113-119.

4. Cooper, C., et al., *Population-Based Study of Survival after Osteoporotic Fractures.* American Journal of Epidemiology, 1993. **137**(9): p. 1001-1005.

5. Gold, D.T., *The Nonskeletal Consequences of Osteoporotic Fractures: Psychologic and Social Outcomes.* Rheumatic Disease Clinics of North America, 2001. **27**(1): p. 255-262.

6. Gold, D.T., *The clinical impact of vertebral fractures: Quality of life in women with osteoporosis.* Bone, 1996. **18**(3, Supplement 1): p. S185-S189.

7. Nevitt, M.C., et al., *The Association of Radiographically Detected Vertebral Fractures with Back Pain and Function: A Prospective Study.* Annals of Internal Medicine, 1998. **128**(10): p. 793-800.

8. Schlaich, C., et al., *Reduced Pulmonary Function in Patients with Spinal Osteoporotic Fractures.* Osteoporosis International, 1998. **8**(3): p. 261-267.

9. van Schoor, N.M., et al., *Impact of vertebral deformities, osteoarthritis, and other chronic diseases on quality of life: a population-based study.* Osteoporosis International, 2005. **16**(7): p. 749-756.

10. *Assessment of Fracture Risk and Its Application to Screening for Postmenopausal Osteoporosis.*, in *WHO Technical Report Series 843*. 1994, World Health Organization: Geneva.

11. Kanis, J.A., et al., *The diagnosis of osteoporosis.* Journal of Bone and Mineral Research, 1994. **9**(8): p. 1137-1141.

12. Watts, N.B., *Fundamentals and pitfalls of bone densitometry using dual-energy X-ray absorptiometry (DXA).* Osteoporos Int, 2004. **15**(11): p. 847-54.

13. Carter, D.R., M.L. Bouxsein, and R. Marcus, *New approaches for interpreting projected bone densitometry data.* J Bone Miner Res, 1992. **7**(2): p. 137-45.

14. Hoffmann, U., et al., *Defining normal distributions of coronary artery calcium in women and men (from the Framingham Heart Study).* Am J Cardiol, 2008. **102**(9): p. 1136-41, 1141 e1.

15. Christiansen, B.A., et al., *Mechanical contributions of the cortical and trabecular compartments contribute to differences in age-related changes in vertebral body strength in men and women assessed by QCT-based finite element analysis.* J Bone Miner Res, 2011. **26**(5): p. 974-83.

16. Samelson, E.J., et al., *QCT measures of bone strength at the thoracic and lumbar spine: the Framingham Study.* J Bone Miner Res, 2012. **27**(3): p. 654-63.

17. Lang, T.F., et al., *Measurement of bone mineral density at the spine and proximal femur by volumetric quantitative computed tomography and dual-energy x-ray absorptiometry in elderly women with and without vertebral fractures.* Bone, 2002. **30**(1): p. 247-250.

18. Lang, T.F., et al., *Assessment of Vertebral Bone Mineral Density Using Volumetric Quantitative CT.* Journal of Computer Assisted Tomography, 1999. **23**(1): p. 130-137.

19. Bouxsein, M.L., et al., *Age- and Sex-Specific Differences in the Factor of Risk for Vertebral Fracture: A Population-Based Study Using QCT.* Journal of Bone and Mineral Research, 2006. **21**(9): p. 1475-1482.

20. Bruno, A.G., et al., *The effect of thoracic kyphosis and sagittal plane alignment on vertebral compressive loading.* Journal of Bone and Mineral Research, 2012: p. 10.1002/jbmr.1658.

21. Iyer, S., et al., *A biomechanical model for estimating loads on thoracic and lumbar vertebrae.* Clin Biomech (Bristol, Avon), 2010. **25**(9): p. 853-8.

22. Bean, J.C., D.B. Chaffin, and A.B. Schultz, *Biomechanical model calculation of muscle contraction forces: A double linear programming method.* Journal of Biomechanics, 1988. **21**(1): p. 59-66.

23. Schultz, A.B. and G.B.J. Andersson, *Analysis of Loads on the Lumbar Spine.* Spine, 1981. **6**(1): p. 76-82.

24. Anderson, D.E., et al., *Regressions for estimating muscle parameters in the thoracic and lumbar trunk for use in musculoskeletal modeling.* Journal of Biomechanics, 2012. **45**: p. 66-75.

25. Narici, M., *Human skeletal muscle architecture studied in vivo by non-invasive imaging techniques: functional significance and applications.* Journal of Electromyography and Kinesiology, 1999. **9**(2): p. 97-103.

26. Genant, H.K., et al., *Vertebral fracture assessment using a semiquantitative technique.* Journal of Bone and Mineral Research, 1993. **8**(9): p. 1137-1148.

27. Riggs, B.L., et al., *Population-Based Study of Age and Sex Differences in Bone Volumetric Density, Size, Geometry, and Structure at Different Skeletal Sites.* Journal of Bone and Mineral Research, 2004. **19**(12): p. 1945-1954.

28. Srinivasan, B., et al., *Relationship of femoral neck areal bone mineral density to volumetric bone mineral density, bone size, and femoral strength in men and women.* Osteoporos Int, 2012. **23**(1): p. 155-62.

29. Robinovitch, S.N., T.A. McMahon, and W.C. Hayes, *Force attenuation in trochanteric soft tissues during impact from a fall.* J Orthop Res, 1995. **13**(6): p. 956-62.

30. Bouxsein, M.L., et al., *Contribution of trochanteric soft tissues to fall force estimates, the factor of risk, and prediction of hip fracture risk.* J Bone Miner Res, 2007. **22**(6): p. 825-31.

31. Nielson, C.M., et al., *Trochanteric soft tissue thickness and hip fracture in older men.* J Clin Endocrinol Metab, 2009. **94**(2): p. 491-6.

32. Davies, K.M., et al., *Prevalence and severity of vertebral fracture: The saunders county bone quality study.* Osteoporosis International, 1996. **6**(2): p. 160-165.

33. Jackson, S.A., A. Tenenhouse, and L. Robertson, *Vertebral fracture definition from population-based data: preliminary results from the Canadian Multicenter Osteoporosis Study (CaMos).* Osteoporos Int, 2000. **11**(8): p. 680-7.

34. O'Neill, T.W., et al., *The prevalence of vertebral deformity in european men and women: the European Vertebral Osteoporosis Study.* J Bone Miner Res, 1996. **11**(7): p. 1010-8.

35. Felsenberg, D., et al., *Incidence of vertebral fracture in europe: results from the European Prospective Osteoporosis Study (EPOS).* J Bone Miner Res, 2002. **17**(4): p. 716-24.

36. Lunt, M., et al., *Bone density variation and its effects on risk of vertebral deformity in men and women studied in thirteen European centers: the EVOS Study.* J Bone Miner Res, 1997. **12**(11): p. 1883-94.

37. Chen, P., et al., *Vertebral fracture status and the World Health Organization risk factors for predicting osteoporotic fracture risk.* J Bone Miner Res, 2009. **24**(3): p. 495-502.

38. O'Neill, T.W., *The Relationship Between Bone Density and Incident Vertebral Fracture in Men and Women.* Journal of Bone and Mineral Research, 2002. **17**(12): p. 2214-2221.

39. Van der Klift, M., et al., *The incidence of vertebral fractures in men and women: the Rotterdam Study.* J Bone Miner Res, 2002. **17**(6): p. 1051-6.

40. Crawford, R.P., C.E. Cann, and T.M. Keaveny, *Finite element models predict in vitro vertebral body compressive strength better than quantitative computed tomography.* Bone, 2003. **33**(4): p. 744-750.

41. Cooper, C., et al., *Incidence of clinically diagnosed vertebral fractures: A population-based study in rochester, minnesota, 1985-1989.* Journal of Bone and Mineral Research, 1992. **7**(2): p. 221-227.

42. Christiansen, B.A. and M.L. Bouxsein, *Biomechanics of vertebral fractures and the vertebral fracture cascade.* Curr Osteoporos Rep, 2010. **8**(4): p. 198-204.

43. Bartynski, W.S., et al., *Severe Thoracic Kyphosis in the Older Patient in the Absence of Vertebral Fracture: Association of Extreme Curve with Age.* AJNR Am J Neuroradiol, 2005. **26**(8): p. 2077-2085.

44. Briggs, A., et al., *The effect of osteoporotic vertebral fracture on predicted spinal loads in vivo.* European Spine Journal, 2006. **15**(12): p. 1785-1795.

45. Briggs, A.M., et al., *Thoracic Kyphosis Affects Spinal Loads and Trunk Muscle Force.* Physical Therapy, 2007. **87**(5): p. 595-607.

46. Freitas, S.S., et al., *Rate and circumstances of clinical vertebral fractures in older men.* Osteoporos Int, 2008. **19**(5): p. 615-23.

Chapter 3: THE EFFECT OF THORACIC KYPHOSIS AND SAGITTAL PLANE ALIGNMENT ON VERTEBRAL COMPRESSIVE LOADING

This chapter was previously published in the Journal of Bone and Mineral Research:

Bruno, A.G., et al., *The effect of thoracic kyphosis and sagittal plane alignment on vertebral compressive loading*. J Bone Miner Res, 2012. 27(10): p. 2144-51.

3.1 Abstract

To better understand the biomechanical mechanisms underlying the association between hyperkyphosis of the thoracic spine and risk of vertebral fracture and other degenerative spinal pathology, we used a previously validated musculoskeletal model of the spine to determine how thoracic kyphosis angle and spinal posture affect vertebral compressive loading. We simulated an age-related increase in thoracic kyphosis (T1-T12 Cobb angle 50° to 75°) during two different activities (relaxed standing and standing with 5 kg weights in the hands) and three different posture conditions: 1) an increase in thoracic kyphosis with no postural adjustment (uncompensated posture), 2) an increase in thoracic kyphosis with a concomitant increase in pelvic tilt that maintains a stable center of mass and horizontal eye gaze (compensated posture), and 3) an increase in thoracic kyphosis with a concomitant increase in lumbar lordosis that also maintains a stable center of mass and horizontal eye gaze (congruent posture). For all posture conditions, compressive loading increased with increasing thoracic kyphosis, with loading increasing more in the thoracolumbar and lumbar regions than in the mid-thoracic region. Loading increased the most for the uncompensated posture, followed by the compensated posture, with the congruent posture almost completely mitigating any increases in loading with increased thoracic kyphosis. These findings indicate that thoracic kyphosis and spinal posture both influence vertebral loading during daily activities, implying that thoracic kyphosis measurements alone are not sufficient to characterize the impact of spinal curvature on vertebral loading.

3.2 Introduction

Thoracic kyphosis refers to forward curvature of the thoracic spine in the sagittal plane. Exaggerated thoracic kyphosis, or hyperkyphosis, is common in the elderly, and this age-related increase in thoracic kyphosis has been attributed to the presence of vertebral fractures [1-3], intervertebral disc degeneration [2, 3], loss of spinal muscle strength [4, 5] and degeneration of the intervertebral ligaments [6]. In addition to being caused by vertebral fractures, hyperkyphosis is also a strong risk factor for incurring new vertebral fractures, independent of bone mineral density [7, 8]. This increased risk of vertebral fractures may be due to an anterior

shift in body mass that effectively increases the moment arm between the spine and the superincumbent body mass that it supports [9, 10]. This increased moment arm would lead to higher spinal moments and trunk muscle forces that would increase spinal compressive loading and vertebral fracture risk. However, the precise relationship between thoracic kyphosis angle and spinal compressive loading has not been systematically explored. Specifically, it is not known how much a given increase in thoracic kyphosis angle increases vertebral compressive loading, and whether this increase is large enough to contribute to the increased fracture risk associated with hyperkyphosis.

In addition to thoracic kyphosis, other postural and morphological parameters can influence the distribution of body mass and therefore the biomechanical environment of the spine. For instance, in response to an age-related increase in thoracic kyphosis a person can make various postural adjustments to maintain a stable center of mass and horizontal eye gaze [11-15]. These postural adjustments include posterior tilting or translation of the pelvis, hip extension, knee flexion, and dorsiflexion of the ankles, all of which act to counter the anterior shift in body mass associated with increased thoracic kyphosis [11, 12]. The postural adjustment strategy that an individual employs, and the degree to which they are able to adjust, will affect the biomechanical environment of the spine, but how these different parameters interact with thoracic kyphosis angle to affect spinal compressive loading is poorly understood.

Another factor that interacts with the thoracic kyphosis angle to influence vertebral compressive loading is whether one's posture is "congruent" [16], meaning that the thoracic curvature is proportional to and balances the lumbar lordosis. Congruency is necessary for maintenance of an upright posture, and the degree to which someone's posture is congruent will influence body mass distribution and the biomechanical environment of the spine. An age-related increase in thoracic kyphosis, without a concomitant change in lumbar lordosis, leads to an "uncompensated incongruent posture" [16], where the thoracic and lumbar regions no longer have complementary amounts of curvature and upright posture is therefore diminished. However, as discussed above, it is possible to make a postural adjustment, such as tilting the pelvis back, to stabilize the body's center of mass. When this occurs, the individual will have a

"compensated incongruent posture" [16] since some adjustment was made to correct balance and redistribute body mass, but the thoracic and lumbar curves are still not balanced.

Our overall objective is to understand the contribution of spine biomechanics to spine-related pathologies, including vertebral fractures. The goals of this study were to systematically investigate the effect of thoracic kyphosis angle and whole-body posture on vertebral compressive loading. We used a musculoskeletal model of the spine to examine how vertebral loading at the mid-thoracic and thoraco-lumbar regions changes with a simulated increase in thoracic kyphosis during three postural conditions: 1) an increase in thoracic kyphosis with no postural adjustment (uncompensated posture), 2) an increase in thoracic kyphosis with a concomitant increase in pelvic tilt that maintains a stable center of mass and horizontal eye gaze (compensated posture), and 3) an increase in thoracic kyphosis with a concomitant increase in lumbar lordosis that also maintains a stable center of mass and horizontal eye gaze (congruent posture) (Fig. 3.1). We hypothesized that spinal loading would be minimally affected by changes in thoracic kyphosis for a congruent posture and most affected for an uncompensated posture.

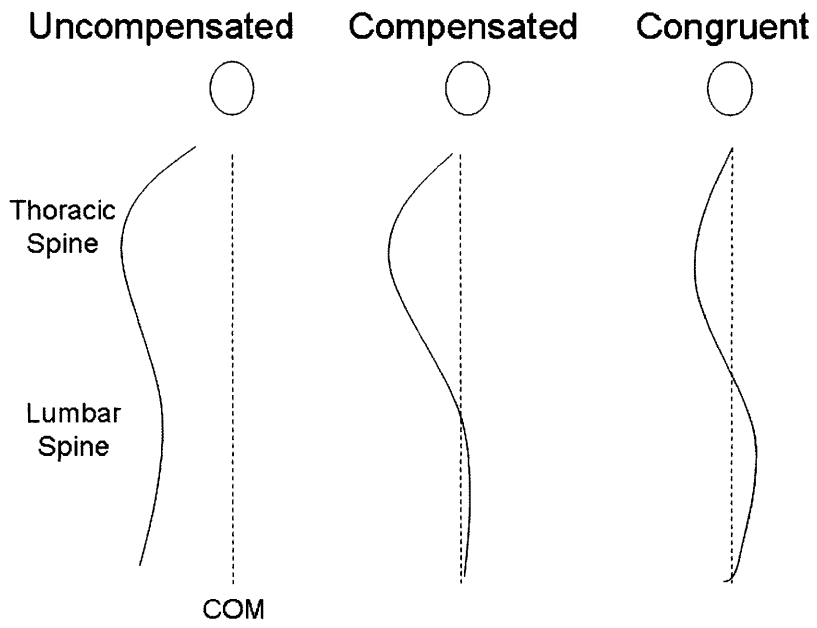

Figure 3.1: Illustration demonstrating the sagittal spinal profiles associated with an uncompensated posture, a compensated posture (in this case tilting the pelvis posteriorly), and a congruent posture.

3.3 Materials and Methods

3.3.1 Musculoskeletal Spine Model

We used a static musculoskeletal model of the spine [17] to estimate compressive force on the T6 through L5 vertebral bodies of a representative 65 year old woman during a simulated increase in thoracic kyphosis. Our spine model has been previously validated against *in vivo* measurements of trunk muscle myoelectric activity and intervertebral disc pressures in the thoracic and lumbar spine during a variety of activities, including relaxed standing, trunk lateral bending, trunk flexion/extension, and standing with a 10kg load and elbows flexed 90° [17]. For the purposes of the current study, vertebral compressive force was estimated for three different posture conditions (described later) and for two different activities: 1) relaxed standing with arms hanging down and 2) standing with elbows flexed 90° and 5 kg weights in each hand (Fig. 3.2).

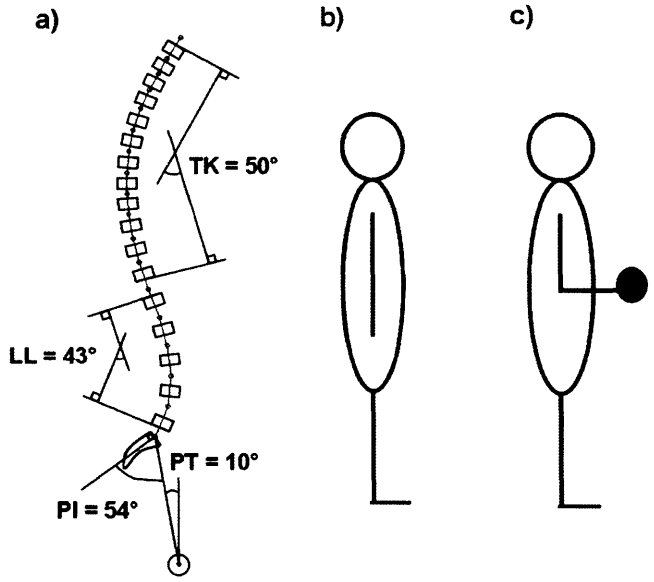

Figure 3.2: a) Sagittal view of the baseline spinal curvature and pelvic orientation used in the biomechanical model, showing the degree of thoracic kyphosis (TK), lumbar lordosis (LL), pelvic incidence (PI), and pelvic tilt (PT); b) cartoon of the first activity modeled: standing upright with the arms hanging straight down at the sides; c) cartoon of the second activity modeled: standing upright with the elbows flexed 90° and 5 kg weights in each hand. Both activities were modeled in 3D and were sagittally symmetric.

Our musculoskeletal model operates on principles similar to those used in previously published biomechanical models of the *lumbar* spine [18-20], except that it also estimates vertebral loading in the thoracic spine by taking into account the mechanical contribution of the

ribs and sternum [17]. In brief, the body was modeled as a series of linked-segments, and for this study the weight, length, and center of mass position for each segment was estimated for a 65 year old woman (height = 1.61 m, weight = 70.31 kg) using published anthropometric data [21-25]. The center of mass of each thoracic and lumbar trunk segment (T1 through L5) was positioned anterior to the vertebral body centroid using data from Pearsall and colleagues [23]. Muscles present in the model included pectoralis major, rectus abdominus, serratus anterior, trapezius, latissimus dorsi, external oblique, internal oblique, sacrospinalis, transversospinalis, psoas major, and quadratus laborum. Trunk muscle cross-sectional areas and moment arm lengths in the medial-lateral and anterior-posterior directions were estimated using regression equations relating these properties to age, sex, height, and weight [26]. The forces and moments applied to each vertebral body due to the weight and position of superincumbent body mass, as well as the weights being held in the hands, were calculated for each activity. Muscle forces required to balance the moments and maintain static equilibrium were determined using a static optimization algorithm that minimized the sum of cubed muscle intensities [17]. The maximum allowable muscle stress was limited to 1 MPa [27] to keep solutions within a physiologically acceptable range. Compressive force on the vertebral body was the sum of the superincumbent weight and muscle loading acting in the axial direction of the vertebral body.

3.3.2 Baseline Spinal Curvature and Pelvic Orientation

The baseline spinal curvature and pelvic orientation for the model were created using average values from the literature (Fig. 3.2) [28, 29] as follows: T1-T12 Cobb angle = 50°, L1-L5 Cobb angle = 43°, pelvic incidence = 54°, pelvic tilt = 10°, sacral slope = 44°, and L5-S1 intersegmental angulation = 21°.

3.3.3 Thoracic Kyphosis Sensitivity Analysis

To determine the effect of increasing thoracic kyphosis on spinal compressive loading, we started with our baseline spinal model, which represents a congruent posture, and increased the T1-T12 Cobb angle from 50° to 75° in 1° increments (Fig. 3.3) to simulate an age-

related increase in thoracic kyphosis [30]. Adjustments to the T1-T12 Cobb angle were evenly added to the different vertebral levels to achieve the desired Cobb angle. For example, to achieve a 75° T1-T12 Cobb angle, the baseline thoracic curvature of 50° was increased 25° by adding 25/11 ≈ 2.27° to each of the 11 intersegmental angles between T1 and T12. For each T1-T12 Cobb angle, we estimated vertebral compressive loading for the two different activities and three different postural conditions: 1) uncompensated posture, 2) compensated posture and 3) congruent posture. For the uncompensated posture condition, the T1-T12 Cobb angle was varied from 50° to 75° while all other spino-pelvic parameters remained fixed at their baseline values. For the compensated posture condition, pelvic tilt was varied (10° to 15.31° in 0.23° increments) concomitantly with the T1-T12 Cobb angle (50° to 75° in 1° increments) to maintain the sagittal alignment of the head and neck directly above the hip joint. For the congruent posture condition, the L1-L5 Cobb angle was varied (43° to 52.10° in 0.36° increments) concomitantly with the T1-T12 Cobb angle (50° to 75° in 1° increments) to maintain the sagittal alignment of the head and neck directly above the hip joint.

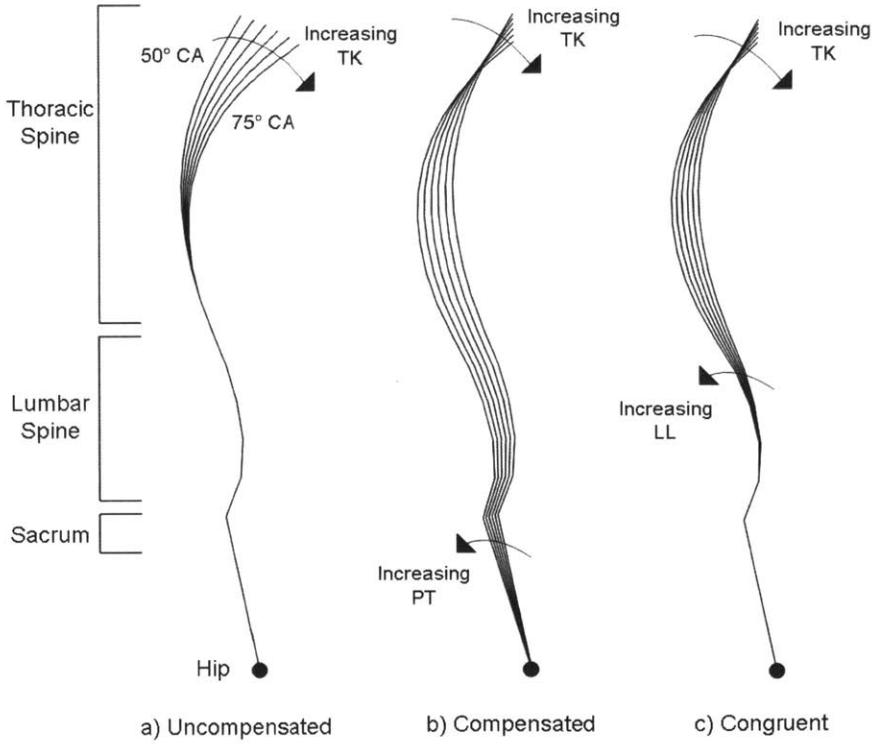

Figure 3.3: Schematic representation of the range of spinal curvatures modeled in this study, starting with a) uncompensated posture, b) compensated posture, and c) congruent posture. The T1-T12 Cobb angle was varied

from 50° to 75° in 1° increments, but for clarity the images above show only the 5° increments with the extreme spinal curves labeled.

Compressive force on the T6 through L5 vertebral bodies was calculated for each T1-T12 Cobb angle during the three posture and two activity conditions. Detailed force versus Cobb angle results are presented for T8 and T12, the most common sites for osteoporotic vertebral fracture [31, 32]. Least-squares linear regressions were fitted to the load versus Cobb angle data for each of the vertebral bodies between T6 and L5 in order to determine the increase in vertebral compressive force for every 1° increase in Cobb angle.

We also explored how subject height and weight might interact with posture, thoracic kyphosis, and activity to influence spinal loading at T12. We varied the height and weight of our subject using values ranging between the 5^{th} and 95^{th} percentiles for US women above age 20 [33]. While varying height, weight was held fixed at the 50^{th} percentile value for women (71 kg) and when varying weight, height was held constant at the 50^{th} percentile value for women (1.62 m).

3.4 Results

Vertebral compressive force was higher at T12 than T8 and higher for standing with weight in the hands than standing with no weight (Fig. 3.4). At the baseline condition (thoracic kyphosis = 50°) the spino-pelvic parameters for the three different posture conditions (uncompensated, compensated, and congruent) were the same, meaning that the shape of the spine and the orientation of the pelvis were identical for all three postures, as were vertebral compressive forces. For this baseline condition the compressive force at T8 was 297 N for standing and 921 N for standing with elbows flexed and weight in the hands, whereas the compressive force at T12 was 422 N for standing and 1471 N for standing with elbows flexed and weight in the hands. At T8, compressive loading increased with increasing thoracic kyphosis for each of the three postures, with the increase in loading being greatest for the uncompensated posture, followed by the compensated posture, and finally the congruent posture (Fig. 3.4). A similar trend was observed at T12 except that the differences in loading

between the different postures at a given thoracic kyphosis angle were greater than those observed for T8.

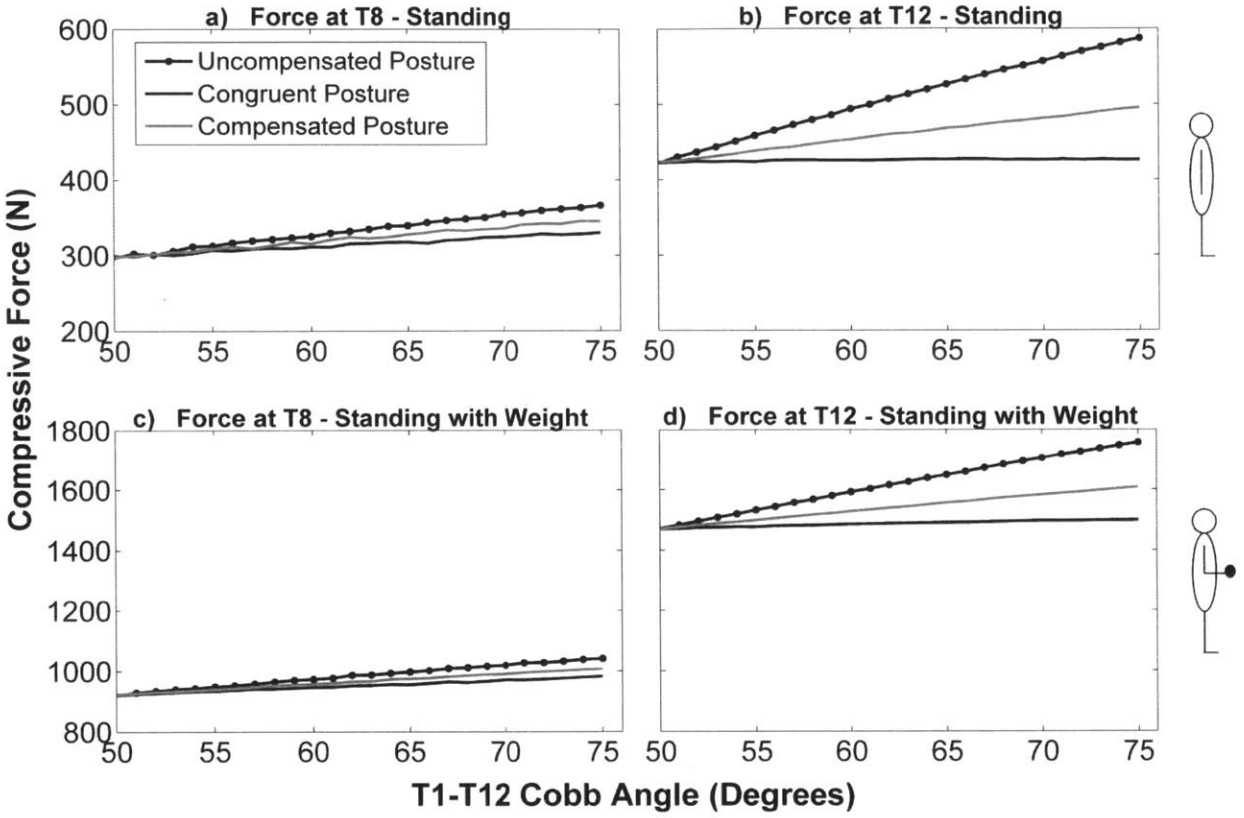

Figure 3.4: Compressive force (Newtons) on T8 and T12 as a function of T1-T12 Cobb angle (degrees) for the two activities, as well as the three different postures.

The uncompensated and compensated postures in general caused greater increases in loading in the lumbar and thoracolumbar regions than in the thoracic spine. The congruent posture appeared to mitigate kyphosis-related increases in loading at all vertebral levels, and even caused loading to decrease with increasing Cobb angle in the lumbar spine (Fig. 3.5).

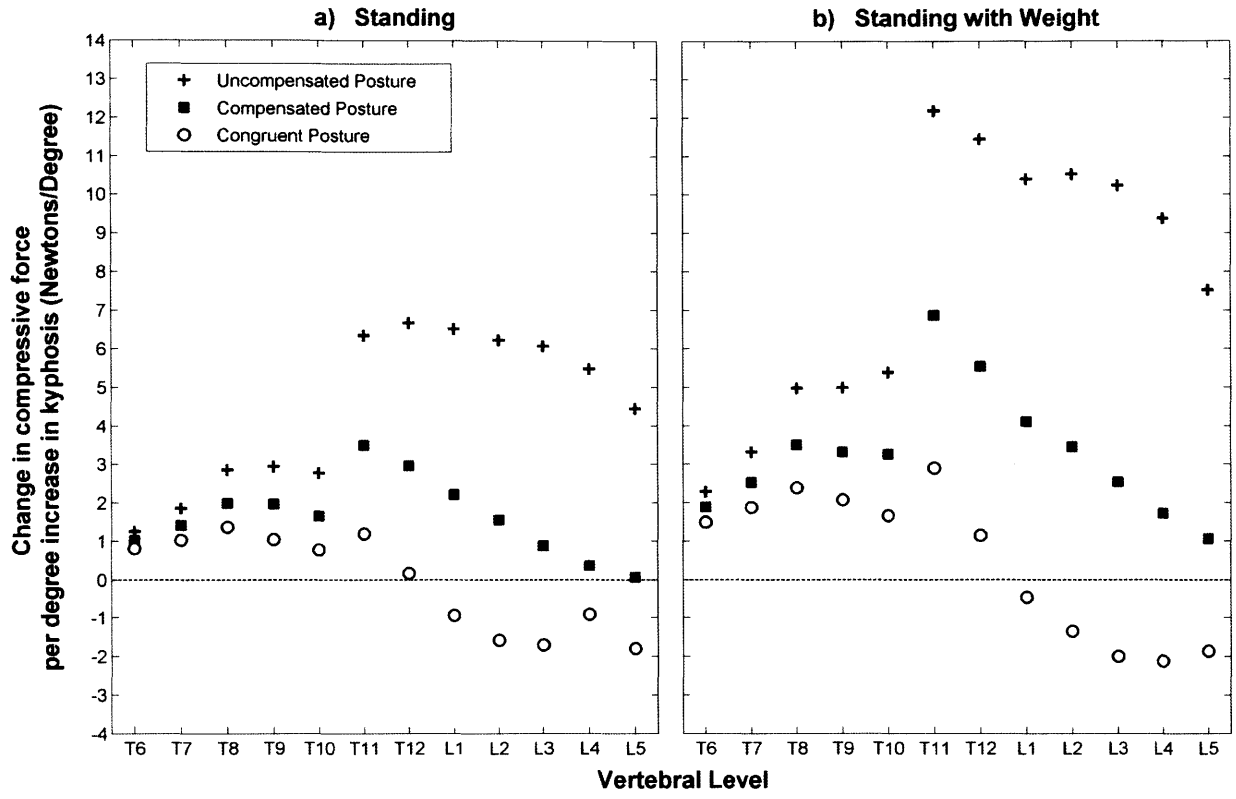

Figure 3.5: Increase in compressive loading for every 1° increase in the T1-T12 Cobb angle. These values are the slopes of least-squares linear regressions fitted to the load versus Cobb angle data for each vertebral body.

For a given posture and thoracic kyphosis angle, the magnitude of vertebral compressive loading was higher when subject height or weight was increased, which was expected (data not shown). Varying subject height had minimal to no effect on the load versus Cobb angle trends already observed at T12 (Fig. 3.6). That is, subject height did not affect the change in compressive force per 1° increase in kyphosis. Increasing subject body weight caused larger kyphosis-related increases in loading for the uncompensated and compensated posture conditions (Fig. 3.6). Interestingly, the congruent posture condition prevented this interaction of subject weight and thoracic kyphosis angle.

Again, all three postures showed an increase in spinal compressive loading with increasing thoracic kyphosis, but the increase was greatest for the uncompensated posture, followed by the compensated posture, and finally the congruent posture.

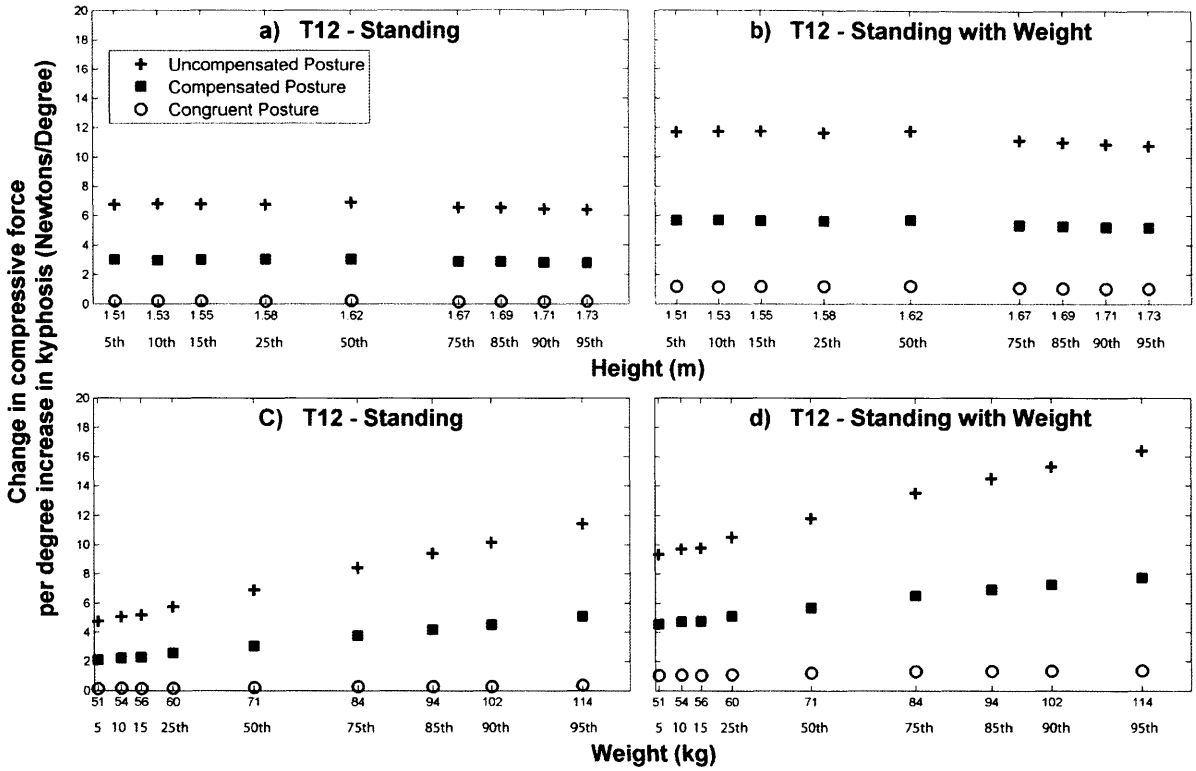

Figure 3.6: Increase in T12 compressive loading for every 1° increase in the T1-T12 Cobb angle. These values are the slopes of least-squares linear regressions fitted to the load versus Cobb angle data at T12 for each height/weight combination. Note that when the subject's height was varied, subject weight was held constant at 71 kg (the 50th percentile value for females) and when the subject's weight was varied, subject height was held constant at 1.62 m (the 50th percentile value for females).

3.5 Discussion

We used a musculoskeletal model of the spine to investigate the effect of increasing thoracic kyphosis on vertebral compressive loading under three different postural conditions (uncompensated, compensated, and congruent) and two different activities (relaxed standing and standing with weight in the hands). We found that an uncompensated increase in thoracic kyphosis resulted in the largest increases in spinal loading, whereas maintenance of a congruent posture minimized the increases in loading. Use of a postural compensation technique also reduced kyphosis-related increases in loading, but not to the same extent as the congruent posture. The differences in loading between the three posture conditions were greater in the thoracolumbar and lumbar regions than in the thoracic region. Varying subject height did not affect kyphosis-related increases in loading. However, increasing subject weight

resulted in larger kyphosis-related increases in loading for the uncompensated and compensated postures, but did not have an effect for the congruent posture.

Vertebral fractures are most common at the mid-thoracic and thoracolumbar regions [31, 32], and therefore these are the most relevant spinal locations in terms of understanding how excessive thoracic kyphosis might increase vertebral fracture risk. Higher loads at T12 compared to T8 were expected considering that T12 is located inferior to T8 and therefore carries a higher percentage of the body's weight. In addition, load sharing with the ribs and sternum likely reduced the compressive force exerted on T8 [17]. In general, we found that the thoracolumbar and lumbar regions of the spine experienced greater kyphosis-related increases in loading then the thoracic region, which is most likely due to the fact that for a given increase in thoracic curvature, lower sections of the spine see a proportionally greater amount of body mass shifted anteriorly. Additionally, the ribs and sternum in the thoracic region likely share a proportion of the increased load. Together, these two effects might explain the marked increase in loading that occurs between the lower-thoracic and thoracolumbar regions (Fig. 3.5).

As body weight increased, the kyphosis-related increase in loading was greater for both the uncompensated and compensated postures, presumably because a greater amount of body mass was being shifted anteriorly, whereas in the congruent posture this additional body mass was more efficiently distributed around the trunk such that increasing thoracic kyphosis did not significantly change the moment arm between the body mass and the T12 vertebral body.

The results of our simulations are largely consistent with prior biomechanical modeling studies [10, 34, 35]. Briggs and colleagues found that during upright standing osteoporotic individuals with a vertebral fracture had higher estimated vertebral compressive loading between T7 and L5 than individuals with no vertebral fracture, and that these differences in loading were due to subtle differences in spinal curvature [34]. Furthermore, during relaxed standing, estimated vertebral compressive forces between T7 and L5 are reported to be up to 14% greater in elderly subjects with high versus low thoracic kyphosis, and an increased thoracic kyphosis angle increased loading more so at T12 than at T8 [10].

In our study, increasing thoracic kyphosis increased spinal compressive loading more in the uncompensated condition than in the compensated or congruent conditions because it shifted a greater amount of body mass forward. This generated higher flexion moments which required larger muscle forces to equilibrate, elevating compressive loads on the vertebral bodies. The congruent and compensated posture conditions countered the anterior shift in body mass associated with an increasing thoracic kyphosis, with the congruent posture condition being more effective. The clinical implication is that some older individuals who have very high thoracic kyphosis may not have increased vertebral loading and be at an elevated risk for fracture because they have congruent posture. In comparison, those who have an age-related increase in thoracic kyphosis and do not have a congruent spinal configuration may have a greater risk for fracture than someone with the same thoracic kyphosis angle but who maintains a congruent posture.

In support of this concept, Keller and colleagues [36] applied a biomechanical model to a large group of young asymptomatic subjects to investigate how various spinal morphology parameters influence loading of the intervertebral disc. Whereas they found a positive correlation between compressive forces on thoracic vertebrae and forward sagittal balance (anterior shift in the center of mass position), they found no association between thoracic compressive forces and any sagittal spinal angles, despite a high variation in thoracic kyphosis angle among the subjects (T1-T12 Cobb angle ranged between 16.3° and 71.5°). The lack of association between thoracic kyphosis angle and thoracic spine compressive forces supports the notion that other postural parameters play a significant role in determining body mass distribution and therefore the spine's biomechanical environment. These results are consistent with the current study's findings that postural congruency and the use of a compensation technique can act to mitigate any increases in compressive loading associated with an elevated thoracic kyphosis angle. The asymptomatic subjects in the Keller study (mean age = 26.7 years) may have exhibited highly congruent postures because of their young age and the notion that congruency is indicative of a healthy spine [16]. Taken together, these observations suggest that thoracic kyphosis measurements alone are not sufficient to characterize the impact of

spinal curvature on vertebral loading, and that whole body postural alignment likely needs to be taken into consideration.

Despite age-related increases in the thoracic kyphosis angle, people are generally able to maintain their center of mass in a narrow range by employing various postural compensation strategies [11-15]. For instance, Schwab and colleagues [12] found that thoracic kyphosis increased with advancing age but that center of mass was maintained at a constant distance from the heel due to posterior translation of the pelvis and an increase in pelvic tilt. Similarly, patients with a variety of degenerative spinal pathologies, including vertebral fracture, spondylolisthesis, lumbar spinal canal stenosis, disc pathology, sciatica, degenerative lumbar scoliosis, and spondylodiscitis, maintain their center of mass in a tight range similar to that of healthy controls [13]. Therefore, it seems unlikely that a fully uncompensated increase in thoracic kyphosis, like that modeled in the current study, would actually occur. Rather, it seems that individuals will always attempt some form of compensation, with the degree and effectiveness of that compensation depending on the severity of the thoracic kyphosis deformity and characteristics of the individual. For instance, individuals with a larger pelvic incidence appear better able to compensate for thoracic kyphosis deformities and sagittal imbalance because they can tilt their pelvis back more than individuals with a smaller pelvic incidence [11]. Understanding the factors that affect one's ability to make postural adjustments is an area that needs further investigation.

The current study examined the effect of spinal curvature and posture on the net compressive load carried by each vertebral body, but did not look at how these factors might affect the spatial distribution of loading on the vertebral body. This was beyond the capability of the current musculoskeletal model, but is an important topic for future investigations. For instance, a majority of vertebral fractures are classified as anterior wedge compression fractures, meaning that the anterior portion of the vertebral body has been reduced in height significantly compared to the posterior and middle sections. It is important to understand what role posture and spinal curvature might play in changing the patterns of stresses and strains within the vertebral body. For instance, compared to flexed postures, upright and extended postures result in increased load transfer through the facet joints [37, 38]. Further, the

presence of intervertebral disc degeneration dramatically increases load transfer through the facets and stress-shields the anterior vertebral body [39, 40]. This may cause a reduction in BMD in the anterior vertebral body, predisposing to anterior wedge fractures during forward flexion [39, 40]. It is essential for future studies to investigate how thoracic kyphosis angle and overall sagittal alignment might interact with factors such as intervertebral disc degeneration to affect the distribution of loading throughout the spinal column. For instance, although a particular posture may reduce the total load on the vertebral body, it might concentrate load in some regions and stress-shield others, predisposing to injury despite the fact that the total load has been decreased.

A limitation of this study was that it only investigated one possible compensation strategy, namely coordinated changes in spinal curvature, whereas there are many other compensation strategies, and combinations of strategies, that an individual could employ to counter an anterior shift in body mass [11]. Further research is required to understand how effective these various strategies are at restoring postural stability and mitigating increases in spinal loading. Another limitation was that our baseline spinal geometry for the model was derived from average values found in the literature, and we increased the thoracic kyphosis angle by uniformly adding to this curvature. However, spinal geometry is highly variable and two individuals with the same thoracic kyphosis angle can have spines that are shaped very differently [41, 42]. Future studies should investigate the role of posture and thoracic kyphosis angle on spinal loading within the context of population variability. Finally, loading was only examined in two sagittally symmetric, static activities. Future studies should examine how thoracic kyphosis affects spinal compressive loading for a variety of static and dynamic activities, including those that are not sagittally symmetric.

In conclusion, there is evidence linking hyperkyphosis of the thoracic spine to vertebral fractures and other spinal degenerative diseases. It is thought that excessively stooped posture increases the forces applied to various spinal tissues to a level capable of causing pathology and degeneration. However, we suggest that the current theory ascribing increased spinal loading to greater amounts of thoracic kyphosis is overly simplistic as it does not take into account other postural adjustments that accompany age-related increases in thoracic kyphosis, and

which act to modulate any increases in loading. Our results indicate that in addition to measuring thoracic kyphosis angle, it is also necessary to evaluate overall posture and spino-pelvic alignment when assessing one's risk for degenerative spinal pathology due to altered spine biomechanics, such as vertebral fractures. Further, when treating spinal deformities, clinicians should strive to restore congruent posture because of its positive effects on spinal loading, balance, and eye gaze.

3.6 Acknowledgements

This work was supported by grants from the National Institutes of Health (R01AR053986, R01AR/AG041398, T32AG023480, T32AG023480-07, 1F31AG041629-01), and by the National Heart, Lung, and Blood Institute (NHLBI) Framingham Heart Study (NIH/NHLBI Contract N01-HC-25195). The contents are solely the responsibility of the authors, and do not necessarily represent the views of the NIH.

Authors' roles: Study design: AB, DA, MB. Study conduct: AB, DA, JD, MB. Data collection: AB, DA, JD. Data analysis: AB, DA, MB. Data interpretation: AB, DA, MB. Drafting manuscript: AB. Revising manuscript content: AB, DA, JD, MB. Approving final version of manuscript: AB, DA, JD, MB. All authors take responsibility for the integrity of the data analysis.

3.7 REFERENCES

1. Milne, J.S. and J. Williamson, *A Longitudinal Study of Kyphosis in Older People.* Age and Ageing, 1983. **12**(3): p. 225-233.

2. Goh, S., et al., *The relative influence of vertebral body and intervertebral disc shape on thoracic kyphosis.* Clinical Biomechanics, 1999. **14**(7): p. 439-448.

3. Manns, R.A., et al., *The relative contribution of disc and vertebral morphometry to the angle of kyphosis in asymptomatic subjects.* Clinical Radiology, 1996. **51**(4): p. 258-262.

4. Katzman, W., et al., *Association of spinal muscle composition and prevalence of hyperkyphosis in healthy community-dwelling older men and women.* J Gerontol A Biol Sci Med Sci, 2012. **67**(2): p. 191-5.

5. Mika, A., V.B. Unnithan, and P. Mika, *Differences in Thoracic Kyphosis and in Back Muscle Strength in Women With Bone Loss due to Osteoporosis.* Spine, 2005. **30**(2): p. 241-246.

6. Birnbaum, K., et al., *Correction of kyphotic deformity before and after transection of the anterior longitudinal ligament – a cadaver study.* Archives of Orthopaedic and Trauma Surgery, 2001. **121**(3): p. 142-147.

7. Huang, M.-H., et al., *Hyperkyphotic Posture and Risk of Future Osteoporotic Fractures: The Rancho Bernardo Study.* Journal of Bone and Mineral Research, 2006. **21**(3): p. 419-423.

8. Roux, C., et al., *Prospective assessment of thoracic kyphosis in postmenopausal women with osteoporosis.* J Bone Miner Res, 2010. **25**(2): p. 362-8.

9. Briggs, A., A. Greig, and J. Wark, *The vertebral fracture cascade in osteoporosis: a review of aetiopathogenesis.* Osteoporosis International, 2007. **18**(5): p. 575-584.

10. Briggs, A.M., et al., *Thoracic Kyphosis Affects Spinal Loads and Trunk Muscle Force.* Physical Therapy, 2007. **87**(5): p. 595-607.

11. Roussouly, P. and C. Nnadi, *Sagittal plane deformity: an overview of interpretation and management.* Eur Spine J, 2010. **19**(11): p. 1824-36.

12. Schwab, F., et al., *Gravity Line Analysis in Adult Volunteers: Age-Related Correlation With Spinal Parameters, Pelvic Parameters, and Foot Position.* Spine, 2006. **31**(25): p. E959-E967.

13. Geiger, E., et al., *Adjustment of pelvispinal parameters preserves the constant gravity line position.* International Orthopaedics, 2007. **31**(2): p. 253-258.

14. Lafage, V., et al., *Standing balance and sagittal plane spinal deformity: analysis of spinopelvic and gravity line parameters.* Spine (Phila Pa 1976), 2008. **33**(14): p. 1572-8.

15. Schwab, F., et al., *Sagittal plane considerations and the pelvis in the adult patient.* Spine (Phila Pa 1976), 2009. **34**(17): p. 1828-33.

16. Knight, R., et al., *White Paper on Sagittal Plane Alignment.* Scoliosis Research Society,, 2003. **accessed from SRS.org**.

17. Iyer, S., et al., *A biomechanical model for estimating loads on thoracic and lumbar vertebrae.* Clin Biomech (Bristol, Avon), 2010. **25**(9): p. 853-8.

18. Bean, J.C., D.B. Chaffin, and A.B. Schultz, *Biomechanical model calculation of muscle contraction forces: A double linear programming method.* Journal of Biomechanics, 1988. **21**(1): p. 59-66.

19. Brown, S.H.M. and J.R. Potvin, *Constraining spine stability levels in an optimization model leads to the prediction of trunk muscle cocontraction and improved spine compression force estimates.* Journal of Biomechanics, 2005. **38**(4): p. 745-754.

20. Schultz, A.B. and G.B.J. Andersson, *Analysis of Loads on the Lumbar Spine.* Spine, 1981. **6**(1): p. 76-82.

21. Contini, R., *Body Segment Parameters, Part II.* Artificial Limbs, 1972. **16**(1): p. 1-19.

22. Liu, Y.K., J.M. Laborde, and W.C. Van Buskirk, *Inertial properties of a segmented cadaver trunk: their implications in acceleration injuries.* Aerospace Medicine 1971. **42**(6): p. 650-7.

23. Pearsall, D., J. Reid, and L. Livingston, *Segmental inertial parameters of the human trunk as determined from computed tomography.* Annals of Biomedical Engineering, 1996. **24**(2): p. 198-210.

24. de Leva, P., *Adjustments to Zatsiorsky-Seluyanov's segment inertia parameters.* Journal of Biomechanics, 1996. **29**(9): p. 1223-1230.

25. Winter, D.A., *Biomechanics and Motor Control of Human Movement*. 2009, John Wiley & Sons: Hoboken, NJ.

26. Anderson, D.E., et al., *Regressions for estimating muscle parameters in the thoracic and lumbar trunk for use in musculoskeletal modeling.* Journal of Biomechanics, 2012. **45**: p. 66-75.

27. Narici, M., *Human skeletal muscle architecture studied in vivo by non-invasive imaging techniques: functional significance and applications.* Journal of Electromyography and Kinesiology, 1999. **9**(2): p. 97-103.

28. Bernhardt, M. and K.H. Bridwell, *Segmental Analysis of the Sagittal Plane Alignment of the Normal Thoracic and Lumbar Spines and Thoracolumbar Junction.* Spine, 1989. **14**(7): p. 717-721.

29. Kuntz, C., et al., *Neutral upright sagittal spinal alignment from the occiput to the pelvis in asymptomatic adults: a review and resynthesis of the literature.* Journal of Neurosurgery: Spine, 2007. **6**(2): p. 104-112.

30. Vialle, R., et al., *Radiographic analysis of the sagittal alignment and balance of the spine in asymptomatic subjects.* The Journal of Bone and Joint Surgery, 2005. **87-A**(2): p. 260-7.

31. Ismail, A.A., et al., *Number and Type of Vertebral Deformities: Epidemiological Characteristics and Relation to Back Pain and Height Loss.* Osteoporosis International, 1999. **9**(3): p. 206-213.

32. Melton, L.J., et al., *Prevalence and incidence of vertebral deformities.* Osteoporosis International, 1993. **3**(3): p. 113-119.

33. McDowell, M.A., et al., *Anthropometric Reference Data for Children and Adults: United States, 2003-2006*, C.f.D.C.a.P. US Department of Health and Human Services, National Center for Health Statistics Editor. 2008.

34. Briggs, A., et al., *The effect of osteoporotic vertebral fracture on predicted spinal loads in vivo.* European Spine Journal, 2006. **15**(12): p. 1785-1795.

35. El-Rich, M., A. Shirazi-Adl, and N. Arjmand, *Muscle Activity, Internal Loads, and Stability of the Human Spine in Standing Postures: Combined Model and In Vivo Studies.* Spine, 2004. **29**(23): p. 2633-2642.

36. Keller, T.S., et al., *Influence of spine morphology on intervertebral disc loads and stresses in asymptomatic adults: implications for the ideal spine.* The Spine Journal, 2005. **5**(3): p. 297-309.

37. Adams, M. and W. Hutton, *The effect of posture on the lumbar spine.* J Bone Joint Surg Br, 1985. **67-B**(4): p. 625-629.

38. Adams, M. and W. Hutton, *The effect of posture on the role of the apophysial joints in resisting intervertebral compressive forces.* J Bone Joint Surg Br, 1980. **62-B**(3): p. 358-362.

39. Adams, M.A., et al., *Intervertebral Disc Degeneration Can Predispose to Anterior Vertebral Fractures in the Thoracolumbar Spine.* Journal of Bone and Mineral Research, 2006. **21**(9): p. 1409-1416.

40. Pollintine, P., et al., *Intervertebral Disc Degeneration Can Lead to "Stress-Shielding" of the Anterior Vertebral Body: A Cause of Osteoporotic Vertebral Fracture?* Spine, 2004. **29**(7): p. 774-782 10.1097/01.BRS.0000119401.23006.D2.

41. Gelb, D.E., et al., *An Analysis of Sagittal Spinal Alignment in 100 Asymptomatic Middle and Older Aged Volunteers.* Spine, 1995. **20**(12): p. 1351-1358.

42. Hammerberg, E.M. and K.B. Wood, *Sagittal Profile of the Elderly.* Journal of Spinal Disorders & Techniques, 2003. **16**(1): p. 44-50.

Chapter 4: DEVELOPMENT AND VALIDATION OF A MUSCULOSKELETAL MODEL OF THE FULLY ARTICULATED THORACOLUMBAR SPINE AND RIB CAGE

This chapter was previously published in the Journal of Biomechanical Engineering:

> Bruno, A.G., M.L. Bouxsein, and D.E. Anderson, *Development and validation of a musculoskeletal model of the fully articulated thoracolumbar spine and rib cage*. Journal of Biomechanical Engineering, Accepted for publication March 24, 2015.

4.1 Abstract

Numerous musculoskeletal models have been developed to study the extremities, lumbar spine, and cervical spine, but modeling of the thorax remains limited. Thus we developed and validated a fully articulated model of the thoracolumbar spine in OpenSim that includes the individual vertebrae, ribs, and sternum. The model builds on published models of the lumbar spine, neck, and shoulder, adding thoracic anatomy and musculature to produce an integrated model of the thoracolumbar spine. To ensure trunk muscles in the model accurately represent muscles *in vivo*, we used a novel approach to adjust the cross-sectional area and position of the trunk muscles based on muscle measurements in CT scans of the trunk sampled from a community-based cohort. For a variety of sagittally symmetric and asymmetric activities, model predictions of vertebral compressive loading and trunk muscle tension were highly correlated to previous *in vivo* measures of intradiscal pressure ($r = 0.91$ for lumbar levels and $r = 0.87$ for the thoracic levels), vertebral loading from telemeterized implants ($r = 0.88$ at L1), and trunk muscle myoelectric activity recorded by EMG ($r = 0.98$ at L3, $r = 0.91$ at L1-L5, and $r = 0.98$ at T4). In conclusion, a novel thoracolumbar spine model was created that accurately predicts vertebral compressive loading and trunk muscle tension. This model will enable future studies aimed at understanding thorax and spine biomechanics, as well as conditions such as vertebral fracture, kyphosis, scoliosis, and back pain.

4.2 Introduction

Musculoskeletal models of the human body are now widely used to gain insight into normal human movement, pathologic conditions, and the effects of surgical or rehabilitative treatments [1]. These models allow the determination of the forces on muscles, bones, and joints that are generally not measurable *in vivo*. However, whereas the extremities, cervical spine, and lumbar spine have been the subjects of significant musculoskeletal modeling efforts, the thorax has not. Prior musculoskeletal models have incorporated the thorax as a single rigid segment [2], have neglected the mechanical contribution of the ribs and sternum [2-5], or have lacked an anatomically realistic model of the rib cage [6], making them unsuitable for predicting thoracic skeletal and muscular loading. A few prior models included an articulated thoracic

spine, but not the rib cage or the detailed thoracic musculature [3, 5, 7-9]. In addition, these prior models were not validated against *in vivo* measures of spine and trunk muscle loading, and were only used to assess vertebral loading during a neutral standing posture. Other computational models of the thorax have utilized finite element analysis, focusing on thorax deformation and predicting injury tolerances in motor vehicle accidents [10]. However, these models do not include muscular anatomy and therefore are also not suitable for studying the *in vivo* thoracic skeletal loads that occur during normal daily activities. A detailed, fully articulated, musculoskeletal model of the thoracolumbar spine and rib cage would allow prediction of the *in vivo* skeletal and muscular loads that occur in the thorax during different activities and facilitate investigations into the biomechanical mechanisms underlying, and potential treatments for, multiple thoracic diseases and conditions, including vertebral fractures, hyperkyphosis, scoliosis, respiratory insufficiency, and back pain.

Musculoskeletal models typically rely on detailed cadaver dissections or anatomical descriptions to determine muscle position and architectural parameters [2, 11-13]. Although this type of data is necessary for creating detailed models that account for a muscle group's individual fascicles and many attachments, the resulting models are generic and reflect input parameters from a small and potentially heterogeneous sample. Further, muscle areas and positions derived from cadavers may not be representative of muscle anatomy *in vivo*, due to the effects of preserving medium and dehydration [14]. Muscle anatomy assessed *in vivo* using medical imaging such as computed tomography (CT) or magnetic resonance imaging (MRI) could be used in combination with detailed cadaver studies to create musculoskeletal models that are more physiologically relevant. Further, the use of clinical imaging data could allow construction of models that are tailored to specific populations or individuals depending on the research or clinical objective.

Therefore, the objectives of this study were to develop and validate an anatomically detailed musculoskeletal model of the spine, including the lumbar and thoracic vertebrae, ribs, and sternum, that accurately predicts lumbar and thoracic vertebral loading during different activities. In developing the model, we employed a novel approach that used CT scans of the trunk from subjects sampled from a community-based cohort to adjust the cross-sectional area

(CSA) and position of the trunk muscles in the model. To validate the accuracy of the model, we compared vertebral loading and trunk muscle tension predicted by the model to previously collected *in vivo* measurements of intradiscal pressure (IDP), vertebral compression from telemeterized implants, and trunk muscle myoelectric activity from electromyography (EMG).

4.3 METHODS

4.3.1 DEFINITION OF SKELETAL ANATOMY AND JOINTS IN THE MODEL

We created a model of the full thoracolumbar spine and rib cage using OpenSim musculoskeletal modeling software [1]. The skeletal anatomy was based on CT scans of a 25 year old male (obtained from the OpenSim geometry file library), 50th percentile for height and weight (height = 175 cm, weight = 78 kg). The positions and orientations of the vertebral bodies, defining the curvature of the spine, were based on average measurements available in the literature with thoracic kyphosis (T1-T12 Cobb angle) set to 50° and lumbar lordosis (L1-L5 Cobb angle) set to -43° [15, 16]. The size and shape of the ribs and sternum were based on published morphometric equations that describe the position of three to five major landmarks on each rib [17]. Cubic splines were fit to these landmarks to model the shape of each individual rib. Point to point actuators were placed between the ends of the ribs and the sternum (ribs 1 through 7) or between the ends of adjacent ribs (ribs 8 through 10) to represent forces transmitted by costal cartilage. The actuators generate a compressive or tensile force along their length, and these forces are determined as part of the same static optimization routine that computes muscle forces in the model (described later). The optimal force of these actuators was set to a high value (1000 N) so that optimization would favor loading of the actuators over the muscles, allowing the costal cartilage to supply as much supporting force as possible to the ends of the ribs. The value of 1000 N for the costal cartilage actuators was chosen based on the results of a sensitivity analysis (described in section 2.4).

The arms, head, and neck were incorporated from other previously published and freely available OpenSim models (Vasavada neck model [13] and Stanford VA Upper Extremity model [18]). The upper extremity model includes shoulder, elbow, wrist, and radioulnar joints, allowing us to simulate physiologic movement of the upper extremities during different

activities, such as lifting and carrying objects. The head and neck were adapted into a single lumped body connected to T1 via a ball joint (3 rotational degrees of freedom). The intervertebral joints (L5/S1 to T1/T2) were modeled as ball joints with a center of rotation placed at the geometric center of the intervertebral disc, allowing for segmental movement of the thoracic and lumbar spine in three dimensions. The hip joint, connecting the pelvis to the ground, was modeled as a pin joint (1 rotational degree of freedom) allowing for anterior and posterior tilting of the pelvis.

For each type of trunk movement (flexion/extension, lateral bending, and axial rotation), prior studies were used to determine the percentage of total motion that occurs at the pelvis and the individual lumbar and thoracic intervertebral joints. For trunk flexion/extension, the ratio of lumbar flexion to pelvic flexion (lumbopelvic ratio) was computed as a function of total trunk flexion, ranging from approximately 2.5 at the beginning of trunk flexion to 1.0 at end range of motion (Supplemental Table 4.1) [19]. The lumbar and thoracic regions were set to contribute approximately equally to the spine component of trunk flexion (51% lumbar and 49% thoracic) [20, 21]. For lateral bending, the lumbar and thoracic spines were set to contribute 27% and 73% of total trunk movement, respectively [20, 22, 23]. For axial rotation, the lumbar and thoracic spines were set to contribute 17% and 83% of total trunk movement, respectively [24, 25]. The distribution of movement at each intervertebral joint is presented in Supplemental Table 4.2.

The costovertebral joints connecting the ribs to the thoracic vertebrae (T1 through T12 on the left and right sides) were modeled as pin joints [26, 27], allowing for the physiologic motion of the ribs during ventilation [28] and the proper transmission of forces between ribs and the thoracic spine during activities. Each rib rotates about its own cervical axis, which is a vector pointing between the costovertebral and costotransverse joints [26, 27]. The positions of these joints on the thoracic vertebral bodies were estimated using data from Schultz and colleagues [29, 30], and used to set the positions and orientations of the costovertebral joints in the model (Supplemental Table 4.3).

The mass and center of mass positions of body segments in the model were based on published anthropometric ratios [31-33]. The mass of the trunk was partitioned among the

vertebral bodies and sacrum, with the mass of each trunk slice and its anterior offset relative to the vertebral body determined from prior cadaver studies [31-33]. The lumped head and neck body was assigned a single mass [31]. The ribs, sternum, clavicles, and scapulae were each assigned an arbitrarily low mass of 0.0001 kg. The mass properties of the humeri, radii, ulnae, and hands from the Stanford VA Upper Extremity model [18] were maintained, since these corresponded to a 50^{th} percentile 25 year old male.

4.3.2 Model muscle anatomy

Muscles that attach to the spine and thorax were incorporated from previously published OpenSim models (Fig. 4.1 and Table 4.1) [2, 13, 18]. As opposed to attaching to a single rigid thorax body, these muscles were edited to attach to the individual thoracic vertebral bodies, ribs, clavicles, scapulae, and sternum. The major lumbar spine and abdominal muscle groups were incorporated from the Christophy lumbar spine model [2, 34], and muscles attaching to the upper and mid-thorax were adapted from the Vasavada cervical spine model [13] and the Stanford VA upper extremity model [18]. Additional muscle groups were then added, including the external and internal intercostals, the thoracic multifidus, the lower portion of the trapezius, the serratus anterior [35, 36], and the transversus abdominis [37]. Each muscle group is represented by multiple fascicles crossing one or more joints, and each fascicle is represented by a Hill-Type model that modulates force generating potential due to changes in muscle fiber length and velocity [38]. Muscle architectural parameters (physiological cross-sectional area, pennation angle, optimal fiber length, and tendon slack length) for muscles incorporated from previous OpenSim models, as well as for the muscles we added, were based on prior literature studies or estimated (Supplemental Table 4.4 lists all muscle architectural parameters used in the model, including their source and how they were calculated or estimated). The maximum isometric force a muscle can generate is equal to its physiologic cross-sectional area (PCSA) multiplied by a constant maximum muscle stress (MMS) [14]. We used a MMS of 100 N/cm^2 for all muscles except the shoulder muscle groups, which were set to 140 N/cm^2 [18]. We performed a sensitivity study to justify our selection of MMS, described in section 2.4.

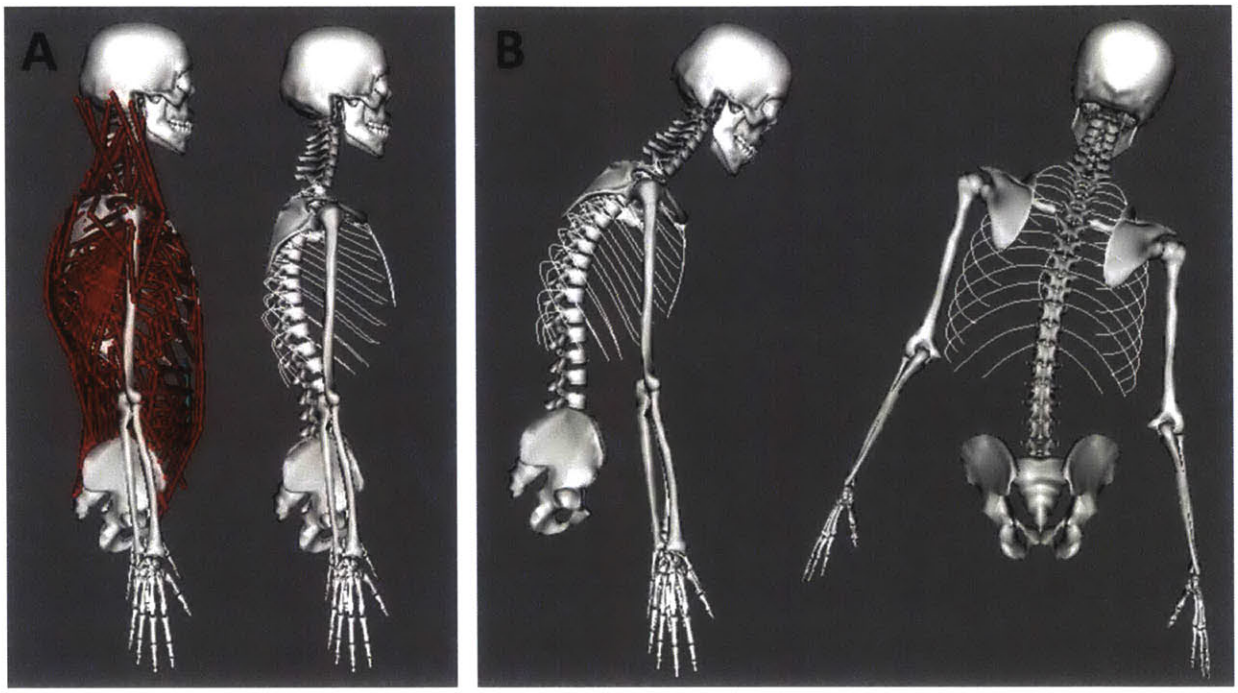

Figure 4.1: a) Image of the new musculoskeletal spine model shown with and without muscles. b) The model can simulate sagittally symmetric and asymmetric activities. Here, the model is simulating 30° trunk flexion and 20° trunk lateral bending to the right.

Table 4.1: Muscle groups incorporated into the model. Muscle fascicles from previously published OpenSim models attached to a single rigid thorax, so these muscles were updated to attach to individual thoracic vertebral bodies, ribs, and the sternum in the new model.

Source	Muscle groups included in model
OpenSim Lumbar Spine Model [2]	Lumbar and thoracic erector spinae, lumbar multifidus, psoas major, quadratus lumborum, latissimus dorsi, external and internal obliques, rectus abdominis
OpenSim Cervical Spine Model [13]	Cervical erector spinae, cervical multifidus, sternocleidomastoid, scalenes, longus colli, splenius, semispinalis, levator scapulae, superior trapezius
OpenSim Upper Extremity Model [18]	Deltoid, supraspinatus, infraspinatus, subscapularis, teres minor, teres major, pectoralis major, coracobrachialis
Added in current study	Internal and external intercostals, serratus anterior, inferior trapezius, thoracic multifidus, transversus abdominis

Because more precise data were lacking, the PCSA of the external and internal intercostals were estimated using rib lengths (approximately between the rib tubercles posteriorly and the ends of the bony ribs anteriorly) multiplied by 5 mm, the estimated thickness of the external and internal intercostal muscle sheets together (2.5 mm thickness for

each sheet). The external intercostals were set to form angles of approximately 40° relative to the superior ribs and the internal intercostals were set to form angles of approximately 120° relative to the inferior ribs [39, 40]. Optimal fiber lengths were computed as the distance between attachment points on adjacent ribs, and pennation angles and tendon slack lengths were assumed to be 0° and 0.1 mm, respectively. Muscle architectural parameters for the thoracic multifidus and the lower trapezius were estimated from the cervical [13] and lumbar multifidus [2] and the upper trapezius, respectively [12, 13].

4.3.3 Adjustment of muscle CSA and position using in vivo CT measurements

The cross-sectional area (CSA) and position of the muscles in this and other models are derived from multiple sources, mostly consisting of dissection studies using a small, heterogeneous group of cadavers [2, 11-13]. Thus, to ensure physiologic size and position we used previously collected CT-based measurements of trunk muscle CSA and position performed in a sample of participants from the community-based Framingham Heart Study Offspring and Third Generation Multidetector CT Study [41] to adjust muscle CSA and position in the model. Specifically, we previously measured the CSA and position (medial-lateral and anterior-posterior moment arms with respect to the vertebra) of several major trunk muscle groups (rectus abdominis, latissimus dorsi, trapezius, external oblique, internal oblique, erector spinae, mutlifidus, psoas major, quadratus lumborum, serratus anterior, and pectoralis major) in 51 men (mean age = 59.4, Ht = 177.6 cm , Wt = 86.3 kg) [42]. Measurements were made at the mid-plane of each vertebral body between T6 and L5. In our spine model, each muscle group consists of multiple fascicles. To facilitate the comparison and then adjustment of our model to the CT cohort data, we calculated an equivalent muscle group CSA and position at each vertebral mid-plane in the model (Fig. 4.2). To do so, for each muscle group at each vertebral mid-plane in the model, we summed the CSAs of the individual fascicles crossing the vertebral mid-plane to compute an equivalent muscle group CSA at that level. Similarly, we computed the centroid of the fascicles crossing the vertebral mid-plane to find the anterior-posterior (AP) and medial-lateral (ML) moment arms of the muscle group relative to the vertebral centroid.

Figure 4.2 illustrates this process by showing how trapezius group CSA and position at T9 were calculated from the model.

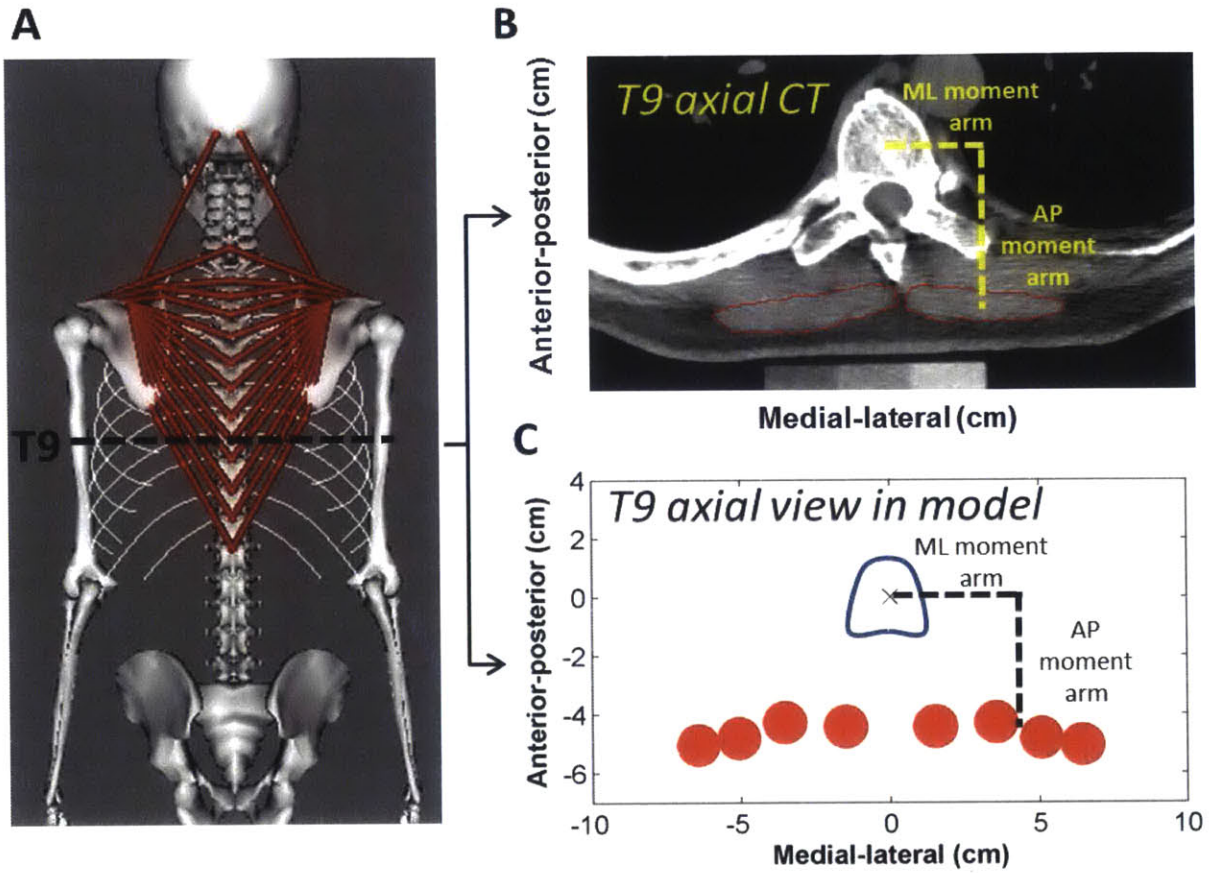

Figure 4.2: Method for calculating muscle group CSA and moment arm in the model at different transverse planes, facilitating comparisons to muscle group CSA and moment arm made on axial CT images. The example above shows the calculation of trapezius CSA and moment arm at the T9 mid-vertebral plane in the model (a), which we would like to compare to measurements of trapezius CSA and moment arm made on axial CT at the T9 mid-plane (b). The four trapezius fascicles in the model that cross the T9 mid-plane are schematically shown in (c), where they are plotted relative to the T9 vertebral body centroid. The size of the circles is equal to the CSA of the individual fascicles, and these areas are summed to get trapezius CSA at T9. The centroid of the fascicles is then calculated and used to find the medial-lateral and anterior-posterior moment arms of the muscle group relative to the vertebral centroid.

We adjusted the CSA of nine muscle groups (rectus abdominis, latissimus dorsi, trapezius, external oblique, internal oblique, erector spinae, mutlifidus, psoas major, and quadratus lumborum) between T6 and L5 in the model to match the average CSA measurements from men in our CT cohort (Table 4.2). We were unable to adjust CSA of the serratus anterior and the pectoralis major because these fascicles were primarily oriented parallel to the transverse plane in the model, whereas our muscle measurements were made

within the transverse plane. We then adjusted the AP and ML moment arms of erector spinae, multifidus, rectus abdominis, and trapezius to match the average male AP and ML moment arm measurements from our CT cohort. The moment arms of the other muscle groups in the model were generally within two standard deviations of the measured moment arms, and therefore did not require adjustment.

Table 4.2: Root mean square error (RMSE) values for the pre-adjusted and adjusted models versus the cohort CT measurements of muscle morphology. CSA was scaled for all nine muscle groups, but anterior-posterior (AP) moment arms and medial-lateral (ML) moment arms were only scaled for rectus abdominis, trapezius, erector spinae, and multifidus. The adjusted model has lower RMSE values for the scaled muscle parameters.

	CSA RMSE (cm^2)		**AP moment arm RMSE (cm)**		**ML moment arm RMSE (cm)**	
	Pre-adjusted Model	Adjusted Model	Pre-adjusted Model	Adjusted Model	Pre-adjusted Model	Adjusted Model
Rectus Abdominis	1.24	0.80	1.07	0.32	2.33	0.42
Latissimus Dorsi	1.77	1.67	1.28	1.25	2.18	2.18
Trapezius	3.11	0.68	1.41	0.43	1.27	0.47
External Oblique	4.38	1.43	1.33	1.59	5.53	5.26
Internal Oblique	1.99	1.17	2.31	2.32	2.34	2.37
Erector Spinae	5.99	2.10	1.92	0.36	1.82	0.34
Multifidus	1.86	0.40	1.11	0.34	0.74	0.21
Psoas Major	2.60	1.37	0.52	0.54	0.73	0.72
Quadratus Lumborum	2.97	0.83	0.55	0.54	1.40	1.38

To adjust the CSA of a muscle group in the model, we multiplied fascicle CSA by the ratio of measured muscle group CSA to model muscle group CSA at each vertebral level where the muscle was present, and then averaged across vertebral levels to compute an adjusted fascicle CSA. The following equation describes the adjustment process for each muscle fascicle in a muscle group:

$$CSA_{adjusted\_fas} = \frac{1}{L}\left(\sum_{i=1}^{L} CSA_{model\_fas,i}\frac{CSA_{measured\_gr,i}}{CSA_{model\_gr,i}}\right) \quad Eq.1 \qquad (1)$$

where $CSA_{measured\_gr}$ is the average CSA of the equivalent muscle group from CT measurements, CSA_{model_gr} is the pre-adjusted CSA of the muscle group in the model, CSA_{model_fas} is the pre-adjusted CSA of the fascicle, $CSA_{adjusted\_fas}$ is the adjusted fascicle CSA, and L is the vertebral

levels where the muscle was measured. The adjusted CSAs of the fascicles were then used to calculate adjusted equivalent muscle group areas in the model, following the same method outlined in Figure 4.2.

To adjust the AP and ML moment arms of a muscle group, we calculated the difference between CT-measured and model equivalent AP and ML moment arms at each vertebral level where the muscle was measured, and used linear interpolation to estimate this difference in the regions between measurements. The attachment points of individual fascicles were then automatically moved this amount within the transverse plane to reduce the difference between the model and the measured data. To evaluate the effectiveness of our CSA and moment arm adjustments, we computed root mean square errors (RMSE) for both the pre-adjusted and the adjusted models versus the measured cohort CT data.

4.3.4 Sensitivity studies

We performed four analyses to assess the sensitivity of our model to key assumptions. First, we characterized the effect of maximum muscle stress (MMS) on vertebral compressive loading. A wide range of values (approximately 20 to 140 N/cm^2) has been reported in the literature for MMS [18, 43]. A value of 46 N/cm^2 is often used in spine models for muscles of the trunk [11], derived by computing the MMS that would allow the extension strength of a lumbar spine model to best match average L5-level trunk extensor moments measured in a different study. Given the uncertainty in this parameter, we varied MMS between 20 and 140 N/cm^2 (in increments of 10). Another source of uncertainty is the PCSA of the internal and external intercostals, so we varied this parameter from 25% to 175% (in increments of 25%) of its baseline value. In another analysis, we tested the sensitivity of our model's vertebral compressive loading predictions to the optimal force of the costal cartilage actuators, which we varied from 0 N (equivalent to no actuators present) to 1000 N in 100 N increments (results are reported in Supplemental Fig. 4.1). Finally, we tested the sensitivity of our model's vertebral compressive loading predictions to the locations of the intervertebral joints. The instantaneous axes of rotation (IAR) of the intervertebral joints vary substantially between individuals, vertebral levels, and with disc health, and for simplicity we located the IAR at the geometric

center of each disc. To assess the impact of this assumption on vertebral compressive loading predictions, we compared loading estimates from our baseline model to those from a model in which the lumbar intervertebral joints were shifted posterior and inferior to match the IARs reported by Pearcy and colleagues (results are reported in Supplemental Fig. 4.2) [44].

4.3.5 *Validation of vertebral compressive loading and muscle force predictions*

To evaluate the accuracy of vertebral loading and muscle force predictions from the model, we simulated a variety of activities for which prior studies have acquired *in vivo* measures of intradiscal pressure (IDP), vertebral implant loads, or myoelectric activity of trunk muscles. A list of these validation studies with the activities they investigated, the characteristics of the study participants, and the primary measurements made is found in Table 4.3 [45-51].

Table 4.3: Studies used for validation of the model. For each study, the average age, height, and weight of the study participants was used to scale the model size, mass, and muscle CSA and moment arms, and the model was then used to simulate the listed isometric activities. Measured intradiscal pressure (IDP), vertebral implant loads, and trunk muscle myoelectric activity (EMG) were compared to vertebral loading and trunk muscle tension predicted by the model. For studies with N>1, we list the mean body mass and height, and the range of ages for the study subjects. BM = body mass and HT = height.

Study	Subjects	Subject Characteristics	Measures	Activities
Andersson et al. 1977 [45]	3F 1M	BM = 61 kg HT = 173 cm Ages 26-34	L3/L4 IDP T4 EMG	10 to 50° lumbar flexion, 10.2 kg each hand
Polga et al. 2004 [46]	4 M 2 W	BM = 73 kg HT = 178 cm Ages = 19-47	T6-T7 or T7-T8 IDP T9-T10 or T10-T11 IDP	Standing Standing, 10-kg in each hand at the side Standing, 10-kg in each hand, elbows 90° 30° trunk flexion 30° trunk flexion, 10-kg in each hand 15° trunk extension 30° axial rotation to the left 20° lateral bend to the right
Rohlmann et al. 2008 [51]	2 M	BM = 70 kg HT = 169 cm	L1 Implant load	Standing 30° trunk flexion

		Ages = 62-71		15° trunk extension 30° axial rotation to the left 20° lateral bend to the right Elevate right arm 90° Elevate arms 90° Abduct arms 90°
Sato et al. 1999 [47]	8 M	BM = 73 kg HT = 174 cm Ages = 22-29	L4/L5 IDP	Standing 30° trunk flexion 15° trunk extension
Schultz et al. 1982 [48]	3 W 1 M	BM = 63 kg HT = 174 cm Ages = 19-23	L3/L4 IDP L1-L5 EMG	Standing Standing, arms in, holding 8 kg Standing, arms out Standing, arms out, holding 8 kg 30° trunk flexion, arms out 30° trunk flexion, arms out, holding 8kg
Takahashi et al. 2006 [49]	3 M	BM = 72 kg HT = 176 cm Ages = 24-26	L4/L5 IDP L3 EMG	Standing Standing, 5 kg in each hand at the side 10° trunk flexion 10° trunk flexion, 5 kg in each hand 20° trunk flexion 20° trunk flexion, 5 kg in each hand 30° trunk flexion 30° trunk flexion, 5 kg in each hand
Wilke et al. 2001 [50]	1 M	BM = 72 kg HT = 174 cm Age = 45	L4/L5 IDP	Standing Standing, 20-kg in left hand at the side Standing, 20-kg in each hand at the side 30° trunk flexion 30° trunk flexion, 10-kg in each hand 90° trunk flexion 15° trunk extension 30° axial rotation to the left 20° lateral bend to the right

For each validation study we created a version of our spine model that was scaled to the average height and weight of the study participants, and we estimated muscle group CSA and AP and ML moment arms from previously published regressions [42] using the average age, sex,

height, and weight of the study participants. We then adjusted the CSA and moment arms in the model to match the CSA and moment arms predicted by regression using our muscle adjustment algorithm (section 2.3). These spine models were used to simulate the static, isometric activities performed in the validation studies so that the model predictions could be correlated with the measured data. For each activity, muscle forces that satisfy static equilibrium were computed using an optimization routine that minimizes the sum of cubed muscle activations, which is equivalent to maximizing muscle endurance [52, 53].

To compare vertebral compressive loads predicted by the model to measured IDP, we converted vertebral compressive loading from the model to an estimated IDP using vertebral body cross-sectional area and a previously published correction factor:

$$IDP_{model} = \frac{F_C}{CSA_{Vert} x\ 0.66} \quad Eq.2 \qquad (2)$$

where F_C is the compressive load in the axial direction of the vertebral body predicted by our model, CSA_{Vert} is the cross-sectional area of the vertebral body, and 0.66 is a correction factor for translating between IDP and compressive loading [54-56]. Although the correction factor has only been computed for lumbar intervertebral discs, we also used this same correction factor to estimate IDP in the thoracic spine, because no study that we are aware of has determined a thoracic-specific correction factor. CSA_{Vert} was measured in three of the studies reporting lumbar IDP [47, 49, 50], and a value of 18 cm^2, reported by Wilke and colleagues [50], was used for the lumbar IDP studies that did not measure CSA_{Vert} [45, 48]. For thoracic levels, we measured CSA_{Vert} in our own CT scans of subjects that closely matched the study participants in sex, age, height, and weight.

Vertebral loads recorded from telemeterized vertebral body implants were reported as a percentage of neutral standing load [51], so vertebral loads predicted by the model were also presented this way for comparison.

Measured myoelectric activity for the erector spinae was correlated with erector spinae tension predicted by the model. The tensions of the erector spinae fascicles closest to the reported electrode locations were summed for comparisons to these validation studies. For instance, Andersson and colleagues [45] measured myoelectric activity to the left and right of

T4, so only the erector spinae fascicles crossing the T4 vertebral level were included in the comparison.

4.4 RESULTS

4.4.1 ADJUSTMENT OF MUSCLE CSA AND POSITION

The adjustment process significantly reduced the difference between muscle CSA and moment arm measured in our CT cohort and muscle CSA and moment arm in our adjusted model, as assessed by root mean square error (Table 4.2). For example, the CSA and AP and ML moment arms of the erector spinae group in the model were generally adjusted to be within one standard deviation of the measured data (Fig. 4.3).

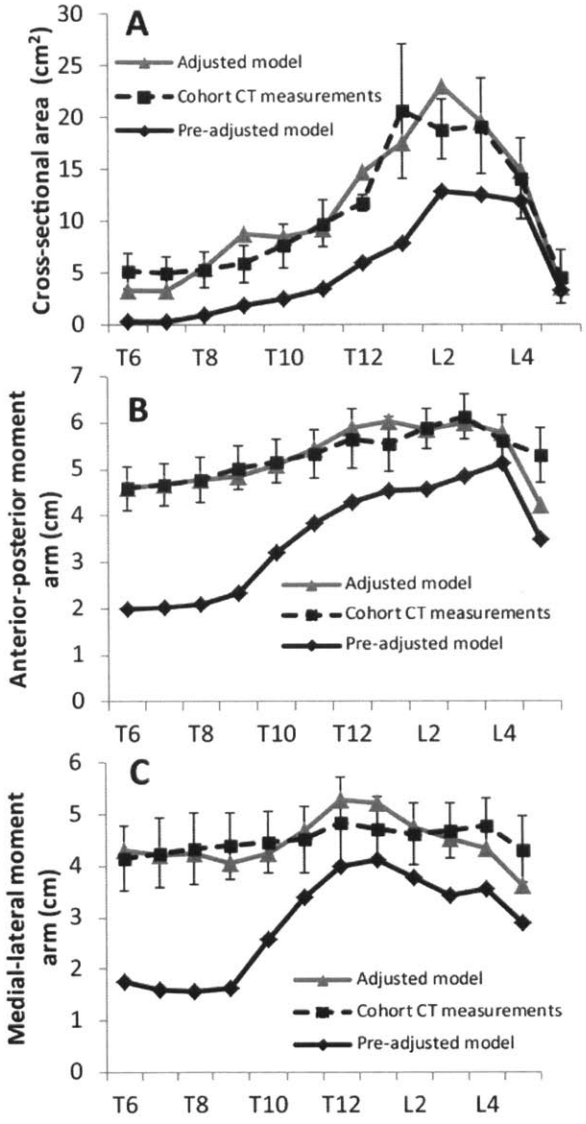

Figure 4.3: Muscle anatomy for the baseline model (pre-adjusted model) was derived from prior cadaver studies and anatomical descriptions. We generated a new model with muscle group CSA and position scaled to match average in vivo values of muscle CSA and position that were measured on CT scans in a sample of older males (cohort CT measurements) at the vertebral mid-slices of T6 through L5 for several major muscle groups. a) through c) shows the improvement in CSA, anterior-posterior moment arm, and medial-lateral moment arm for the erector spinae muscle group in the adjusted versus pre-adjusted model. The error bars are ±1 standard deviations of the measured data.

4.4.2 Sensitivity studies

We found that the model was unable to satisfy equilibrium even for low intensity activities, such as 30° trunk flexion and 20° trunk lateral bending, for MMS values below 40 N/cm^2. For higher intensity activities, such as 30° trunk flexion with 10 kg weights in each hand and upright standing while holding 10 kg weights in each hand and elbows flexed 90°, the

model was unable to satisfy equilibrium for MMS values below 60 N/cm^2. To ensure that our model muscle strength was strong enough to satisfy equilibrium for all of the activities in the validation studies, we chose to set MMS at 100 N/cm^2, which is at the higher end of the range of measured values [43]. For the shoulder muscle groups, we retained the value of 140 N/cm^2 used by Holzbaur and colleagues [18]. For values of MMS for which the model was able to satisfy equilibrium, there were very small differences in vertebral loading for increasing values of MMS. For instance, the differences in vertebral compressive loading for MMS values between 60 N/cm^2 and 100 N/cm^2 were less than 1.5% for vertebral levels below T7, less than 6% for levels T3 through T7, and less than 13% at T1 and T2.

Varying the PCSA of the intercostals had a minimal effect on vertebral compressive loading in the lumbar spine, but a larger effect in the thoracic spine. For 30° trunk flexion, using 25% of the baseline PCSA caused vertebral loading to increase by 2 to 7% for vertebrae in the upper thoracic spine, and decrease by up to 5% for vertebrae in the mid- to lower thoracic spine. Using 175% of the baseline PCSA caused vertebral loading to decrease by 2 to 10% for vertebrae in the upper thoracic spine and increase by up to 4% for vertebrae in the mid- to lower thoracic spine. For upright standing while holding 10 kg weights in each hand and elbows flexed 90°, using 25% of the baseline PCSA caused vertebral loading to increase by up to 39% between T1 and T12, and using 175% of the baseline PCSA caused vertebral loading to decrease by 1 to 18% between T1 and T12.

4.4.3 VALIDATION STUDIES

Vertebral compressive loading estimates from the lumbar and thoracic regions of the model were strongly correlated to previously reported IDP measurements for a variety of sagittally symmetric and asymmetric activities ($r = 0.91$ for lumbar and $r = 0.87$ for thoracic loading, Fig. 4.4). The slopes and intercepts of the linear trend lines relating measured IDP to model IDP were not significantly different than one and zero, respectively (95% confidence intervals for the slopes were 0.767 to 1.096 for lumbar loading and 0.989 to 1.966 for thoracic loading, and 95% confidence intervals for the intercepts were -0.205 to 0.147 for lumbar loading and -1.178 to 0.178 for thoracic loading). However, the model slightly under predicted

the magnitude of lumbar loading and over predicted the magnitude of thoracic loading for certain activities. L1 vertebral compressive loading predicted by the model was highly correlated with the loads recorded from telemeterized L1 vertebral body implants from two patients for a variety of activities (r = 0.88, Fig. 4.5), except for extension in which the model predictions of compressive load exceeded the recorded measurements. The slope and intercept of the linear trend line were not significantly different than one and zero, respectively (95% confidence interval for the slope was 0.302 to 1.044 and 95% confidence interval for the intercept was -4.312 to 101.634).

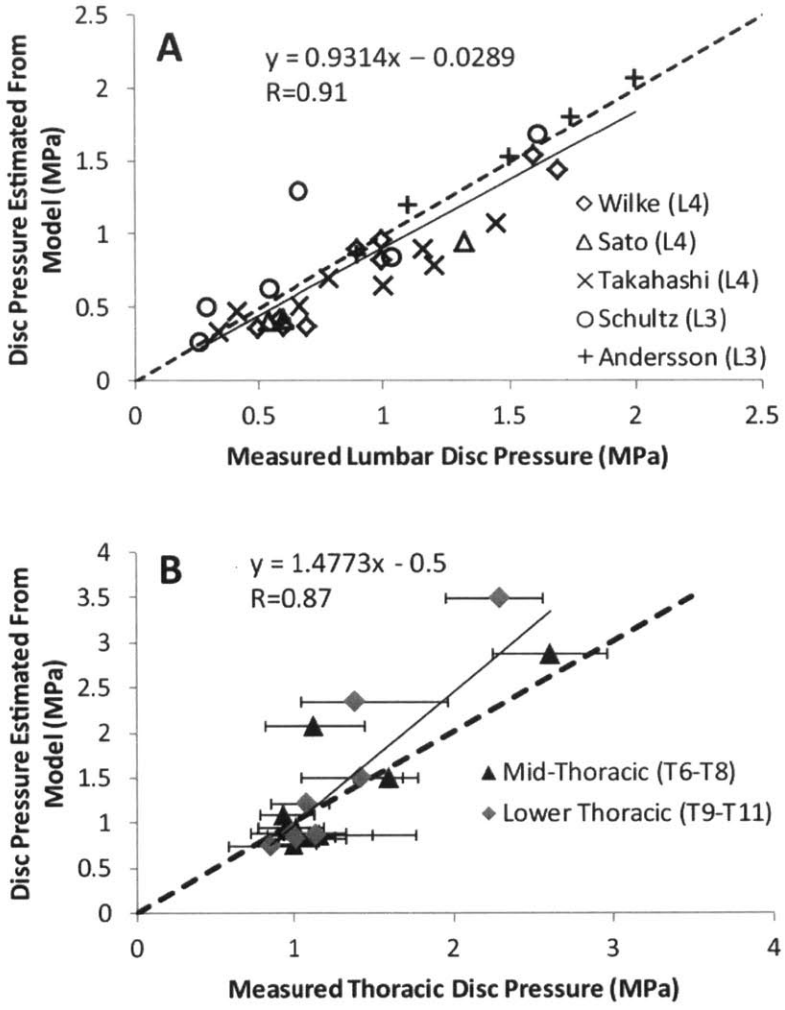

Figure 4.4: The model was used to simulate activities for which IDP measurements have been previously reported. Vertebral compressive force predicted by the model was converted to an estimated IDP using vertebral area and a correction factor of 0.66. IDP estimated by the model was correlated with IDP measurements made in the lumbar (a) and thoracic spine (b). The error bars in (b) are the range of IDP reported by Polga and colleagues [46]. The dashed lines represent unity.

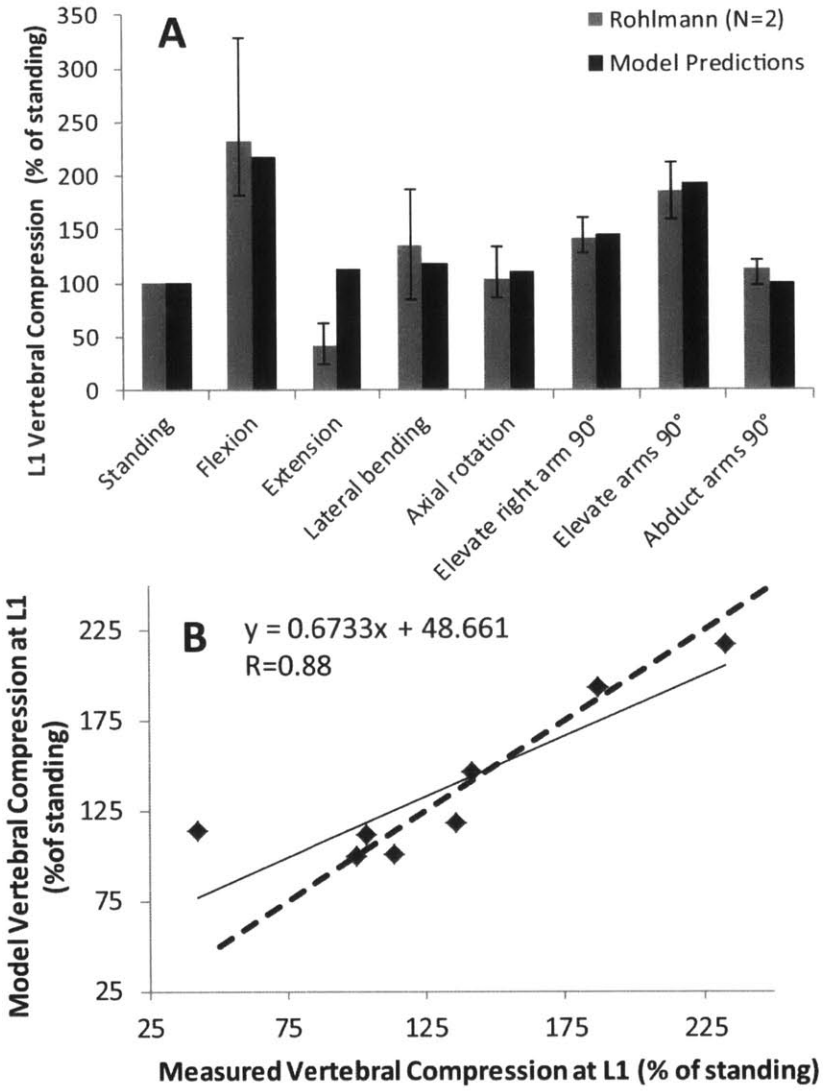

Figure 4.5: The model was used to simulate the activities reported in Rohlmann and colleagues [51], for which vertebral loading at L1 was recorded from telemeterized vertebral implants in two individuals. a) Vertebral loading is expressed as a percentage of standing load. Error bars are the range of data reported in the study. b) The correlation between measured and model predicted loading is shown.

Finally, erector spinae muscle tension predicted by the model was highly correlated with measured myoelectric activity in both the lumbar and thoracic regions of the spine, with correlation coefficients of r = 0.98, r = 0.98 and r = 0.91 at T4, L3 and L1-L5, respectively (Fig. 4.6).

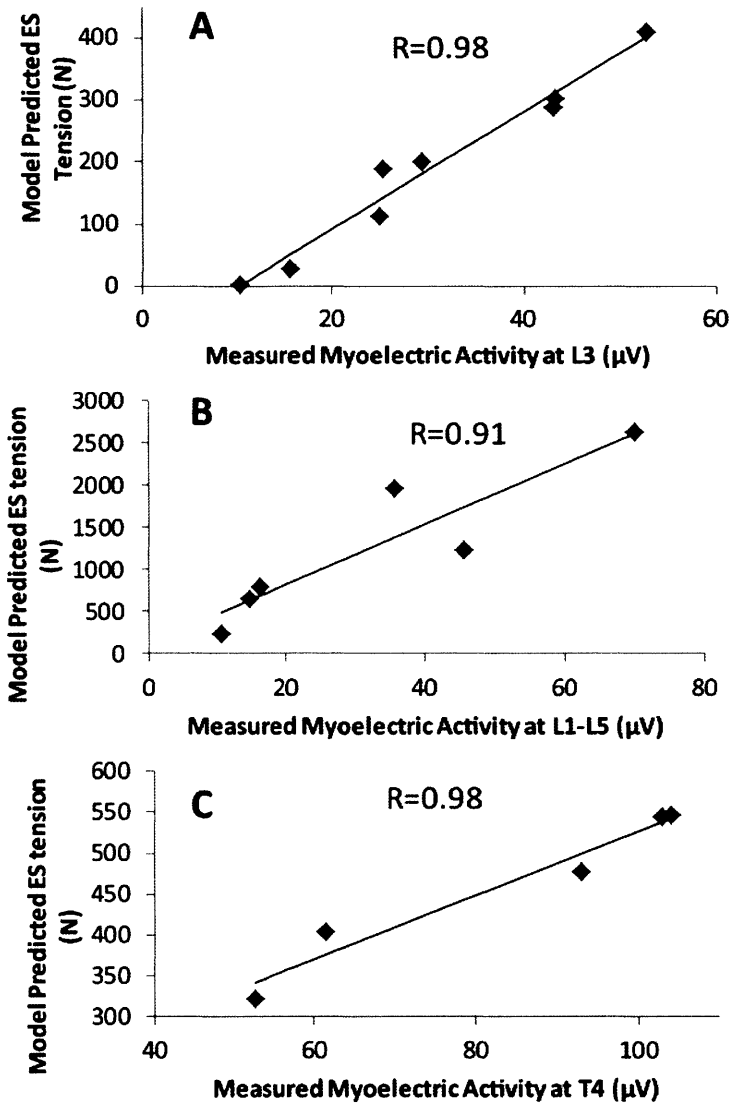

Figure 4.6: The model was used to simulate a range of activities for which trunk muscle myoelectric activity has been previously reported by a) Takahashi and colleages at L3 [49], b) Schultz and colleagues at L1-L5 [48], and c) Andersson and colleagues at T4 [45]. Measured myoelectric activity was correlated with the sum of erector spinae fascicle tensions predicted by the model at the spine levels measured.

4.5 Discussion

We created a fully articulated model of the thoracic and lumbar spine that included the individual vertebrae, ribs, sternum, and the major trunk muscle groups. The model can simulate daily activities in a quasi-static fashion, with muscle forces being solved via an optimization routine that minimizes the sum of cubed muscle activations, which is equivalent to maximizing muscle endurance. The unique features of this model are the detailed anatomy of

the rib cage, including the associated musculature, and the ability to compute thoracic as well as lumbar vertebral loading. Moreover, the ribs can move relative to the thoracic vertebral bodies in a realistic fashion via the costovertebral pin joints, and the thoracic and lumbar vertebral bodies can move relative to each other via intervertebral ball joints, allowing for realistic spine motion. The costal cartilages connecting the ribs to the sternum are modeled as actuators that can provide a tensile or compressive force along their length. These connections, along with the costovertebral joints and the intercostal muscles, facilitate load sharing amongst the skeletal structures comprising the thorax. Overall, our model's predictions of vertebral loading and trunk muscle tension were well correlated with measurements of IDP, loading from telemeterized implants, and trunk muscle myoelectric activity. The high correlations between model predictions and measured values imply that our model is correctly capturing the relative change in vertebral loading and muscle tension that occurs between different activities.

Our model's predictions of lumbar vertebral loading and trunk muscle tension were highly correlated ($r>0.90$) to *in vivo* measures of IDP and myoelectric activity taken from a variety of prior studies, indicating that our model's lumbar loading estimates have an accuracy equivalent to previous models of the lumbar spine [4, 48]. A major strength of the current study was our conversion of vertebral compressive force from the model to an estimated IDP using vertebral cross-sectional area and a previously published correction factor [54-56]. This conversion process allowed us to determine how accurately our model was predicting loading magnitude. The slope and intercept of the linear trend line relating measured IDP to model estimated IDP did not differ significantly from one and zero, respectively, indicating that loading magnitudes from the model were well matched to measured disc pressure magnitudes.

Vertebral compressive loading predicted by the model at L1 closely matched *in vivo* measurements of L1 compressive load recorded from telemeterized implants for all activities except trunk extension (Fig. 4.5) [51]. The range of loading measured by Rohlmann and colleagues for extension was lower than the model predictions (42% versus 114% standing load). However, the precise amount of trunk extension performed in the study by Rohlmann and colleagues was not specified, so an initial assumption of 15° was used in the model. In an

attempt to explain the discrepancy between the model predictions and the measured data we also simulated 5° and 30° of trunk extension, which generated vertebral compressive loads of 94% and 137% standing load, respectively, indicating that positioning effects do not explain why the *in vivo* load was substantially lower than the model predictions. Another possible reason for the lower measured *in vivo* load could be due to the fact that the patients had bisegmental spinal fixators implanted posteriorly to stabilize the spine. These fixators could offload the vertebral body implant during extended postures. Further, the facet joints have been shown to transfer compressive load during trunk extension, thereby offloading the vertebral body. The model estimates total vertebral loading, and does not differentiate between the vertebral body and the facet joints, while the measurement only includes the vertebral body. This could also be a reason for why the model predicts higher vertebral loading during trunk extension than is measured in vertebral bodies. Removing extension from the correlation analysis improved the correlation coefficient between measured and model from r = 0.88 to r = 0.97. Han and colleagues found a similar result when comparing their model of the lumbar spine [4] to the telemeterized vertebral loads reported by Rohlmann and colleagues. The model predictions from Han and colleagues matched the implant loads closely, except for extension in which they predicted 120% of standing load versus the measured value of 42% of standing load.

There was only one study that measured thoracic IDP *in vivo* [46], limiting our ability to fully validate the model's predictions of vertebral compressive loading in the thoracic spine. Nonetheless, thoracic vertebral loading predicted by the model generally correlated well with measured IDP from this study. In addition, thoracic erector spinae tension predicted by the model was highly correlated with measured myoelectric activity at T4. The model over-predicted thoracic IDP for a few lifting activities: 30° trunk flexion with weights in each hand (at the mid and lower thoracic spine) and standing upright with weights in each hand and elbows flexed 90° (at the lower thoracic spine). One possible cause for this could be the absence of intra-abdominal pressure and intra-thoracic pressure from the model [4, 57, 58]. Prior studies have shown that both intra-abdominal pressure and intra-thoracic pressure are elevated during heavy lifting and other strenuous activities [48, 59], and these pressures could act to unload the

thoracic and lumbar spines [58]. Although thoracic IDP was over-predicted by the model for these heavy lifting activities, lumbar IDP was not. In the future, the mechanical effects of intra-abdominal pressure and intra-thoracic pressure should be incorporated into the model to clarify their effects on both lumbar and thoracic spine loading.

Other mechanical factors that might influence thoracic spine loads *in vivo* include the stiffness of the intervertebral joint and the bending stiffness of the costal cartilage, both of which could act to change the forces and moments applied to the spine. These factors were not included in the present version of the model due to limited experimental data on the value of these properties. For instance, most *in vitro* studies measuring intervertebral joint stiffness have focused on only a few lumbar spinal levels. Future experimental studies measuring costal cartilage stiffness and intervertebral joint stiffness at multiple thoracic and lumbar levels is an important area of future work, as well as developing methods to incorporate these factors into musculoskeletal models.

A final source of potential error in the model's thoracic load predictions could be the pattern of intercostal muscle activation. Although the role of the external and internal intercostals is well documented during ventilation [40, 60], the extent to which these muscles activate during daily activities and lifting is less clear. McGill and colleagues demonstrated significant myoelectric activity of the intercostal muscles for a few activities, including a squat lift of between 72 and 91 kg [61], providing evidence that the intercostals activate during daily activities, especially strenuous ones. Higher intercostal activation and tension could change the stiffness and load-sharing characteristics of the thorax, either increasing or decreasing the amount of load carried by the thoracic vertebrae. The current model, combined with measurements of intercostal myoelectric activity during daily activities, could be used in the future to elucidate the important non-ventilation related roles of this muscle group.

A major strength of the current study was the use of *in vivo* muscle morphology measurements to adjust the cross-sectional area and position of several major trunk muscle groups in the model. Prior models have typically relied on detailed cadaver dissection to account for a muscle group's individual fascicles and many attachments. For instance, the erector spinae muscle group in the OpenSim lumbar spine model [2], which was incorporated

into the current study's model, consists of 76 individual fascicles based on the detailed dissections of Macintosh and Bogduk [11, 62]. However, the data from cadaver dissection is derived from a small, heterogeneous sample and may not be representative of a broader population. Moreover, our base musculoskeletal model was derived by combining several existing models and adding new muscle fascicles, and it was not clear whether this process would lead to a physiologically accurate and broadly representative model. Indeed, prior to adjustment, the CSA and AP and ML moment arms of the erector spinae were more than 2 standard deviations smaller than the averages from our measured CT cohort. After adjustment, the CSA and AP and ML moment arms in the model matched the measured data very closely (Fig. 4.3 and Table 4.2). In the future, medical imaging data from other regions (ie: shoulder, upper thoracic, and cervical spines) could be used to adjust the CSA and position of muscles in these other areas to further enhance the biofidelity of the model. Moreover, this method of adjusting a musculoskeletal model to match *in vivo* muscle morphology measurements can be used to tailor a model to a specific research question or to an individual person. For instance, the study of vertebral fracture etiology requires a model representative of an older adult population. Other factors that vary between individuals and likely influence *in vivo* loads, such as spine curvature [63-65] and rib cage size and shape [17, 66, 67], can also easily be incorporated in future versions of the model to provide an even better subject-specific model.

In conclusion, we used OpenSim to develop an anatomically detailed, fully articulated model of the thoracic and lumbar spine that includes the individual ribs, sternum, and associated musculature. We also created a unique approach for adjusting the size and position of muscle fascicles in this model using *in vivo* CT measurements of muscle morphology. Comparison of vertebral loading and muscle activation predictions to multiple prior reports of *in vivo* intradiscal pressure, vertebral implant loads, and myoelectric activity demonstrated that the model accurately predicts vertebral compressive loading and trunk muscle tension for a variety of activities. Altogether, this new thoracolumbar spine model will be useful for future studies aimed at understanding the biomechanical pathology of various thoracic conditions, such as vertebral fracture and thoracic back pain.

4.6 NOMENCLATURE

$CSA_{measured\_gr}$	average cross-sectional area of a muscle group from CT measurements
CSA_{model_gr}	pre-adjusted cross-sectional area of a muscle group in the model
CSA_{model_fas}	pre-adjusted cross-sectional area of a fascicle in the model
$CSA_{adjusted\_fas}$	adjusted cross-sectional area of a fascicle in the model
CSA_{Vert}	cross-sectional area of the vertebral body
F_C	compressive load in the axial direction of the vertebral body
IDP_{model}	intradiscal pressure estimated from the model
L	vertebral levels where a muscle group was measured on CT

4.7 APPENDIX

Supplemental Figure 4.1: We tested the sensitivity of our model's vertebral compressive loading predictions to the optimal force of the costal cartilage actuators, which we varied from 0 N (equivalent to no actuators present) to 1000 N in 100 N increments. We performed this analysis for three different activities: a) neutral standing, b) standing with 10 kg weights in each hand and the elbows flexed 90°, and c) 30° forward trunk flexion. We found that vertebral loads in the mid- and upper-thoracic regions of the spine were the most sensitive to the costal cartilage optimal force, especially while holding weights in the hands (b). Vertebral loading is only sensitive to the costal cartilage optimal force when it is between 0 N and 300 N, but for optimal force values greater than 300 N vertebral loading is unaffected. Therefore, we selected an optimal force of 1000 N for the model so that the optimization routine would always favor activation and loading of the costal cartilage actuators over the muscles for any arbitrary activity we might simulate in the future.

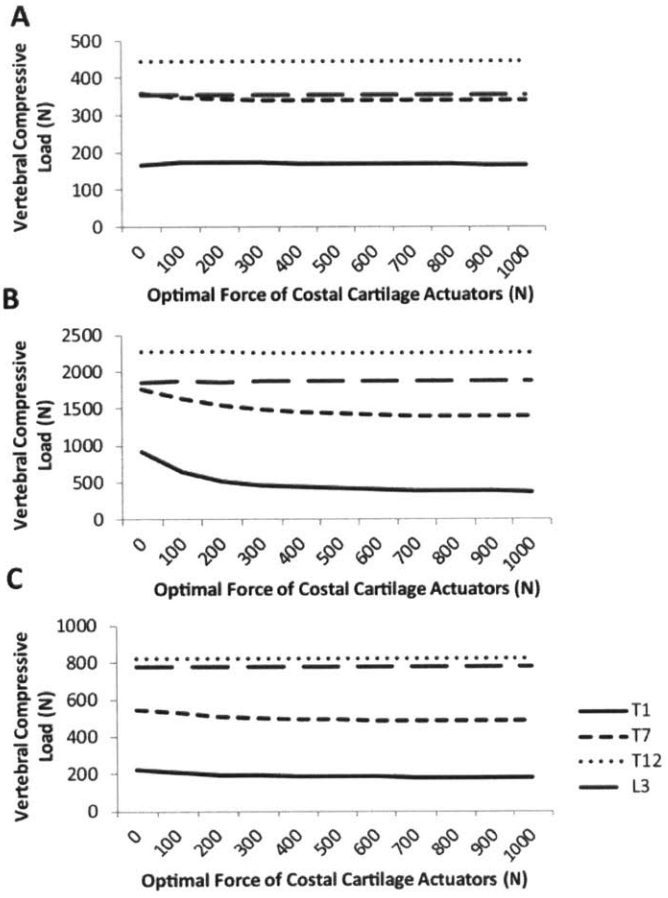

Supplemental Figure 4.2: We tested the sensitivity of our model's vertebral compressive loading predictions to the locations of the lumbar intervertebral joint centers. Vertebral compressive loading predicted by our baseline model (with the joint centers placed at the geometric centers of the intervertebral discs) was compared to load predictions from a model with the lumbar joint centers shifted to match the average locations reported by Pearcy and colleagues (between 0.44 and 0.93 cm posterior/inferior of the disc center) [44]. Vertebral loading was assessed for the following activities: 1) neutral standing, 2) standing with 10 kg weights in each hand and the elbows flexed 90°, and 3) 30° forward trunk flexion. We found that vertebral loading was minimally affected by joint center location, with differences ranging between -0.5 and 9% for standing, -16 to 11% for trunk flexion, and -4 to 3% for standing with weights.

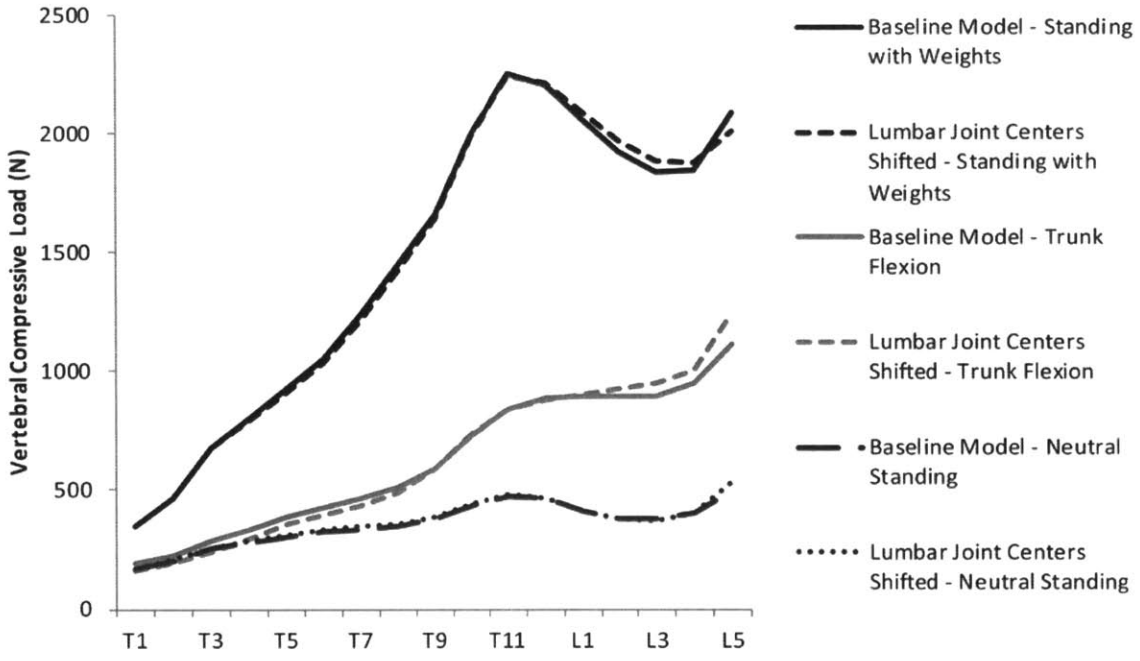

Supplemental Table 4.1: Method for partitioning total trunk flexion into pelvis, lumbar spine, and thoracic spine components. A second order polynomial was fit to data from Tafazzol and colleagues [20] relating the measured lumbopelvic (LB) ratio to the amount of trunk flexion, expressed as a percentage of total range of motion (ROM): $LB\ ratio = 0.9749 + 0.0236(ROM) - 4x10^{-5}(ROM)^2$. Representative values of the lumbopelvic ratio are shown below using 121° as the trunk flexion ROM [20]. Total trunk flexion is the sum of lumbar, thoracic, and pelvic flexion, and the lumbar and thoracic regions contribute 51% and 49% of the spine component of flexion.

% Trunk ROM	Lumbopelvic ratio	Total trunk flexion (°)	Lumbar flexion (°)	Thoracic flexion (°)	Pelvic flexion (°)
0	2.6	0.0	0.0	0.0	0.0
10	2.5	12.1	5.1	5.0	2.0
20	2.4	24.2	10.1	9.9	4.2
30	2.3	36.3	15.1	14.7	6.5
40	2.2	48.4	19.9	19.4	9.1
50	2.1	60.5	24.6	23.9	12.0
60	1.9	72.6	29.0	28.2	15.4
70	1.7	84.7	33.1	32.2	19.4
80	1.5	96.8	36.7	35.7	24.4
90	1.3	108.9	39.5	38.5	30.8
100	1.0	121.0	41.3	40.2	39.5

Supplemental Table 4.2: Coefficients determining the amount of trunk motion at each intervertebral joint. For axial rotation and lateral bending, the coefficients represent a percentage of total trunk movement. For flexion extension, the thoracic coefficients (T1/T2 to T12/L1) represent the percentage of thoracic flexion and the lumbar coefficients (L1/L2 to L5/S1) represent the percentage of lumbar flexion. The method for computing the amount of lumbar and thoracic flexion is shown in Supplemental Table 4.1.

	Axial Rotation	Lateral Bending	Flexion/Extension
T1/T2	0.046	0.057	0.053
T2/T3	0.062	0.053	0.053
T3/T4	0.054	0.057	0.053
T4/T5	0.062	0.037	0.053
T5/T6	0.070	0.033	0.053
T6/T7	0.074	0.045	0.066
T7/T8	0.089	0.070	0.079
T8/T9	0.097	0.053	0.079
T9/T10	0.105	0.066	0.079
T10/T11	0.101	0.074	0.118
T11/T12	0.050	0.094	0.158
T12/L1	0.019	0.090	0.158
L1/L2	0.029	0.051	0.300
L2/L3	0.031	0.068	0.247
L3/L4	0.038	0.066	0.211
L4/L5	0.038	0.049	0.147
L5/S1	0.036	0.037	0.068

Supplemental Table 4.3: Positions and orientations of the right side costovertebral (CV) joints. The position of each CV joint is expressed in the vertebral body frame that the rib is connected to (ie: T1/R1 CV joint position is expressed in the T1 body frame). The x-axis of the CV joint is located along the rib cervical axis, which runs between the CV and costotransverse joints. The acute angle between the CV joint x-axis and the vertebral body x-axis is given (CV joints are oriented posterior-laterally). Note that the vertebral body frame is located at the center of the inferior intervertebral disc. The z-axis of the CV joint was oriented parallel to the y-axis of the vertebral body according to the convention in [27].

CV joint	X-position (mm)	Y-position (mm)	Z-position (mm)	Orientation of CV joint X-axis (°)
T1/R1	-3.3	19.5	18.8	40.2
T2/R2	-3.1	20.3	12.0	39.0
T3/R3	-4.4	22.2	13.3	37.7
T4/R4	-6.1	24.5	14.9	36.2
T5/R5	-7.9	26.3	16.2	34.6
T6/R6	-8.9	25.7	15.7	32.8
T7/R7	-10.1	25.9	15.7	30.8
T8/R8	-10.5	24.6	14.6	28.5
T9/R9	-11.7	25.1	14.7	25.9
T10/R10	-14.9	29.0	17.0	22.9
T11/R11	-16.0	18.8	16.8	19.6
T12/R12	-22.0	22.1	21.4	15.7

Supplemental Table 4.4: Input parameters for the muscle fascicles included in the model. Maximum isometric force was calculated as the product of PCSA and maximum muscle stress, which was set to 140 N/cm^2 for shoulder group muscles, and 100 N/cm^2 for all other muscle groups. Adjusted PCSA is the fascicle area after adjustment to the average male CT cohort data, and blank entries indicate that the muscle group was not adjusted. For the muscles adapted from Christophy and colleagues [2], optimal fiber length (OFL) was computed as: OFL = L^{MT} * (L^f/L^{mt}) * (L^{s0}/L^s), where L^{MT} is the musculotendon length from our model, L^f/L^{mt} is the ratio of muscle fiber length to musculotendon length at rest reported by Christophy and colleagues, and L^{s0}/L^s is the ratio of optimal sarcomere length to sarcomere length reported by Chirstophy and colleagues. Tendon slack length (TSL) was then computed as: TSL = L^{MT} – [L^{MT} * (L^f/L^{mt})]*cos(α), where α is the pennation angle reported by Christophy and colleagues.

	Fascicle Name	Adjusted PCSA (cm^2)	Pre-adjusted PCSA (cm^2)	OFL (cm)	TSL (cm)	α (°)
Rectus Abdominis						
(Christophy et al. 2012)	rect_abd_r	6.62	5.72	30.34	8.25	0.0
Latissimus Dorsi						
(Christophy et al. 2012)	LD_L1_r	0.90	0.90	33.19	7.25	0.0
	LD_L2_r	0.85	0.90	35.71	7.80	0.0
	LD_L3_r	1.05	1.10	37.80	8.25	0.0
	LD_L4_r	1.01	1.10	39.49	8.62	0.0
	LD_L5_r	1.02	1.10	41.73	8.57	0.0
	LD_T12_r	0.54	0.50	31.59	6.49	0.0
	LD_T11_r	0.63	0.60	29.51	6.06	0.0
	LD_T10_r	0.64	0.60	29.13	4.56	0.0
	LD_T9_r	0.41	0.40	25.49	3.99	0.0
	LD_T8_r	0.41	0.40	23.68	4.86	0.0
	LD_T7_r	0.37	0.40	22.30	4.58	0.0
	LD_R12_r	0.43	0.40	27.37	5.62	0.0
	LD_R11_r	0.63	0.60	23.90	4.91	0.0
	LD_Il_r	0.65	0.70	46.50	2.01	0.0
External Obliques						
(Stokes et al. 1999 and Christophy et al. 2012)	E0_R5_r	0.53	1.96	8.16	0.91	0.0
	E0_R6_r	0.65	2.32	13.77	1.53	0.0
*OFL and TSL were estimated as 90% and 10% of the musculotendon length in the model, respectively.	E0_R7_r	1.28	2.43	18.43	2.05	0.0
	E0_R8_r	1.73	2.34	22.61	2.51	0.0
	E0_R9_r	1.98	1.68	26.73	2.97	0.0
	E0_R10_r	1.41	1.68	13.74	1.53	0.0
	E0_R11_r	1.41	1.68	10.71	1.19	0.0

	Fascicle Name	Adjusted PCSA (cm^2)	Pre-adjusted PCSA (cm^2)	OFL (cm)	TSL (cm)	α (°)
	E0_R12_r	1.53	1.68	8.70	0.97	0.0
Internal Obliques						
(Christophy et al. 2012)	IO1_r	1.96	1.85	10.10	1.12	0.0
	IO2_r	2.02	2.24	10.49	1.17	0.0
	IO3_r	1.92	2.26	12.42	1.38	0.0
	IO4_r	2.33	2.68	10.46	1.16	0.0
	IO5_r	2.04	2.35	10.67	1.19	0.0
	IO6_r	1.80	2.07	10.03	1.11	0.0
Erector Spinae						
(Christophy et al. 2012)	IL_L1_r	1.47	1.09	5.70	12.92	13.8
	IL_L2_r	1.83	1.54	4.05	9.19	13.8
	IL_L3_r	2.17	1.83	2.69	6.11	13.8
	IL_L4_r	4.15	1.89	1.87	4.24	13.8
	IL_R5_r	0.57	0.24	18.42	25.79	13.8
	IL_R6_r	0.73	0.30	17.89	21.61	13.8
	IL_R7_r	0.88	0.39	17.55	18.44	13.8
	IL_R8_r	0.78	0.35	16.13	16.29	13.8
	IL_R9_r	0.96	0.50	18.61	10.95	13.8
	IL_R10_r	1.92	1.00	16.26	9.57	13.8
	IL_R11_r	2.35	1.24	13.62	6.82	13.8
	IL_R12_r	2.06	1.48	10.07	5.04	13.8
	LTpT_T1_r	3.26	0.28	11.02	26.10	12.6
	LTpT_T2_r	2.41	0.57	11.54	27.74	12.6
	LTpT_T3_r	1.73	0.57	11.70	28.14	12.6
	LTpT_T4_r	0.61	0.22	11.72	28.19	12.6
	LTpT_T5_r	0.57	0.22	10.96	26.35	12.6
	LTpT_T6_r	0.81	0.33	11.46	26.19	12.6
	LTpT_T7_r	0.80	0.39	13.04	24.67	12.6
	LTpT_T8_r	1.20	0.63	13.91	21.97	12.6
	LTpT_T9_r	1.39	0.74	13.68	23.18	12.6
	LTpT_T10_r	1.21	0.80	12.57	21.31	12.6
	LTpT_T11_r	1.15	0.83	10.92	18.50	12.6
	LTpT_T12_r	0.94	0.70	8.63	14.62	12.6
	LTpT_R4_r	0.60	0.22	15.13	25.64	12.6
	LTpT_R5_r	0.57	0.22	14.22	24.11	12.6
	LTpT_R6_r	0.81	0.33	15.27	23.39	12.6
	LTpT_R7_r	0.80	0.39	14.49	24.23	12.6
	LTpT_R8_r	1.30	0.63	12.09	24.66	12.6
	LTpT_R9_r	1.11	0.74	10.61	25.92	12.6
	LTpT_R10_r	1.20	0.80	12.58	21.62	12.6
	LTpT_R11_r	1.15	0.83	11.76	16.75	12.6

	Fascicle Name	Adjusted PCSA (cm^2)	Pre-adjusted PCSA (cm^2)	OFL (cm)	TSL (cm)	α (°)
	LTpT_R12_r	0.94	0.70	7.36	14.31	12.6
	LTpL_L5_r	1.58	1.15	5.15	0.10	12.6
	LTpL_L4_r	1.52	1.11	4.37	4.71	12.6
	LTpL_L3_r	1.21	1.02	5.92	6.43	12.6
	LTpL_L2_r	1.08	0.91	7.57	8.33	12.6
	LTpL_L1_r	1.06	0.78	9.04	10.53	12.6
Multifidus						
(Christophy et al. 2012)	MF_m1s_r	0.81	0.40	5.34	2.22	0.0
	MF_m1t_1_r	0.72	0.42	8.77	2.63	0.0
	MF_m1t_2_r	0.60	0.36	10.80	3.24	0.0
	MF_m1t_3_r	1.00	0.60	11.80	3.54	0.0
	MF_m2s_r	0.54	0.39	5.50	2.13	0.0
	MF_m2t_1_r	0.57	0.39	7.46	2.27	0.0
	MF_m2t_2_r	1.46	0.99	9.34	2.84	0.0
	MF_m2t_3_r	1.61	0.99	10.44	3.18	0.0
	MF_m3s_r	0.84	0.54	4.71	1.96	0.0
	MF_m3t_1_r	0.91	0.52	11.28	3.75	0.0
	MF_m3t_2_r	0.91	0.52	9.49	3.16	0.0
	MF_m3t_3_r	0.91	0.52	9.49	3.16	0.0
	MF_m4s_r	1.01	0.52	4.29	2.71	0.0
	MF_m4t_1_r	0.90	0.47	6.15	2.49	0.0
	MF_m4t_2_r	0.90	0.47	8.02	3.25	0.0
	MF_m4t_3_r	0.90	0.47	9.17	3.71	0.0
	MF_m5s_r	0.35	0.23	1.47	0.93	0.0
	MF_m5t_1_r	0.35	0.23	7.60	3.07	0.0
	MF_m5t_2_r	0.35	0.23	5.68	2.30	0.0
	MF_m5t_3_r	0.35	0.23	4.07	1.65	0.0
	MF_m1_laminar_r	0.39	0.19	3.69	1.40	0.0
	MF_m2_laminar_r	0.31	0.22	3.11	1.18	0.0
	MF_m3_laminar_r	0.36	0.23	3.31	1.26	0.0
	MF_m4_laminar_r	0.26	0.17	3.49	1.33	0.0
	MF_m5_laminar_r	0.56	0.36	2.56	0.97	0.0
(Vasavada et al. 1998)	supmult-T1-C4	2.84	1.83	6.80	2.74	5.0
	supmult-T1-C5	2.84	1.83	6.80	2.74	5.0
	supmult-T2-C6	2.84	1.83	6.80	2.74	5.0
	deepmult-T1-C5	2.84	1.83	6.80	2.74	5.0
	deepmult-T1-C6	2.84	1.83	6.80	2.74	5.0
	deepmult-T2-C7	2.84	1.83	6.80	2.74	5.0
	deepmult-T2-T1	2.84	1.83	6.80	2.74	5.0
(Estimated from Vasavada et al. 1998 and	multifidus_L2_T12	2.29	1.83	5.02	1.92	5.0
	multifidus_L1_T11	2.41	1.83	5.00	1.91	5.0

	Fascicle Name	Adjusted PCSA (cm^2)	Pre-adjusted PCSA (cm^2)	OFL (cm)	TSL (cm)	α (°)
Christophy et al. 2012) *The average L^f/L^{mt} and L^{s0}/L^s reported by Christophy et al. for the lumbar multifidus was used to calculate OFL and TSL. Pennation angle and pre-adjusted PCSA were taken from the cervical mutlifidus reported by Vasavada et al.	multifidus_T12_T10	2.25	1.83	4.91	1.88	5.0
	multifidus_T11_T9	2.20	1.83	4.66	1.78	5.0
	multifidus_T10_T8	1.85	1.83	3.72	1.42	5.0
	multifidus_T9_T7	1.54	1.83	2.72	1.04	5.0
	multifidus_T8_T6	1.99	1.83	3.55	1.36	5.0
	multifidus_T7_T5	2.52	1.83	3.55	1.36	5.0
	multifidus_T6_T4	2.84	1.83	3.53	1.35	5.0
	multifidus_T5_T3	2.84	1.83	3.43	1.31	5.0
	multifidus_T4_T2	2.84	1.83	3.27	1.25	5.0
	multifidus_T3_T1	2.84	1.83	3.06	1.17	5.0
Psoas Major						
(Christophy et al. 2012)	Ps_L1_VB_r	2.67	2.11	19.36	5.75	10.7
	Ps_L1_TP_r	0.77	0.61	19.07	5.66	10.7
	Ps_L1_L2_IVD_r	1.47	1.20	17.83	5.30	10.7
	Ps_L2_TP_r	2.59	2.11	16.58	4.93	10.7
	Ps_L2_L3_IVD_r	1.51	1.19	15.31	4.55	10.7
	Ps_L3_TP_r	1.28	1.01	14.31	4.25	10.7
	Ps_L3_L4_IVD_r	0.45	0.36	12.85	3.82	10.7
	Ps_L4_TP_r	2.03	1.61	12.25	3.64	10.7
	Ps_L4_L5_IVD_r	0.85	0.79	10.47	3.11	10.7
	Ps_L5_TP_r	1.86	1.73	10.34	3.07	10.7
	Ps_L5_VB_r	2.33	1.91	9.03	2.68	10.7
Quadratus Lumborum						
(Christophy et al. 2012)	QL_post_I_1-L3_r	0.76	0.40	4.42	3.71	7.4
	QL_post_I_2-L4_r	1.56	0.53	2.53	2.13	7.4
	QL_post_I_2-L3_r	0.59	0.31	3.96	3.33	7.4
	QL_post_I_2-L2_r	0.37	0.19	5.71	4.80	7.4
	QL_post_I_3-L1_r	0.77	0.28	7.75	6.51	7.4
	QL_post_I_3-L2_r	0.56	0.30	5.65	4.74	7.4
	QL_post_I_3-L3_r	0.96	0.50	3.99	3.35	7.4
	QL_mid_L3-12_3_r	0.42	0.13	6.16	3.20	7.4
	QL_mid_L3-12_2_r	0.48	0.14	6.65	3.45	7.4
	QL_mid_L3-12_1_r	0.80	0.24	6.82	3.54	7.4
	QL_mid_L2-12_1_r	1.56	0.20	4.64	2.41	7.4
	QL_mid_L4-12_3_r	0.42	0.12	7.71	4.00	7.4
	QL_ant_I_2-T12_r	0.45	0.15	11.52	5.98	7.4
	QL_ant_I_3-T12_r	0.85	0.29	11.34	5.89	7.4
	QL_ant_I_2-12_1_r	0.28	0.10	10.69	5.55	7.4
	QL_ant_I_3-12_1_r	0.53	0.19	10.55	5.48	7.4
	QL_ant_I_3-12_2_r	0.35	0.13	10.07	5.23	7.4
	QL_ant_I_3-12_3_r	0.41	0.15	8.74	4.54	7.4

	Fascicle Name	Adjusted PCSA (cm^2)	Pre-adjusted PCSA (cm^2)	OFL (cm)	TSL (cm)	α (°)
Neck Muscles						
(Estimated from Vasavada et al. 1998 and Kamibayashi et al. 1998) *Added additional splenius capitis fascicle attaching to T2 and splenius cervicis fascicles attaching to T3, T5, and T6. For the splenius fascicles, OFL was computed as the product of musculotendon length in the model and the ratio of optimal fiber length to musculotendon length reported by Kamibayashi et al. TSL was computed as the difference between musculotendon length in model and OFL.	stern_mast		1.97	10.80	5.61	15.0
	cleid_mast		0.99	10.80	3.52	15.0
	cleid_occ		0.99	10.80	6.95	15.0
	scalenus_ant		1.47	4.20	5.34	10.0
	scalenus_med		2.06	5.00	6.15	10.0
	scalenus_post		1.57	6.20	7.28	10.0
	long_col_c1thx		0.27	8.91	8.75	5.0
	long_col_c5thx		0.27	5.76	5.48	5.0
	splen_cap_skl_T1		0.71	13.59	4.01	0.0
	splen_cap_skl_T2		0.71	12.13	3.57	0.0
	splen_cerv_c3_T3		0.35	10.15	5.55	0.0
	splen_cerv_c3_T4		0.35	11.83	6.47	0.0
	splen_cerv_c3_T5		0.35	13.70	7.50	0.0
	splen_cerv_c3_T6		0.35	15.58	8.52	0.0
	semi_cap_sklthx		1.83	6.80	6.89	5.0
	semi_cerv_c3thx		1.83	6.80	2.74	5.0
	levator_scap		2.18	11.30	2.19	0.0
	longissi_cerv_c4thx		0.57	13.18	4.23	0.0
	iliocost_cerv_c5rib		0.57	8.09	2.57	0.0
Trapezius						
(Estimated from Vasavada et al. 1998 and Kamibayashi et al. 1998) *OFL was computed as the product of musculotendon length in the model and the ratio of optimal fiber length to musculotendon length reported by Kamibayashi et al. TSL was computed as the difference between musculotendon length in model and OFL.	trap_cl	1.24	2.22	8.40	11.92	30.0
	trap_acr_scap	1.51	2.69	12.34	4.56	0.0
	trap_acr_T1	1.51	2.69	11.98	4.42	0.0
	trap_acr_T2	1.51	2.69	12.34	4.56	0.0
	trap_acr_T3	1.51	2.69	12.85	4.75	0.0
	trap_inf_T4	0.68	1.21	9.84	1.76	0.0
	trap_inf_T5	0.68	1.21	11.11	1.99	0.0
	trap_inf_T6	0.79	1.21	12.55	2.25	0.0
	trap_inf_T7	0.77	1.21	14.51	2.59	0.0
	trap_inf_T8	0.72	1.21	16.20	2.90	0.0
	trap_inf_T9	0.66	1.21	17.73	3.17	0.0
	trap_inf_T10	0.62	1.21	20.27	3.63	0.0
	trap_inf_T11	0.59	1.21	22.82	4.08	0.0
	trap_inf_T12	0.59	1.21	25.62	4.58	0.0
Shoulder Muscles						
(Holzbaur et al. 2005)	PECM1		2.60	14.40	0.30	17.0
	PECM2		3.70	13.80	8.90	25.0
	PECM3		2.80	13.80	13.20	25.0
	DELT1		8.16	9.76	9.30	22.0
	DELT2		8.16	10.78	10.95	15.0

	Fascicle Name	Adjusted PCSA (cm^2)	Pre-adjusted PCSA (cm^2)	OFL (cm)	TSL (cm)	α (°)
	DELT3		1.86	13.67	3.80	18.0
	SUPSP		3.48	6.82	3.95	7.0
	INFSP		8.65	7.55	3.08	18.5
	SUBSC		9.84	8.73	3.30	20.0
	TMIN		2.53	7.41	7.13	24.0
	TMAJ		3.04	16.24	2.00	16.0
	CORB		1.73	9.32	9.70	0.0
Transversus Abdominis						
(Brown et al. 2011) *TSL was computed as the difference between musculotendon length in model and reported OFL.	TR1_r		1.60	7.30	4.40	0.0
	TR2_r		0.63	14.8	11.60	0.0
	TR3_r		0.63	14.8	7.80	0.0
	TR4_r		0.63	14.8	8.10	0.0
	TR5_r		1.90	7.30	3.30	0.0
Serratus Anterior						
(Garner et al. 2001 and Garner et al. 2003) *Musculotendon length of fascicles in model was used to determine what percentage of PCSA each fascicle was assigned from the total PCSA reported by Garner et. al.	SerrAnt1_1_R		1.36	11.35	0.28	0.0
	SerrAnt2_1_R		1.80	11.35	0.28	0.0
	SerrAnt2_2_R		1.65	11.35	0.28	0.0
	SerrAnt3_1_R		1.49	17.91	0.75	0.0
	SerrAnt4_1_R		2.03	17.91	0.75	0.0
	SerrAnt5_1_R		1.60	17.91	0.75	0.0
	SerrAnt6_1_R		2.23	17.91	0.75	0.0
	SerrAnt7_1_R		2.83	23.15	0.01	0.0
	SerrAnt8_1_R		3.12	23.15	0.01	0.0
	SerrAnt9_1_R		2.41	23.15	0.01	0.0
External Intercostals						
*PCSA was estimated using rib lengths (approximately between the rib tubercles posteriorly and the ends of the bony ribs anteriorly) multiplied by 2.5 mm, the estimated thickness of the external intercostal muscle sheet. Optimal fiber lengths were computed as the distance between attachment points on adjacent ribs, and pennation angles and tendon slack lengths were assumed to be 0° and 0.1 mm, respectively.	ExtIC_IS1_1_R		1.48	4.45	0.10	0.0
	ExtIC_IS1_3_R		1.48	3.86	0.10	0.0
	ExtIC_IS1_5_R		1.48	5.43	0.10	0.0
	ExtIC_IS2_1_R		1.49	3.76	0.10	0.0
	ExtIC_IS2_3_R		1.49	4.04	0.10	0.0
	ExtIC_IS2_5_R		1.49	5.34	0.10	0.0
	ExtIC_IS2_7_R		1.49	5.68	0.10	0.0
	ExtIC_IS3_1_R		1.65	4.24	0.10	0.0
	ExtIC_IS3_3_R		1.65	4.05	0.10	0.0
	ExtIC_IS3_5_R		1.65	4.28	0.10	0.0
	ExtIC_IS3_7_R		1.65	5.78	0.10	0.0
	ExtIC_IS4_1_R		1.75	4.41	0.10	0.0
	ExtIC_IS4_3_R		1.75	4.14	0.10	0.0
	ExtIC_IS4_5_R		1.75	4.27	0.10	0.0
	ExtIC_IS4_7_R		1.75	5.63	0.10	0.0
	ExtIC_IS5_1_R		1.80	4.45	0.10	0.0

	Fascicle Name	Adjusted PCSA (cm^2)	Pre-adjusted PCSA (cm^2)	OFL (cm)	TSL (cm)	α (°)
	ExtIC_IS5_3_R		1.80	4.49	0.10	0.0
	ExtIC_IS5_5_R		1.80	4.88	0.10	0.0
	ExtIC_IS5_7_R		1.80	5.76	0.10	0.0
	ExtIC_IS6_1_R		1.75	4.19	0.10	0.0
	ExtIC_IS6_3_R		1.75	4.55	0.10	0.0
	ExtIC_IS6_5_R		1.75	4.65	0.10	0.0
	ExtIC_IS6_7_R		1.75	5.29	0.10	0.0
	ExtIC_IS7_1_R		1.60	4.97	0.10	0.0
	ExtIC_IS7_3_R		1.60	5.10	0.10	0.0
	ExtIC_IS7_5_R		1.60	5.31	0.10	0.0
	ExtIC_IS7_7_R		1.60	5.15	0.10	0.0
	ExtIC_IS8_1_R		1.38	5.78	0.10	0.0
	ExtIC_IS8_3_R		1.38	4.88	0.10	0.0
	ExtIC_IS8_5_R		1.38	4.96	0.10	0.0
	ExtIC_IS8_7_R		1.38	4.41	0.10	0.0
	ExtIC_IS9_1_R		1.58	5.06	0.10	0.0
	ExtIC_IS9_3_R		1.58	4.91	0.10	0.0
	ExtIC_IS9_5_R		1.58	5.60	0.10	0.0
	ExtIC_IS10_1_R		1.38	6.71	0.10	0.0
	ExtIC_IS10_3_R		1.38	6.44	0.10	0.0
	ExtIC_IS11_1_R		0.63	5.57	0.10	0.0
	ExtIC_IS11_3_R		0.63	5.78	0.10	0.0
Internal Intercostals						
*PCSA was estimated using rib lengths (approximately between the rib tubercles posteriorly and the ends of the bony ribs anteriorly) multiplied by 2.5 mm, the estimated thickness of the internal intercostal muscle sheet. Optimal fiber lengths were computed as the distance between attachment points on adjacent ribs, and pennation angles and tendon slack lengths were assumed to be 0° and 0.1 mm, respectively.	IntIC_IS1_1_R		1.08	3.06	0.10	0.0
	IntIC_IS1_3_R		1.08	4.04	0.10	0.0
	IntIC_IS1_5_R		1.08	8.16	0.10	0.0
	IntIC_IS2_1_R		1.37	2.86	0.10	0.0
	IntIC_IS2_3_R		1.37	3.74	0.10	0.0
	IntIC_IS2_5_R		1.37	5.08	0.10	0.0
	IntIC_IS2_7_R		1.37	4.32	0.10	0.0
	IntIC_IS3_1_R		1.74	3.04	0.10	0.0
	IntIC_IS3_3_R		1.74	3.14	0.10	0.0
	IntIC_IS3_5_R		1.74	4.45	0.10	0.0
	IntIC_IS3_7_R		1.74	5.19	0.10	0.0
	IntIC_IS4_1_R		1.97	3.11	0.10	0.0
	IntIC_IS4_3_R		1.97	3.13	0.10	0.0
	IntIC_IS4_5_R		1.97	4.19	0.10	0.0
	IntIC_IS4_7_R		1.97	3.60	0.10	0.0
	IntIC_IS5_1_R		2.19	3.20	0.10	0.0
	IntIC_IS5_3_R		2.19	3.36	0.10	0.0
	IntIC_IS5_5_R		2.19	4.17	0.10	0.0

Fascicle Name	Adjusted PCSA (cm^2)	Pre-adjusted PCSA (cm^2)	OFL (cm)	TSL (cm)	α (°)
IntIC_IS5_7_R		2.19	3.41	0.10	0.0
IntIC_IS6_1_R		2.40	2.91	0.10	0.0
IntIC_IS6_3_R		2.40	3.31	0.10	0.0
IntIC_IS6_5_R		2.40	4.08	0.10	0.0
IntIC_IS6_7_R		2.40	2.05	0.10	0.0
IntIC_IS7_1_R		1.77	3.13	0.10	0.0
IntIC_IS7_3_R		1.77	3.56	0.10	0.0
IntIC_IS7_5_R		1.77	3.77	0.10	0.0
IntIC_IS7_7_R		1.77	4.04	0.10	0.0
IntIC_IS8_1_R		1.68	3.16	0.10	0.0
IntIC_IS8_3_R		1.68	3.51	0.10	0.0
IntIC_IS8_5_R		1.68	3.59	0.10	0.0
IntIC_IS8_7_R		1.68	3.16	0.10	0.0
IntIC_IS9_1_R		1.98	2.91	0.10	0.0
IntIC_IS9_3_R		1.98	3.56	0.10	0.0
IntIC_IS9_5_R		1.98	3.80	0.10	0.0
IntIC_IS10_1_R		2.17	4.89	0.10	0.0
IntIC_IS10_3_R		2.17	4.54	0.10	0.0
IntIC_IS11_1_R		1.25	4.11	0.10	0.0
IntIC_IS11_3_R		1.25	4.22	0.10	0.0

4.8 REFERENCES

1. Delp, S.L., et al., *OpenSim: open-source software to create and analyze dynamic simulations of movement.* IEEE Trans Biomed Eng, 2007. **54**(11): p. 1940-50.

2. Christophy, M., et al., *A musculoskeletal model for the lumbar spine.* Biomech Model Mechanobiol, 2012. **11**(1-2): p. 19-34.

3. Briggs, A.M., et al., *Thoracic Kyphosis Affects Spinal Loads and Trunk Muscle Force.* Physical Therapy, 2007. **87**(5): p. 595-607.

4. Han, K.S., et al., *An enhanced and validated generic thoraco-lumbar spine model for prediction of muscle forces.* Med Eng Phys, 2012. **34**(6): p. 709-16.

5. Keller, T.S., et al., *Influence of spine morphology on intervertebral disc loads and stresses in asymptomatic adults: implications for the ideal spine.* The Spine Journal, 2005. **5**(3): p. 297-309.

6. Iyer, S., et al., *A biomechanical model for estimating loads on thoracic and lumbar vertebrae.* Clin Biomech (Bristol, Avon), 2010. **25**(9): p. 853-8.

7. Briggs, A., et al., *The effect of osteoporotic vertebral fracture on predicted spinal loads in vivo.* European Spine Journal, 2006. **15**(12): p. 1785-1795.

8. Harrison, D.E., et al., *Anterior thoracic posture increases thoracolumbar disc loading.* European Spine Journal, 2005. **14**(3): p. 234-242.

9. Keller, T.S., et al., *Prediction of Osteoporotic Spinal Deformity.* Spine, 2003. **28**(5): p. 455-462.

10. Murakami, D., et al., *Finite element analysis of hard and soft tissue contributions to thoracic response: sensitivity analysis of fluctuations in boundary conditions.* Stapp Car Crash J, 2006. **50**: p. 169-89.

11. Bogduk, N., J.E. Macintosh, and M.J. Pearcy, *A universal model of the lumbar back muscles in the upright position.* Spine (Phila Pa 1976), 1992. **17**(8): p. 897-913.

12. Kamibayashi, L.K. and F.J. Richmond, *Morphometry of human neck muscles.* Spine (Phila Pa 1976), 1998. **23**(12): p. 1314-23.

13. Vasavada, A.N., S. Li, and S.L. Delp, *Influence of muscle morphometry and moment arms on the moment-generating capacity of human neck muscles.* Spine (Phila Pa 1976), 1998. **23**(4): p. 412-22.

14. Narici, M., *Human skeletal muscle architecture studied in vivo by non-invasive imaging techniques: functional significance and applications.* Journal of Electromyography and Kinesiology, 1999. **9**(2): p. 97-103.

15. Bernhardt, M. and K.H. Bridwell, *Segmental Analysis of the Sagittal Plane Alignment of the Normal Thoracic and Lumbar Spines and Thoracolumbar Junction.* Spine, 1989. **14**(7): p. 717-721.

16. Kuntz, C., et al., *Neutral upright sagittal spinal alignment from the occiput to the pelvis in asymptomatic adults: a review and resynthesis of the literature.* Journal of Neurosurgery: Spine, 2007. **6**(2): p. 104-112.

17. Gayzik, F.S., et al., *Quantification of age-related shape change of the human rib cage through geometric morphometrics.* J Biomech, 2008. **41**(7): p. 1545-54.

18. Holzbaur, K.R., W.M. Murray, and S.L. Delp, *A model of the upper extremity for simulating musculoskeletal surgery and analyzing neuromuscular control.* Ann Biomed Eng, 2005. **33**(6): p. 829-40.

19. Tafazzol, A., et al., *Lumbopelvic rhythm during forward and backward sagittal trunk rotations: combined in vivo measurement with inertial tracking device and biomechanical modeling.* Clin Biomech (Bristol, Avon), 2014. **29**(1): p. 7-13.

20. White, A.A., 3rd and M.M. Panjabi, *The basic kinematics of the human spine. A review of past and current knowledge.* Spine (Phila Pa 1976), 1978. **3**(1): p. 12-20.

21. Wong, K.W., et al., *Continuous dynamic spinal motion analysis.* Spine (Phila Pa 1976), 2006. **31**(4): p. 414-9.

22. Fujimori, T., et al., *Kinematics of the thoracic spine in trunk lateral bending: in vivo three-dimensional analysis.* Spine J, 2013.

23. Rozumalski, A., et al., *The in vivo three-dimensional motion of the human lumbar spine during gait.* Gait Posture, 2008. **28**(3): p. 378-84.

24. Fujii, R., et al., *Kinematics of the lumbar spine in trunk rotation: in vivo three-dimensional analysis using magnetic resonance imaging.* Eur Spine J, 2007. **16**(11): p. 1867-74.

25. Fujimori, T., et al., *Kinematics of the thoracic spine in trunk rotation: in vivo 3-dimensional analysis.* Spine (Phila Pa 1976), 2012. **37**(21): p. E1318-28.

26. Duprey, S., et al., *Biomechanical properties of the costovertebral joint.* Med Eng Phys, 2010. **32**(2): p. 222-7.

27. Lemosse, D., et al., *Characterization of the mechanical behaviour parameters of the costo-vertebral joint.* Eur Spine J, 1998. **7**(1): p. 16-23.

28. Wilson, T.A., et al., *Geometry and respiratory displacement of human ribs.* J Appl Physiol (1985), 1987. **62**(5): p. 1872-7.

29. Andriacchi, T., et al., *A model for studies of mechanical interactions between the human spine and rib cage.* J Biomech, 1974. **7**(6): p. 497-507.

30. Schultz, A.B., D.R. Benson, and C. Hirsch, *Force-deformation properties of human costo-sternal and costo-vertebral articulations.* J Biomech, 1974. **7**(3): p. 311-8.

31. de Leva, P., *Adjustments to Zatsiorsky-Seluyanov's segment inertia parameters.* Journal of Biomechanics, 1996. **29**(9): p. 1223-1230.

32. Liu, Y.K., J.M. Laborde, and W.C. Van Buskirk, *Inertial properties of a segmented cadaver trunk: their implications in acceleration injuries.* Aerospace Medicine 1971. **42**(6): p. 650-7.

33. Pearsall, D., J. Reid, and L. Livingston, *Segmental inertial parameters of the human trunk as determined from computed tomography.* Annals of Biomedical Engineering, 1996. **24**(2): p. 198-210.

34. Stokes, I.A. and M. Gardner-Morse, *Quantitative anatomy of the lumbar musculature.* J Biomech, 1999. **32**(3): p. 311-6.

35. Garner, B.A. and M.G. Pandy, *Musculoskeletal model of the upper limb based on the visible human male dataset.* Comput Methods Biomech Biomed Engin, 2001. **4**(2): p. 93-126.

36. Garner, B.A. and M.G. Pandy, *Estimation of musculotendon properties in the human upper limb.* Ann Biomed Eng, 2003. **31**(2): p. 207-20.

37. Brown, S.H., et al., *Architectural analysis of human abdominal wall muscles: implications for mechanical function.* Spine (Phila Pa 1976), 2011. **36**(5): p. 355-62.

38. Thelen, D.G., *Adjustment of muscle mechanics model parameters to simulate dynamic contractions in older adults.* J Biomech Eng, 2003. **125**(1): p. 70-7.

39. Saumarez, R.C., *An analysis of action of intercostal muscles in human upper rib cage.* J Appl Physiol (1985), 1986. **60**(2): p. 690-701.

40. Wilson, T.A., et al., *Respiratory effects of the external and internal intercostal muscles in humans.* J Physiol, 2001. **530**(Pt 2): p. 319-30.

41. Hoffmann, U., et al., *Defining normal distributions of coronary artery calcium in women and men (from the Framingham Heart Study).* Am J Cardiol, 2008. **102**(9): p. 1136-41, 1141 e1.

42. Anderson, D.E., et al., *Regressions for estimating muscle parameters in the thoracic and lumbar trunk for use in musculoskeletal modeling.* Journal of Biomechanics, 2012. **45**: p. 66-75.

43. Narici, M.V., G.S. Roi, and L. Landoni, *Force of knee extensor and flexor muscles and cross-sectional area determined by nuclear magnetic resonance imaging.* Eur J Appl Physiol Occup Physiol, 1988. **57**(1): p. 39-44.

44. Pearcy, M.J. and N. Bogduk, *Instantaneous axes of rotation of the lumbar intervertebral joints.* Spine (Phila Pa 1976), 1988. **13**(9): p. 1033-41.

45. Andersson, G.B., R. Ortengren, and A. Nachemson, *Intradiskal pressure, intra-abdominal pressure and myoelectric back muscle activity related to posture and loading.* Clin Orthop Relat Res, 1977(129): p. 156-64.

46. Polga, D.J., et al., *Measurement of In Vivo Intradiscal Pressure in Healthy Thoracic Intervertebral Discs.* Spine, 2004. **29**(12): p. 1320-1324 10.1097/01.BRS.0000127179.13271.78.

47. Sato, K., S. Kikuchi, and T. Yonezawa, *In vivo intradiscal pressure measurement in healthy individuals and in patients with ongoing back problems.* Spine (Phila Pa 1976), 1999. **24**(23): p. 2468-74.

48. Schultz, A., et al., *Loads on the lumbar spine. Validation of a biomechanical analysis by measurements of intradiscal pressures and myoelectric signals.* The Journal of Bone & Joint Surgery, 1982. **64**(5): p. 713-720.

49. Takahashi, I., et al., *Mechanical load of the lumbar spine during forward bending motion of the trunk-a biomechanical study.* Spine (Phila Pa 1976), 2006. **31**(1): p. 18-23.

50. Wilke, H.-J., et al., *Intradiscal pressure together with anthropometric data - a data set for the validation of models.* Clinical Biomechanics, 2001. **16**(Supplement 1): p. S111-S126.

51. Rohlmann, A., et al., *Loads on a telemeterized vertebral body replacement measured in two patients.* Spine (Phila Pa 1976), 2008. **33**(11): p. 1170-9.

52. Crowninshield, R.D. and R.A. Brand, *A physiologically based criterion of muscle force prediction in locomotion.* J Biomech, 1981. **14**(11): p. 793-801.

53. Hughes, R.E., *Effect of optimization criterion on spinal force estimates during asymmetric lifting.* J Biomech, 2000. **33**(2): p. 225-9.

54. Dreischarf, M., et al., *Is it possible to estimate the compressive force in the lumbar spine from intradiscal pressure measurements? A finite element evaluation.* Med Eng Phys, 2013. **35**(9): p. 1385-90.

55. Nachemson, A., *Lumbar intradiscal pressure. Experimental studies on post-mortem material.* Acta Orthop Scand Suppl, 1960. **43**: p. 1-104.

56. Nachemson, A., *The load on lumbar disks in different positions of the body.* Clin Orthop Relat Res, 1966. **45**: p. 107-22.

57. de Zee, M., et al., *A generic detailed rigid-body lumbar spine model.* J Biomech, 2007. **40**(6): p. 1219-27.

58. Stokes, I.A., M.G. Gardner-Morse, and S.M. Henry, *Intra-abdominal pressure and abdominal wall muscular function: Spinal unloading mechanism.* Clin Biomech (Bristol, Avon), 2010. **25**(9): p. 859-66.

59. Cholewicki, J., P.C. Ivancic, and A. Radebold, *Can increased intra-abdominal pressure in humans be decoupled from trunk muscle co-contraction during steady state isometric exertions?* Eur J Appl Physiol, 2002. **87**(2): p. 127-33.

60. De Troyer, A. and A.M. Boriek, *Mechanics of the respiratory muscles.* Compr Physiol, 2011. **1**(3): p. 1273-300.

61. McGill, S.M. and M.T. Sharratt, *Relationship between intra-abdominal pressure and trunk EMG.* Clin Biomech (Bristol, Avon), 1990. **5**(2): p. 59-67.

62. Macintosh, J.E. and N. Bogduk, *The attachments of the lumbar erector spinae.* Spine (Phila Pa 1976), 1991. **16**(7): p. 783-92.

63. Boyle, J.J., N. Milne, and K.P. Singer, *Influence of age on cervicothoracic spinal curvature: an ex vivo radiographic survey.* Clin Biomech (Bristol, Avon), 2002. **17**(5): p. 361-7.

64. Bruno, A.G., et al., *The effect of thoracic kyphosis and sagittal plane alignment on vertebral compressive loading.* J Bone Miner Res, 2012. **27**(10): p. 2144-51.

65. Manns, R.A., et al., *The relative contribution of disc and vertebral morphometry to the angle of kyphosis in asymptomatic subjects.* Clinical Radiology, 1996. **51**(4): p. 258-262.

66. Shi, X., et al., *A statistical human rib cage geometry model accounting for variations by age, sex, stature and body mass index.* J Biomech, 2014. **47**(10): p. 2277-85.

67. Weaver, A.A., S.L. Schoell, and J.D. Stitzel, *Morphometric analysis of variation in the ribs with age and sex.* J Anat, 2014. **225**(2): p. 246-61.

Chapter 5: USING CT-BASED MEASUREMENTS OF TRUNK ANATOMY TO CREATE PATIENT-SPECIFIC MUSCULOSKELETAL MODELS OF THE SPINE

5.1 ABSTRACT

Musculoskeletal models of the spine can be used to predict *in vivo* trunk muscle forces and vertebral loads that occur during daily or occupational activities. However, most models do not account for individual variations in trunk anatomy, such as spine curvature and trunk muscle morphology, which may significantly influence loading predictions. The goals of this study were to 1) describe a set of methods to create subject-specific musculoskeletal models of the thoracolumbar spine by incorporating spine curvature and muscle morphology measurements from computed tomography (CT) scans and 2) to determine whether incorporation of subject-specific spine curvature and muscle morphology measurements alters vertebral loading predictions. To accomplish these goals, we measured spine curvature and muscle morphology from spine CT scans of 20 men and 20 women, and then created four sets of subject-specific models: 1) height and weight adjusted models (Ht/Wt models); 2) height, weight, and spine curvature adjusted models (+SC models); 3) height, weight, and muscle morphology adjusted models (+MM models); and 4) height, weight, spine curvature, and muscle morphology adjusted models (+SC/MM models). We found that vertebral compressive loads estimated from musculoskeletal models incorporating either spine curvature, muscle morphology, or both spine curvature and muscle morphology were substantially different from those estimated using musculoskeletal models adjusted for subject height and weight. Vertebral compressive loads predicted by the subject-specific CT-based models were between -25% to +50% different than the vertebral loads from the height- and weight-adjusted models, but this difference varied by subject, vertebral level, specific activity, and model type. In summary, we provide a robust method for rapid, automated generation of subject-specific musculoskeletal models of the thoracolumbar spine using CT-based measurements of spine curvature and trunk muscle morphology. Our results indicate that individual variations in spine curvature and muscle morphology must be accounted for when estimating subject-specific vertebral loading.

5.2 INTRODUCTION

Musculoskeletal models are useful tools for estimating the forces that occur on muscles, bones, and joints *in vivo* [1]. Models of the human spine and trunk are used to estimate spinal loads and trunk muscle forces during daily activities or occupational tasks, with the goals of understanding basic spine biomechanics, evaluating risk of injury, or optimizing the performance of a particular activity. Prior studies have typically used generic musculoskeletal models of the spine that do not incorporate subject-specific traits that may influence the model outcomes. The degree of anatomical detail incorporated into these models varies widely, from simple sagittally symmetric models with a lumped spinal extensor muscle group at a fixed distance from the spine [2], to sophisticated three-dimensional models with numerous muscle fascicles, realistic skeletal anatomy, and multiple degrees of freedom [3, 4]. Models that are more anatomically realistic were developed to improve the accuracy of trunk loading predictions. However, the utility of these models is still limited by their generic nature. Factors such as body mass, trunk muscle morphology, and spine curvature vary markedly between individuals and will have a strong effect on the *in vivo* loads generated by the trunk muscles and applied to the spine [5]. Subject-specific models will be necessary to investigate how variations in trunk anatomy influence trunk loading patterns, and will ultimately provide insights into the differential risk of spine injury and back pain that exists in the population.

Medical imaging, such as computed tomography (CT) or magnetic resonance imaging (MRI), can provide subject-specific measures of trunk muscle morphology and spine curvature that can, in theory, be incorporated into a subject-specific model. However, prior efforts to incorporate imaging-based measures of trunk anatomy into spine models have been limited. For instance, a few studies have incorporated subject-specific spine curvature [6-8] into models already scaled for height and weight, but no studies have incorporated subject-specific trunk muscle morphology, although prior studies have incorporated subject-specific muscle measures into models of the lower extremity [9]. Other studies have used muscle morphology parameters predicted by regression to adjust their models [10-12], which will not be as accurate as using subject-specific measurements.

Therefore, the objectives of the current study were: 1) to describe a set of methods for creating subject-specific spine models using measures of spine curvature and muscle morphology derived from clinical CT images of the trunk, and 2) to determine whether individual variations in spine curvature and muscle morphology influence vertebral loading predictions.

5.3 MATERIALS AND METHODS

5.3.1 BASELINE MUSCULOSKELETAL SPINE MODELS

Subject-specific spine models were created by adjusting either a baseline 50th percentile male (Fig. 5.1) or female model. The development and validation of the male version of the model was described in detail previously [13][Chapter 4]. In brief, the male model was created using OpenSim musculoskeletal modeling software [1], and includes a fully articulated thoracolumbar spine and rib cage, a lumped head and neck body, and the upper extremities. The skeletal anatomy was based on CT scans of a 25 year old 50th percentile male (Height = 175 cm, Weight = 78 kg) taken from the OpenSim geometry file library [1, 14]. The positions and orientations of the vertebrae, defining the curvature of the spine, were based on average measurements available in the literature [15, 16], and the size and shape of the rib cage were derived from previously published morphometric equations [17]. The female version of the model was created by scaling the size and weight of the body segments in the male model to match a 50th percentile female (Height = 163 cm, Weight = 61 kg) [14].

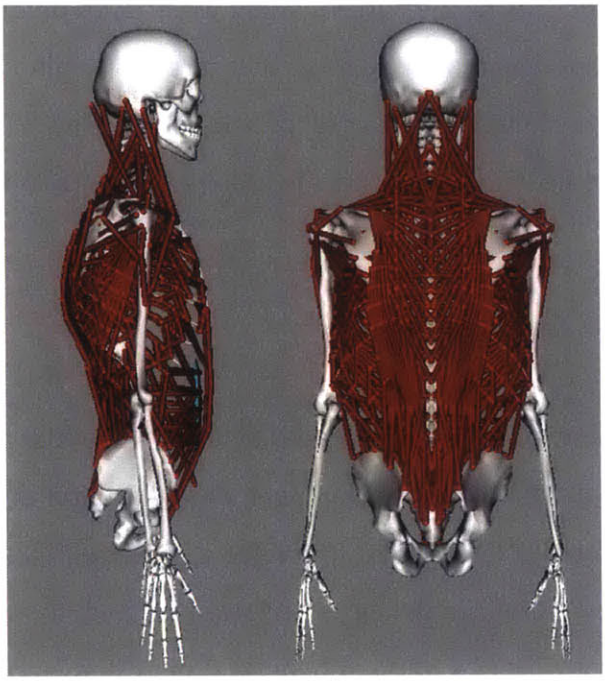

Figure 5.1: Medial-lateral and anterior-posterior views of the baseline 50th percentile male musculoskeletal model used in this study. The model includes a fully articulated thoracolumbar spine and rib cage, a lumped head and neck body, upper extremities, and 552 Hill-type muscle fascicles. The curvature of the spine in the model was set based on average measurements available in the literature, and has a T4-T12 Cobb angle of 42° and a L1-L4 Cobb angle of 25° [15, 16].

The major muscles that attach to the trunk were incorporated into the models using 552 individual Hill-Type muscle fascicles [18], simulating the detailed anatomy and multi-level attachments of these muscle groups (Fig. 5.1). In each baseline model, muscle group cross-sectional area and position were adjusted to match average CT-based measures of muscle cross-sectional area and position made in a sample of older males and females [13][Chapter 4]. The algorithms used to adjust muscle group cross-sectional area and position were described in detail previously [13][Chapter 4], and were used in the current study to create subject-specific models adjusted using each individual's CT-based measurements of muscle morphology (muscle measurement procedure described later).

5.3.2 *Subjects and acquisition of 3D-QCT scans of the trunk*

Subject-specific models were created for a sample of 20 men and 20 women from the Framingham Heart Study (FHS) Multidetector CT Study, a community-based study in which participants had previously acquired abdominal and thoracic CT scans to measure coronary,

aortic, and valvular calcium [19]. The CT scans were acquired using an 8-detector helical QCT scanner (Lightspeed Plus, General Electric, Milwaukee, WI), with the following scan settings: 120 kVP, 320 mAs, in-plane pixel size = 0.68 x 0.68 mm, and slice thickness of 2.5 mm. The scans included lateral 2D scout views extending from the upper thoracic (T4) to sacral (S1) vertebral levels, and these images were used to measure spine curvature in each subject (described later). The thoracic scan was set to image approximately vertebral levels T6 – T12 and the abdominal scan was set to image approximately vertebral levels L1 – L4. We randomly selected 20 men and 20 women from the subset of Framingham Heart Study participants (n=2109) in whom all spine levels between T6 and L4 were included in their scans (Table 5.1). These subjects did not differ in age, height, weight, or sex from the larger group of Framingham Heart Study participants who underwent CT scans.

Table 5.1: Characteristics of the 40 subjects selected from the Framingham cohort and used in this study to create subject-specific models using CT-based measurements of trunk anatomy.

	Men (N=20)		**Women (N=20)**	
	Mean ± SD	Range	Mean ± SD	Range
Age (yrs)	55.1 ± 13.4	41 - 83	60.9 ± 11.5	45 - 89
Height (cm)	174.2 ± 6.4	163.2 - 187.3	159.6 ± 6.8	148.6 - 175.3
Weight (kg)	85.5 ± 12.1	62.6 - 109.3	73.1 ± 16.1	56.2 - 127.0
T4-T12 Cobb Angle (°)	33.6 ± 10.8	14.4 - 52.8	39.3 ± 9.8	22.6 - 59.1
L1-L4 Cobb Angle (°)	14.4 ± 6.6	2.2 - 26.4	23.6 ± 10.3	9.0 - 40.6

5.3.3 HEIGHT AND WEIGHT ADJUSTED MODELS

For the 40 subjects, we used the OpenSim scale tool to create subject-specific models in which the length and weight of the body segments were scaled by patient height and weight (Ht/Wt models). Building from these height and weight-adjusted models, we then created three additional sets of subject-specific models that incorporated CT-based measures of 1) spine curvature (+SC models), 2) muscle morphology (+MM models), or 3) spine curvature and muscle morphology (+SC/MM models).

5.3.4 SPINE CURVATURE MEASUREMENTS/MODEL ADJUSTMENT

Spine curvature was measured in all Framingham Heart Study participants (n=2109) using a semi-automated program (SpineAnalyzer, Optasia Medical, Cheadle, UK) which places six morphometry points around each vertebral body from T4 to L4 on the lateral CT scout views (Fig. 5.2a). The coordinates of these points were then used to compute thoracic kyphosis (T4-T12 Cobb angle) and lumbar lordosis (L1-L4 Cobb angle) in each subject. The placement of the morphometry points was shown previously to have excellent intra- and inter-reader reliability, with intraclass correlation coefficients (ICCs) greater than 0.95 [20]. In 20 randomly selected Framingham Heart Study participants (10 men and 10 women, age range of 35 to 75 years), we performed another reliability study for the curvature measures, which were computed using the morphometry points. Curvature was measured twice by two readers, and we determined the intra-reader and inter-reader reliability was excellent for both the T4-T12 Cobb angle (ICCs = 0.98 and 0.97, respectively) and for the L1-L4 Cobb angle (ICCs = 0.87 and 0.81, respectively).

In addition to calculating Cobb angles with the morphometry points from SpineAnalyzer, we also used these vertebral morphometry points to create OpenSim musculoskeletal models with subject-specific spine curvatures. In each patient, we used the morphometry points surrounding the intervertebral discs (T4-T5 to L3-L4) to find disc centroid locations. In a model that was already scaled to match a patient's height and weight, we then adjusted the locations of the intervertebral joints in the model (located at the disc centroids) to match the disc centroids measured from CT, thus creating a model that was adjusted for height, weight, and spine curvature (+SC models). In a small number of cases, we were unable to place vertebral morphometry points because of poor visualization (ie: scan quality, the presence of large osteophytes). In these cases, we estimated the location of the missing disc centroid(s) by fitting a cubic spline to the location of the other disc centroids, and estimating the position of the missing centroid as a point on the spline mid-way between its adjacent discs.

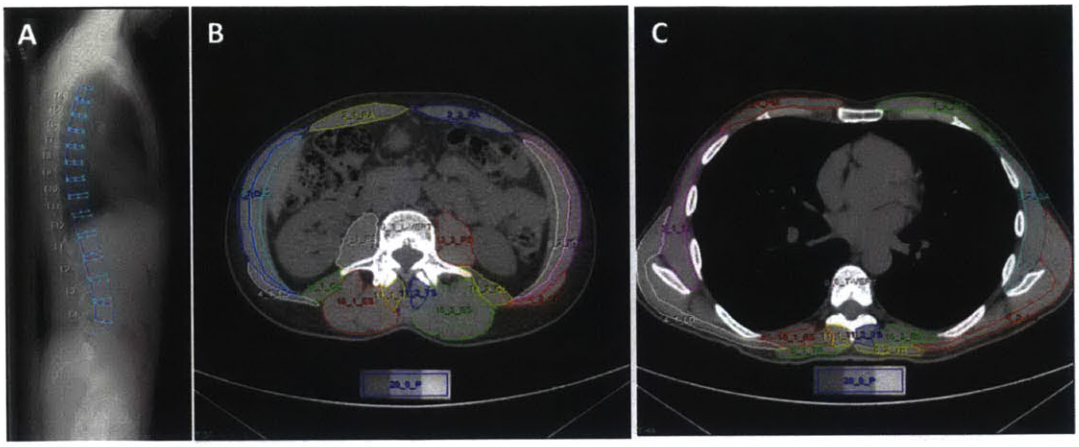

Figure 5.2: A) An example spine curvature measurement made on a lateral CT-scout image using a semi-automated contouring program called SpineAnalyzer (Optasia Medical, Cheadle, UK). The program places six standard morphometry points around each vertebral body (T4 to L4), and we used these points to calculate Cobb angles (T4-T12 and L1-L4) and to set the curvature of the spine in subject-specific musculoskeletal models. B) Example muscle measurements performed on an axial CT image at the L3 vertebral mid-plane. The major muscle groups were contoured by a reader, allowing us to compute muscle cross-sectional areas, medial-lateral moment arms, and anterior-posterior moment arms. C) Similarly, an example of muscle contours made in the thoracic region, specifically at the T8 vertebral mid-plane. Muscle measurements were performed at all vertebral mid-planes for which we had CT-coverage in all patients (T4 to L4).

5.3.5 *Muscle morphology measurements/model adjustment*

Cross-sectional areas and positions of the trunk muscles were measured from transverse CT scans using a commercial image processing platform (Analyze, Biomedical Imaging Resource, Rochester, MN) that we customized for this purpose [21]. We performed measurements on pectoralis major, rectus abdominis, serratus anterior, latissimus dorsi, trapezius, external and internal obliques, erector spinae, multifidus, psoas major, and quadratus lumborum at each vertebral mid-plane from T6 to L4 (Table 5.2).

Table 5.2: This table shows which muscle groups were present/measured at each vertebral level. Measurements were performed on the axial CT slice closest to each vertebral mid-plane.

	T6	T7	T8	T9	T10	T11	T12	L1	L2	L3	L4
Pectoralis Major	✓	✓	✓	✓							
Rectus Abdominis					✓	✓	✓	✓	✓	✓	✓
Serratus Anterior	✓	✓	✓	✓	✓	✓					
Latissimus Dorsi	✓	✓	✓	✓	✓	✓	✓	✓	✓	✓	
Trapezius	✓	✓	✓	✓	✓	✓					
External Oblique				✓	✓	✓	✓	✓	✓	✓	✓
Internal Oblique									✓	✓	✓
Erector Spinae	✓	✓	✓	✓	✓	✓	✓	✓	✓	✓	✓
Multifidus	✓	✓	✓	✓	✓	✓	✓	✓	✓	✓	✓
Psoas Major								✓	✓	✓	✓
Quadratus Lumborum								✓	✓	✓	✓

Briefly, each CT image was spatially filtered to reduce noise and preserve edges [22], and then each muscle was contoured using a semi-automated approach at each mid-vertebral slice (Fig. 5.2b and c). Muscle size was calculated as cross-sectional area (CSA) within the muscle contour, and moment arms were computed as the anterior-posterior (AP) and medial-lateral (ML) distances between the muscle and vertebral body centroids. To determine intra- and inter-reader reliability of the muscle measurements, two readers each performed two sets of measurements in randomly selected Framingham Heart Study participants in the thoracic region (at T7, T8, and T12 in 10 men and 10 men, age range of 50 to 73 years) and in the lumbar region (at L2, L3, and L4 in 5 men and 5 women, age range of 40 to 85 years). We found that 77-100% of thoracic muscle measures and 83-100% of lumbar muscle measures had ICCs greater than 0.75.

For each patient, we used CT-based measures of muscle CSA and AP/ML moment arm to adjust the muscles in an OpenSim model that had already been adjusted for height and weight (+MM models). In our baseline model, the CSA of each trunk muscle is multiplied by a constant maximum muscle stress of 100 N/cm^2 to determine maximum isometric strength. Each muscle group in the model consists of multiple fascicles that may span different levels of the spine; however our CT-based measures are restricted to just the muscle groups, and cannot resolve the CSA and moment arm of individual fascicles. Therefore, we developed algorithms (described in detail previously [13][Chapter 4] to adjust muscle groups in the model (consisting

of multiple fascicles) by muscle group measurements from CT. We were unable to adjust the CSA or moment arm of certain muscle groups that formed a large oblique angle with the transverse plane of the model. For instance, we were unable to adjust the CSA and moment arms of the serratus anterior and pectoralis major because these fascicles were primarily oriented parallel to the transverse plane in the model, whereas our muscle measurements were made within the transverse plane on CT. Similarly, we were unable to adjust the moment arms of the external and internal obliques and the latissimus dorsi, but we were able to adjust the CSA of these groups. For the erector spinae, multifidus, trapezius, psoas major, and quadratus lumborum we were able to adjust both CSA and anterior-posterior and medial-lateral moment arms.

Finally, we created a set of models that were scaled for height, weight, and both spine curvature and muscle morphology (+SC &MM models). This was done by adjusting muscle morphology in models that had already been adjusted for height, weight, and spine curvature. Therefore, each subject had a total of four subject-specific models: Ht/Wt model, +SC model, +MM model, and +SC/MM model.

5.3.6 Accuracy of muscle morphology adjustment

In the models adjusted using all available subject-specific parameters (+SC/MM), we computed 'model-equivalent' muscle group CSAs and moments arms at each vertebral mid-plane by summing the CSAs of the individual fascicles crossing the mid-plane of each vertebral body, and then computing the AP and ML moment arms between vertebral body centroid and fascicle centroid within the mid-plane [13][Chapter 4]. These model-equivalent muscle group CSAs and moment arms (for all subjects, muscle groups, and spine levels) were then correlated with the actual CT measurements of CSA and moment arm that we were trying to match with our adjustment algorithm. We also performed this comparison between 'model-equivalent' and measured muscle parameters in the set of models adjusted for height, weight, spine curvature, but not muscle morphology (+SC). This would allow us to test whether our muscle adjustment process was improving the biofidelity of the models. Further, because prior studies have used trunk muscle CSAs and moment arms predicted by regression to adjust their musculoskeletal models, we created an additional set of models adjusted to match CSAs and

moments predicted using previously published regressions [10]. These regressions use each subject's age, sex, height, and weight to predict CSA and ML/AP moments arms for the same muscles and spine levels for which we have measured muscle data (Table 5.2). Models were adjusted to match the regression estimates using the same algorithms we used to adjust based on the measured muscle data. We hypothesized that we would observe the strongest correlation and lowest root mean square error (RMSE) between model-equivalent and measured muscle parameters for the +SC/MM models, followed by the regression-adjusted models, and finally the +SC models.

5.3.7 *Subject-specific vertebral loading predictions*

For each subject-specific model, we estimated vertebral loading at T8, T12, and L3 for four different activities: 1) neutral standing, 2) standing with 10 kg weights in each hand and elbows flexed 90°, 3) 40° trunk flexion while holding 5 kg weights in each hand, and 4) 10° trunk lateral bending to the right while holding a 5 kg weight in the right hand. For each activity, we used an optimization routine to determine the pattern of muscle forces that would maintain static equilibrium while at the same time minimizing the sum of cubed muscle activations, which is equivalent to maximizing muscle endurance (40 subjects x 4 models per subject x 4 activities per model = 640 simulations/optimizations) [23, 24].

5.3.8 *Data Analysis*

To determine whether incorporating CT-based measures of spine curvature and muscle morphology into musculoskeletal spine models influenced vertebral loading predictions, we compared vertebral loading estimates from the three CT-based musculoskeletal models to loading estimates derived from models adjusted only for height and weight. For each subject, we computed the percent differences and root mean square (RMS) differences in vertebral loading (at T8, T12, and L3) between the Ht/Wt-adjusted models and each CT-based model (+SC, +MM, +SC/MM).

For the models incorporating subject-specific spine curvatures (+SC and +SC/MM), we tested whether the difference between an individual's measured spine curvature and the curvature in the Ht/Wt model (TK = 42°, LL = 25°) was associated with the difference in

vertebral loading estimates between the Ht/Wt and CT-based models. To accomplish this, we performed a multiple regression analyses where the dependent variables were the difference in vertebral loading between the Ht/Wt models and either the +SC models or the +SC/MM models (at T8, T12, and L3 for the four activities). The independent variables were the differences in TK and LL (measured - baseline).

5.4 Results

5.4.1 Spine curvature adjustment

Thoracic kyphosis and lumbar lordosis varied significantly among subjects. Figure 5.3 shows the distributions of T4-T12 and L1-L4 Cobb angles in the sample of men and women, and how these distributions compared to the Cobb angles used in our baseline musculoskeletal model. For each subject, we were successfully able to incorporate the CT-based measures of spine curvature into subject-specific musculoskeletal models by matching the model-intervertebral joint locations to disc centroid locations measured from CT. Figure 5.4 shows example spine curvature measurements, and the corresponding models adjusted for spine curvature, from two subjects at the extremes of the TK distribution.

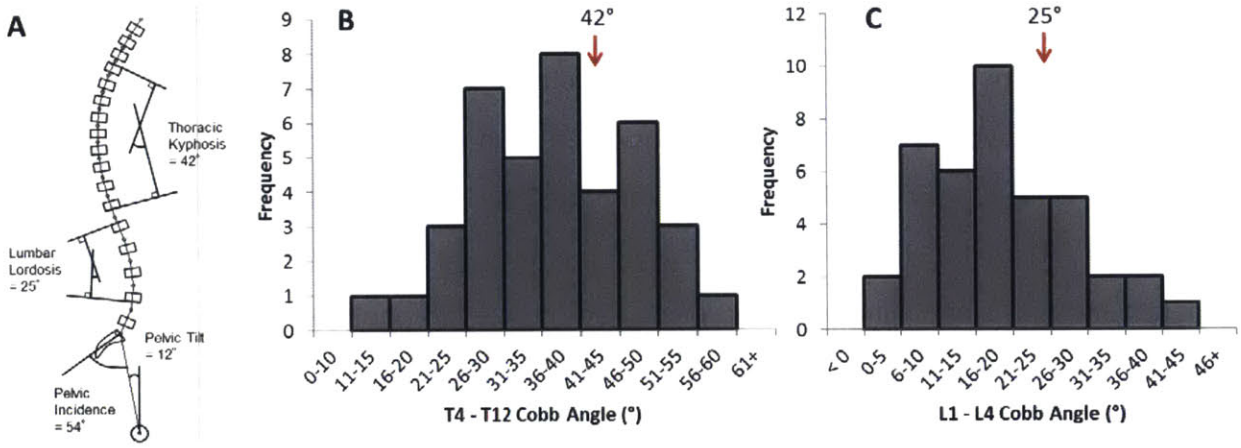

Figure 5.3: A) Generic spinal curvature used in our baseline spine model; B) Distribution of thoracic kyphosis (T4-T12 Cobb angle) and C) lumbar lordosis (L1-L4 Cobb angle) in 40 Framingham cohort members. There is significant variation in both thoracic kyphosis and lumbar lordosis, and the generic spine curvature used in our baseline model captures only a small slice of this variation.

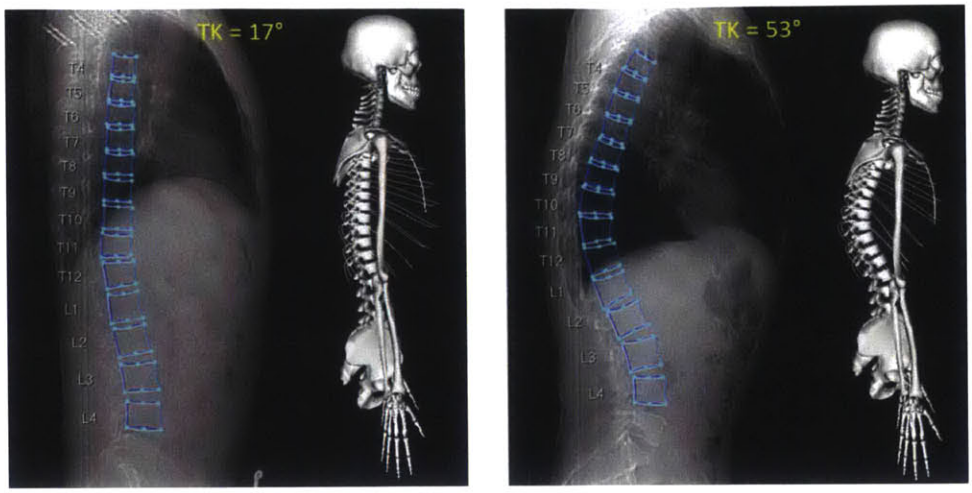

Figure 5.4: Spine curvature measurements were used to adjust spine curvature in OpenSim musculoskeletal models. Left) a subject with low thoracic kyphosis (TK), and Right) a subject with high thoracic kyphosis.

5.4.2 *Muscle morphology adjustment*

In the spine models adjusted for height, weight, and spine curvature (+SC) there were moderate to strong correlations between model-equivalent and measured trunk muscle CSAs (R^2 = 0.77) (Fig. 5.5), ML moment arms (R^2 = 0.91) (Fig. 5.6), and AP moment arms (R^2 = 0.97) (Fig. 5.7). However, the root mean square errors (RMSEs) between model-equivalent and measured muscle parameters were large: RMSE = 4.82 cm^2 for CSA, RMSE = 0.66 cm for ML moment arm, and RMSE = 1.03 cm for AP moment arm. In the spine models adjusted for height, weight, spine curvature, and muscle morphology predicted from regression, the correlations and RMSEs comparing model-equivalent and measured muscle parameters were slightly improved: R^2 = 0.82, RMSE = 4.30 cm^2 for CSA; R^2 = 0.96, RMSE = 0.45 cm for ML moment arm; R^2 = 0.99, RMSE = 0.60 cm for AP moment arm. For the spine models adjusted for height, weight, spine curvature, and measured muscle morphology (+SC/MM) there was a larger improvement in the correlations and RMSEs comparing model-equivalent to measured muscle parameters: R^2 = 0.92, RMSE = 2.67 cm^2 for CSA; R^2 = 0.99, RMSE = 0.26 cm for ML moment arm; R^2 = 0.99, RMSE = 0.26 cm for AP moment arm. Supplemental Tables 5.1 to 5.3 show RMSEs by muscle group and spine level for the +SC models versus CT-measurements and the +SC/MM models versus CT-measurements.

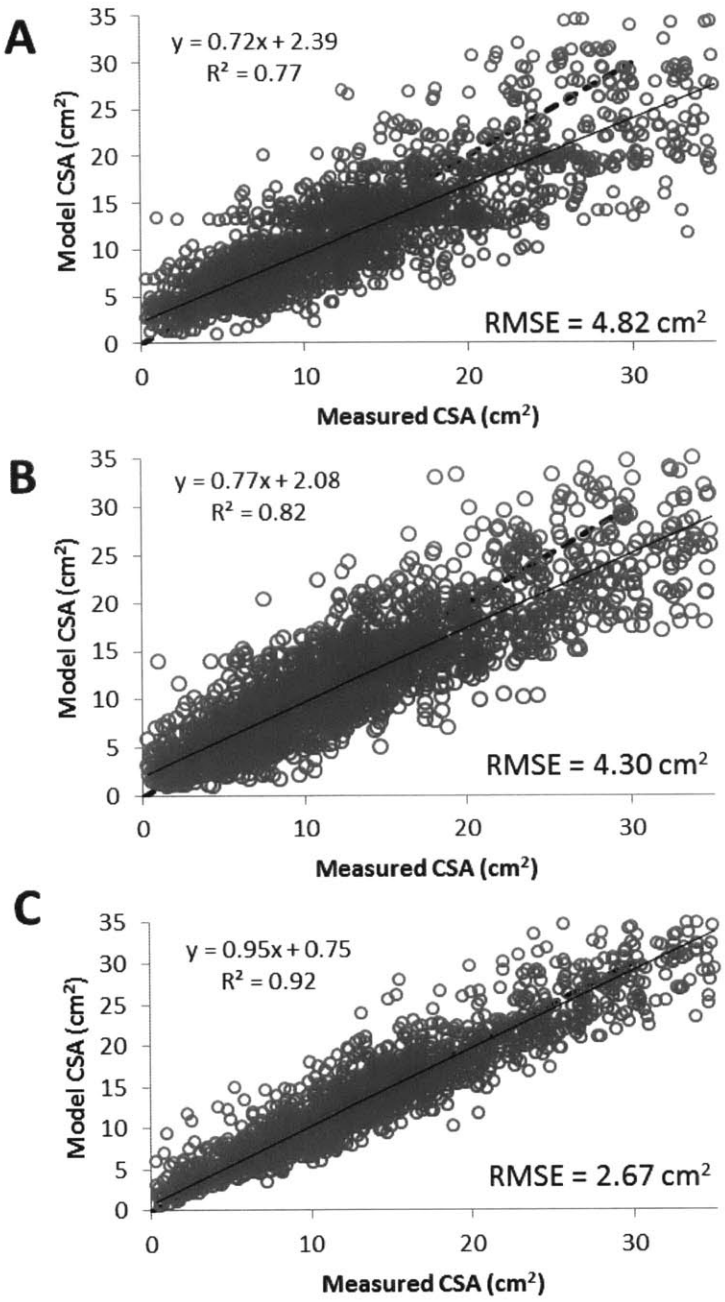

Figure 5.5: Comparison of CT-measured muscle group CSAs and model-equivalent muscle CSAs in A) the +SC models (no muscle adjustment), B) the regression-adjusted models, and C) the +SC/MM models.

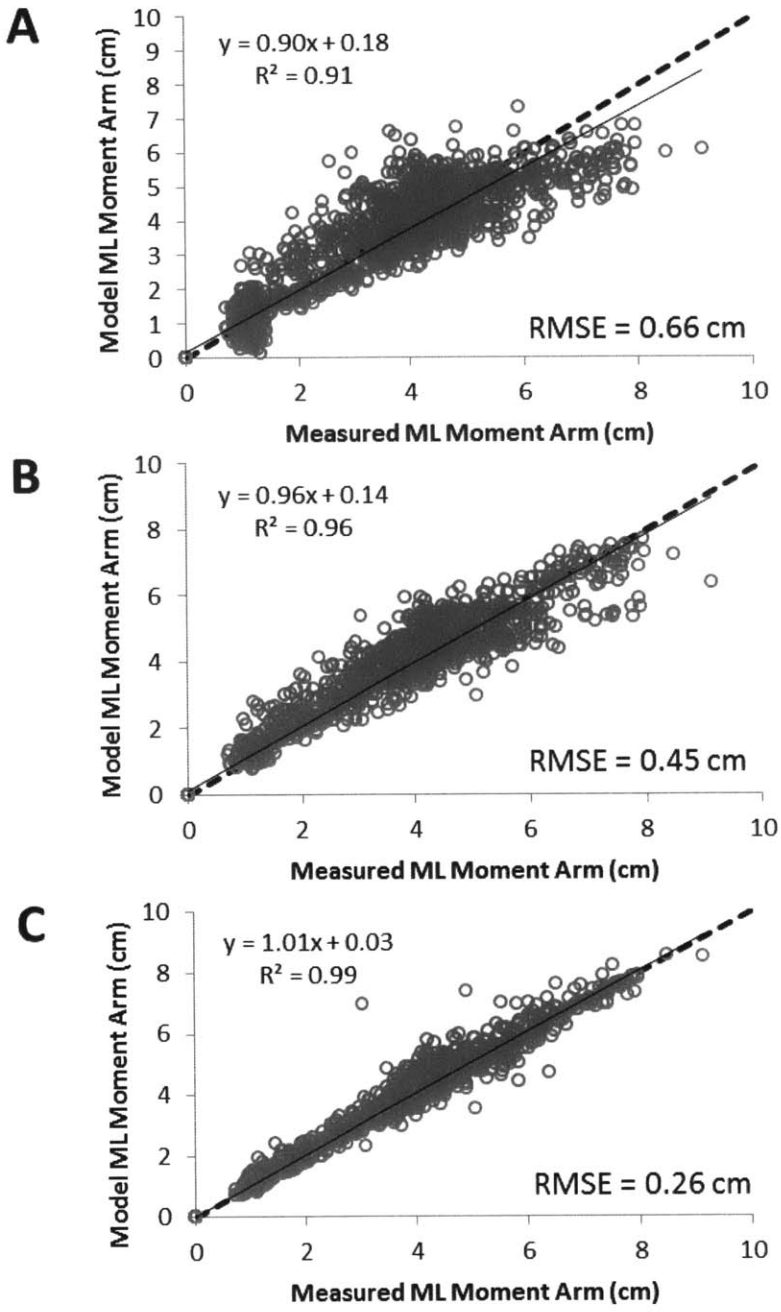

Figure 5.6: Comparison of CT-measured muscle group medial-lateral moment arms and model-equivalent medial-lateral moment arms in A) the +SC models (no muscle adjustment), B) the regression-adjusted models, and C) the +SC/MM models.

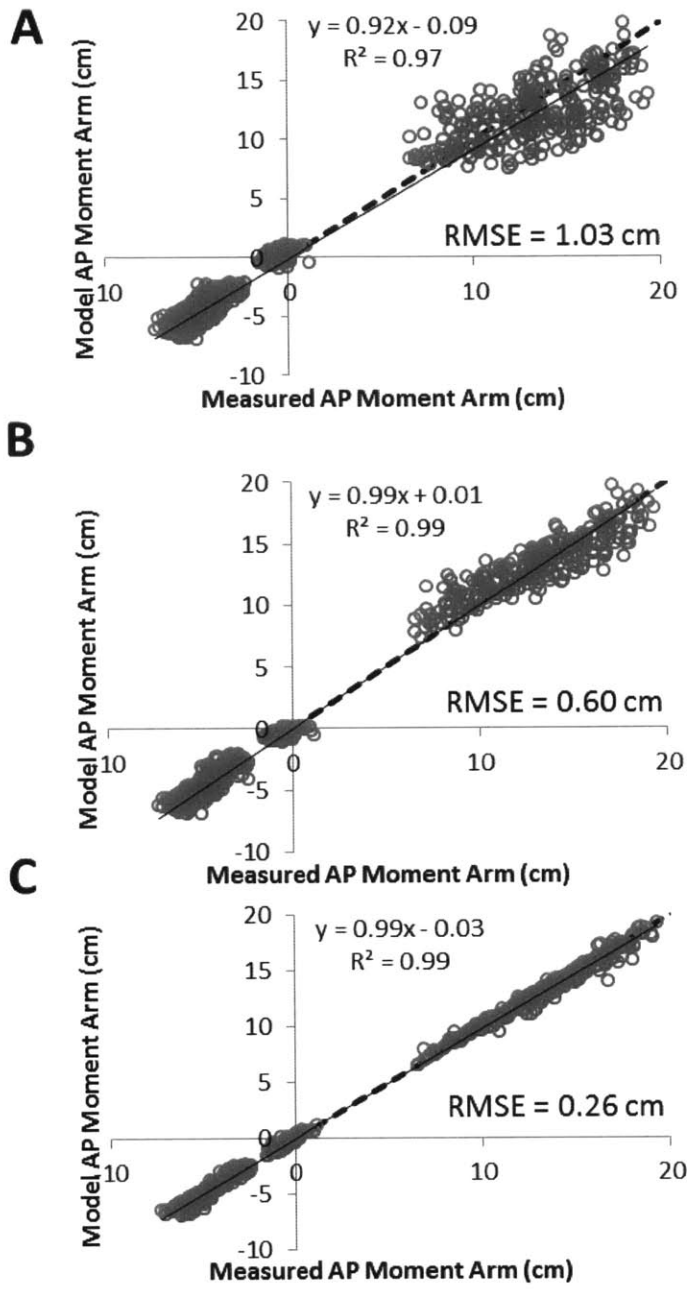

Figure 5.7: Comparison of CT-measured muscle group anterior-posterior moment arms and model-equivalent anterior-posterior moment arms in A) the +SC models (no muscle adjustment), B) the regression-adjusted models, and C) the +SC/MM models.

5.4.3 *Subject-specific vertebral loading*

Vertebral compressive loads (mean ± standard deviation) are presented for the three CT-based models (+SC, +MM, +SC/MM) and the models adjusted only for height and weight

(Ht/Wt) (Table 5.3). Vertebral loads were highest for standing with weight (10 kg in each hand with the elbows flexed 90°), followed by 40° trunk flexion with weight (5 kg in each hand), followed by 10° trunk lateral bending with weight (5 kg in the right hand), and finally neutral standing. Vertebral loads were higher in men than women, and the highest vertebral loads occurred at T12, followed by L3, and then T8.

Table 5.3: Vertebral loads (mean ± standard deviation, in N) from the CT-based models and the height and weight adjusted models.

	Standing		Standing with Weights		Trunk Flexion with Weights		Trunk Lateral Bending with Weight	
	Men	Women	Men	Women	Men	Women	Men	Women
T8 (N)								
Ht/Wt	369 ± 51	318 ± 71	1461 ± 58	1429 ± 84	902 ± 90	829 ± 128	611 ± 58	507 ± 78
+SC	334 ± 63	302 ± 76	1428 ± 114	1314 ± 158	882 ± 97	760 ± 129	572 ± 61	489 ± 81
+MM	380 ± 50	314 ± 69	1535 ± 88	1431 ± 132	966 ± 97	836 ± 140	617 ± 59	506 ± 70
+SC/MM	342 ± 57	307 ± 76	1487 ± 131	1340 ± 187	932 ± 99	777 ± 135	572 ± 62	490 ± 73
T12 (N)								
Ht/Wt	494 ± 68	417 ± 94	2234 ± 85	2131 ± 117	1591 ± 160	1397 ± 220	802 ± 79	652 ± 105
+SC	451 ± 81	398 ± 106	2102 ± 153	1894 ± 225	1462 ± 158	1234 ± 227	731 ± 74	606 ± 110
+MM	500 ± 64	414 ± 92	2269 ± 100	2091 ± 136	1621 ± 149	1376 ± 209	801 ± 72	646 ± 97
+SC/MM	452 ± 74	399 ± 108	2110 ± 201	1857 ± 277	1478 ± 150	1217 ± 230	727 ± 72	603 ± 106
L3 (N)								
Ht/Wt	401 ± 55	341 ± 77	1861 ± 72	1780 ± 99	1585 ± 164	1371 ± 223	631 ± 63	529 ± 86
+SC	416 ± 65	352 ± 89	1878 ± 110	1686 ± 169	1598 ± 136	1348 ± 239	638 ± 58	529 ± 95
+MM	401 ± 55	341 ± 77	1868 ± 84	1756 ± 128	1589 ± 153	1352 ± 225	625 ± 60	525 ± 83
+SC/MM	413 ± 60	350 ± 88	1847 ± 141	1643 ± 213	1575 ± 136	1313 ± 249	627 ± 56	528 ± 93

Although the average vertebral loads predicted by the different sets of models did not vary greatly (Table 5.3), there were large differences between model types for individual subjects (Fig. 5.8). Because some subjects had an increase in loading after incorporation of CT-based spine curvature and muscle morphology measures and others had a decrease in loading, this caused the average difference in vertebral loading predictions between model types to be small, and almost zero in some cases. For example, for neutral standing vertebral loads predicted by the +SC/MM models at T12 were -25% to +50% (-113 N to +228 N) different than the Ht/Wt model predictions, depending on the subject (Fig. 5.8). For standing with weights, the loading differences at T12 for the +SC/MM models versus the Ht/Wt models ranged from -29% to +32% (-633 N to +698 N).

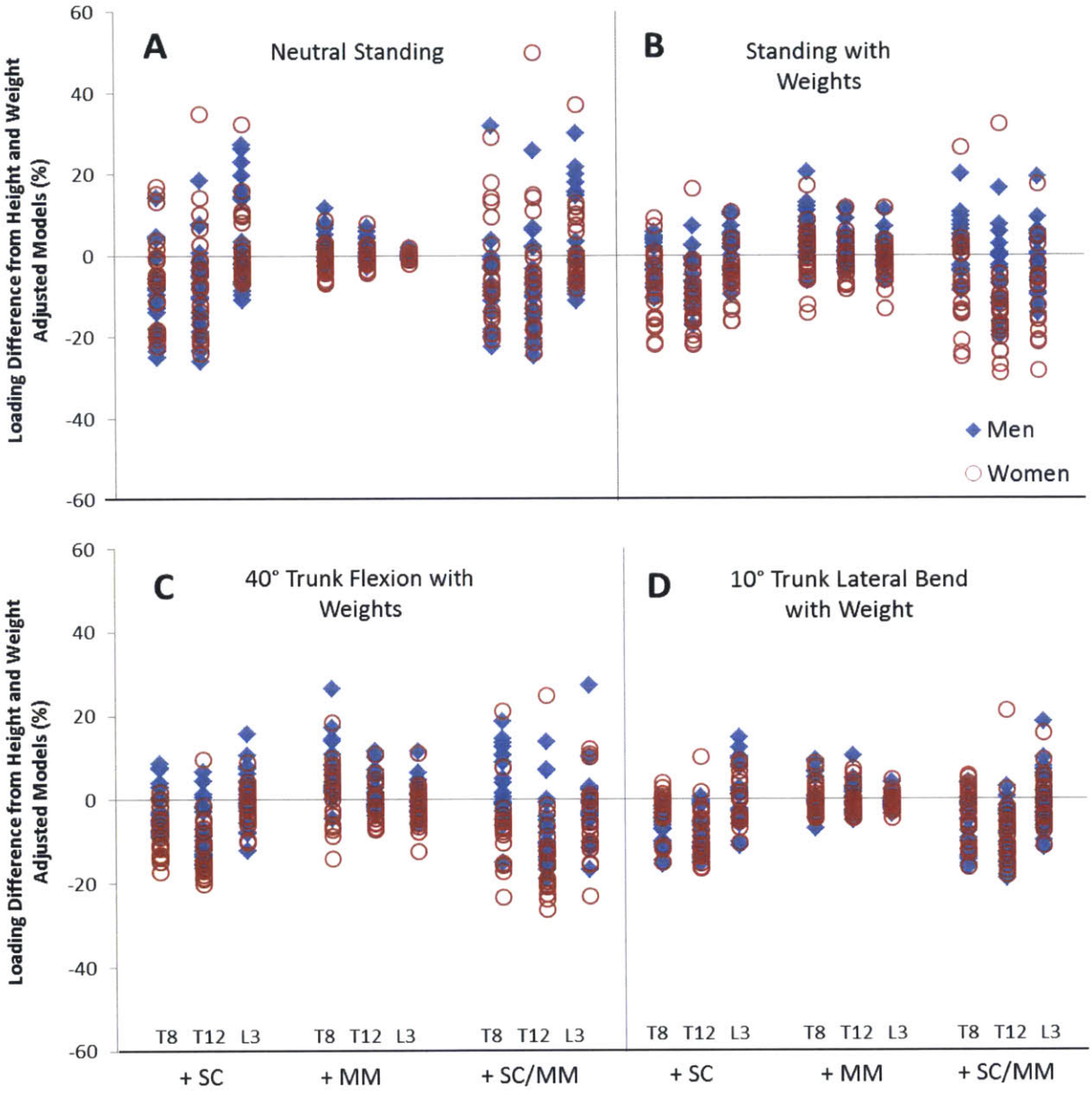

Figure 5.8: For the 40 subjects in this study, we computed the differences in vertebral compressive loading between a set of models adjusted for height and weight only (Ht/Wt), and 1) a set of models adjusted for height, weight and spine curvature (+SC), 2) a set of models adjusted for height, weight, and muscle morphology (+MM), and 3) a set of models adjusted for height, weight, spine curvature, and muscle morphology (+SC & +MM). Loading differences are reported as percent change from the Ht/Wt models. Loading differences at T8, T12, and L3 are shown for A) neutral standing, B) standing while holding a load (elbows flexed 90° with 10 kg in each hand), C) 40° trunk flexion while holding 5 kg in each hand, and D) 10° trunk lateral bending to the right, with 5 kg in the right hand.

The RMS differences between CT-based model predictions and the Ht/Wt model predictions were large, and generally higher for the models incorporating spine curvature

rather than muscle morphology only (Table 5.4). Furthermore, the RMS differences were higher for the more strenuous activities, such as standing with weights in the hands, which produced the highest vertebral loads. The highest RMS differences between CT-based models and the Ht/Wt models occurred in the women for the standing with weights activity (RMS difference = 300 N for the +SC vs Ht/Wt models; RMS difference = 376 N for the +SC/MM models vs Ht/Wt models).

Table 5.4: Root mean square differences (N) between vertebral loads from the CT-based models and the height and weight adjusted models.

	Standing		Standing with Weights		Trunk Flexion with Weights		Trunk Lateral Bending with Weight	
	Men	Women	Men	Women	Men	Women	Men	Women
T8 (N)								
+SC	49	40	82	171	54	83	47	33
+MM	17	13	111	98	86	59	25	18
+SC/MM	47	44	110	187	77	94	55	39
T12 (N)								
+SC	68	57	191	300	173	190	82	63
+MM	15	12	108	113	78	68	29	21
+SC/MM	69	68	237	376	173	232	90	74
L3 (N)								
+SC	52	33	111	158	108	72	46	31
+MM	3	3	76	90	64	64	12	11
+SC/MM	50	35	152	228	140	130	46	34

5.4.4 *THE ASSOCIATION BETWEEN SPINE CURVATURE AND VERTEBRAL LOADING*

The multiple regression analyses relating differences in thoracic kyphosis and lumbar lordosis (+SC models vs Ht/Wt models and +SC/MM models vs Ht/Wt models) to vertebral loading differences varied by activity and level, generally showing weak to moderate associations (Fig. 5.9). The strongest associations occurred for trunk flexion while holding weights (R^2 = 0.52 for difference in T8 Load), and associations were generally stronger at T8 compared to T12 and L3. The change in LL was more often a significant predictor of loading differences than the change in TK. In general, there was a trend that higher TK (more curvature compared to the baseline model) and lower LL (less curvature compared to the baseline model) resulted in higher loads compared to the baseline Ht/Wt model.

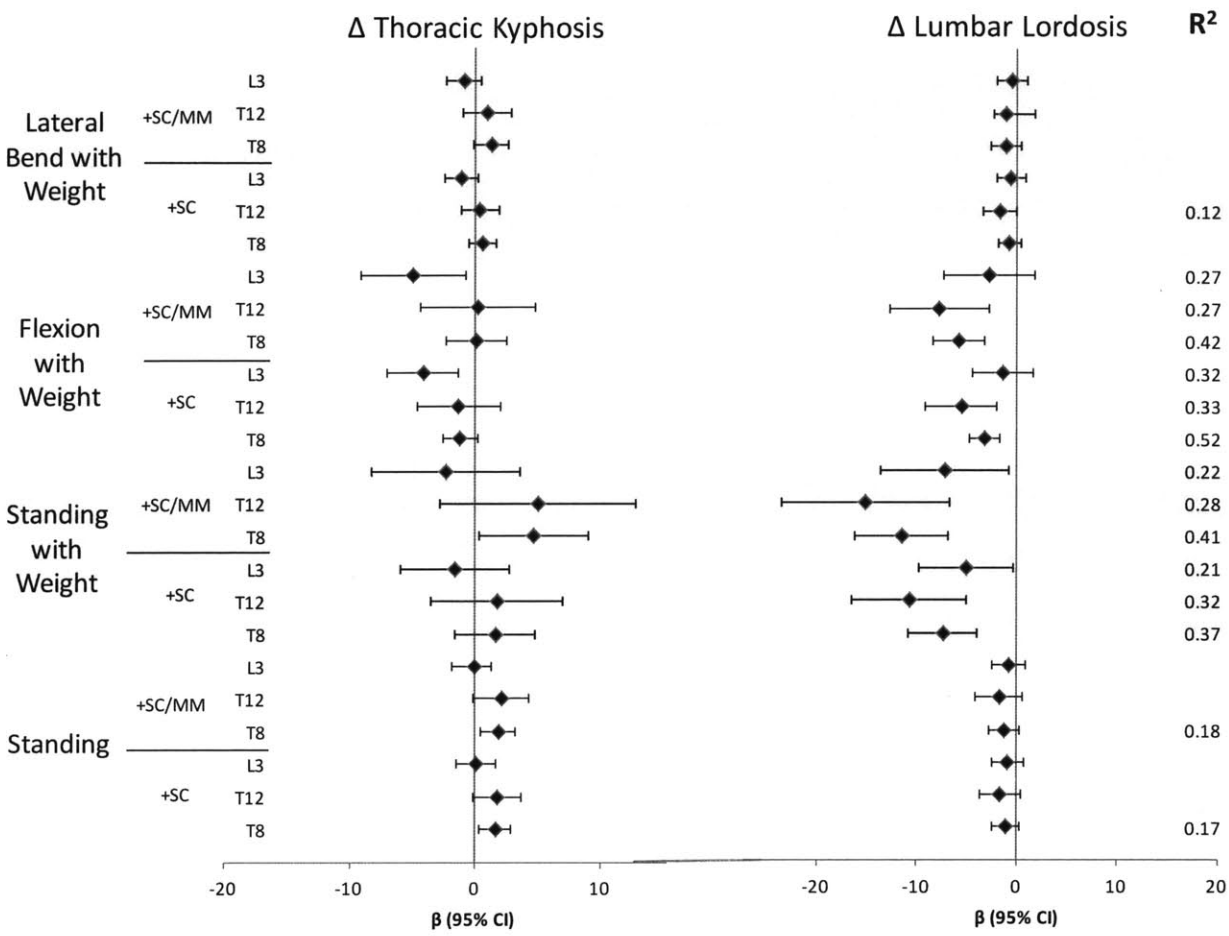

Figure 5.9: Multiple regression analysis was used to determine if the subject-specific difference in thoracic kyphosis and lumbar lordosis between the +SC and +SC/MM models and the baseline Ht/Wt model is associated with the difference in vertebral loading estimated by the models.

5.5 Discussion

In this study we describe a set of methods for using CT-based measurements of spinal curvature and muscle morphology to generate subject-specific musculoskeletal models of the thoracolumbar spine. We used these models to make 40 subject-specific thoracolumbar spine models, successfully adjusting spine curvature and trunk muscle morphology to closely match the CT-based measurements. Models that incorporated CT-based measurements of trunk anatomy predicted substantially different vertebral loads than models only adjusted for height and weight, indicating that individual variation in spine curvature and muscle morphology had a significant effect on *in vivo* spine loads, and therefore must be accounted for in subject-specific models.

Incorporating spine curvature into the models changed loading predictions more than incorporating muscle morphology, as demonstrated by the generally higher differences in loading estimates (from the Ht/Wt models) for the +SC and +SC/MM models compared to the +MM models. Prior studies have also shown that spine curvature influences vertebral loading. For instance, we previously used a musculoskeletal spine model to parametrically simulate an age-related increase in thoracic kyphosis and found that vertebral compressive loading increased along the spine with increasing thoracic kyphosis, and that the increase in loading was higher while standing with weights compared to neutral standing without weight [5]. Further, we found that the increases in loading due to thoracic kyphosis could be mitigated by postural adjustments, such as posterior tilting of the pelvis, or changing the amount of lumbar lordosis. Briggs and colleagues created subject-specific spine models for 44 older women using spine curvature (T1 to L5) and body segment positions measured from standing lateral-radiographs. They found that a high thoracic kyphosis group (mean T4-T9 Cobb angle = 38°) had significantly higher estimated vertebral compressive loads and trunk muscle forces than a low kyphosis group (mean T4-T9 Cobb angle = 25°). In our study, there was a trend for individuals with higher thoracic kyphosis and lower lumbar lordosis compared to the baseline model to have higher predicted vertebral loads compared to their baseline Ht/Wt model. This makes sense from a mechanical perspective, as a higher thoracic kyphosis and lower lumbar lordosis will cause an anterior shift in posture, and require higher spinal-extensor muscle forces to maintain static equilibrium of the trunk. However, there were only weak to moderate associations relating changes in thoracic kyphosis and lumbar lordosis to differences in vertebral loading (Ht/Wt models vs subject-specific spine curvature models), indicating that other aspects of spine curvature not captured by the thoracic and lumbar Cobb angles have important effects on vertebral loading.

This is the first study to our knowledge that has incorporated subject-specific measures of trunk muscle morphology into a detailed thoracolumbar spine model. Since the baseline version of the model contained multiple fascicles per muscle group (Fig. 5.1), we needed to use previously published algorithms [13][Chapter 4] to adjust fascicle CSA and moment arms to match data from measured muscle groups. The adjustment process resulted in the +SC/MM

models matching the CT-measurements better than both the +SC models and the regression-adjusted models [10]. Although there were large reductions in the RMSEs between +SC/MM model-equivalent muscle morphology and CT-measured muscle morphology, the errors were not completely eliminated by the adjustment process, especially for muscle CSA. This remaining error may stem from the fact that each fascicle in a muscle group can span multiple levels of the spine, but can only have one defined CSA in the model, making it impossible to get a perfect match to the measured data at each spine level. In reality, the CSA of an individual fascicle may vary along its length. Therefore, this is an inherent difficulty in adjusting very detailed musculoskeletal models of the trunk. Including the detailed fascicular anatomy and multilevel attachments of the trunk muscles is desirable to more accurately model trunk musculoskeletal mechanics, but this complicated anatomy is difficult to adjust using standard 2D measures of muscle group size and position taken in the transverse plane of the body. This limitation may be overcome in the future by the development of 3D muscle models, rather than the traditional 1D line of action muscles used in the current model.

We showed that incorporating CT-based measures of muscle morphology into patient specific models substantially changed predictions of vertebral loading compared to more basic Ht/Wt models, although to a lesser extent than incorporating subject-specific measures of spine curvature. Incorporating CT-based muscle morphology had smaller effects on vertebral loading for less strenuous activities, but larger effects for the more strenuous activities. This implies that for activities that don't require large muscle activations and forces, accounting for individual variation in muscle morphology may not be important. However, for activities that require much greater muscle forces to balance the spine, factors such as muscle size (and therefore maximum isometric strength), and muscle moment arms will substantially change the predictions of vertebral loading.

A limitation of this study was that our muscle morphology measurements were restricted to the transverse plane of the body, and therefore limited our ability to adjust the CSA and moment arms of several major trunk muscle groups that were significantly oblique or parallel to this plane, such as the pectoralis major and the serratus anterior. However, we were still able to adjust a large number of muscle groups at multiple thoracic and lumbar spine levels

(T6 to L4). As already mentioned, another limitation was that our muscle adjustment procedure could not completely match the CT-measurements, although it markedly reduced the error compared to the unadjusted and regression-adjusted models. The final limitations of this study were that our spine curvature measurements (T4-L4) did not include the entire spine, and that we did not perform any measurements of rib cage anatomy. However, these measurements would be relatively easy to make and then incorporate into models given appropriate imaging data, such as full length lateral radiographs of the spine, and CT scans including the entire rib cage in the field of view [17]. However, the aforementioned limitations do not change our key finding that individual variation in spine curvature and muscle morphology significantly influenced predictions of *in vivo* vertebral loading compared to height and weight adjusted models, and therefore must be accounted for in subject-specific models. Further, the methods we have presented in this study can be generalized for different sources (ie: CT vs MRI) and amounts (ie: different vertebral levels) of imaging-based subject-specific data.

A major strength of this study was the use of a randomly selected sample of men and women spanning a large age range from a community-based cohort. There was large inter-individual variation in TK and LL angles, and this variability was representative of the variability in the whole Framingham cohort. This gives us confidence that the variations in spine curvature and vertebral loading we observed in this study are generalizable to an adult Caucasian population. Another strength of this study was the use of clinical CT-scans to make highly reliable measurements of spine curvature and muscle morphology, demonstrating the utility of clinical imaging technology in the creation of very detailed subject-specific models. Lastly, we used a previously validated model of the fully articulated thoracolumbar spine and rib cage as our baseline model, giving us confidence in the accuracy of our vertebral loading predictions in both the lumbar and thoracic regions of the spine.

In conclusion, we have described a set of methods to rapidly create subject-specific musculoskeletal models of the thoracolumbar spine using measurements of spine curvature and muscle morphology from clinical CT scans. We demonstrated that individual variations in both spine curvature and muscle morphology substantially influence predictions of vertebral

loading compared to simple height and weight adjusted models. Subject-specific spine models that account for individual differences in trunk anatomy will be essential for understanding the differential risk of spine injury and back pain among individuals.

5.6 Acknowledgements

This work was supported by grants from the National Institutes of Health (R01AR053986, F31AG041629, and K99AG042458), and by the National Heart, Lung, and Blood Institute (NHLBI) Framingham Heart Study (NIH/NHLBI Contract N01-HC-25195). The contents are solely the responsibility of the authors, and do not necessarily represent the views of the NIH.

5.7 Supplemental Tables

Supplemental Table 5.1: RMSEs comparing model-equivalent CSAs and CT-measured CSAs in models adjusted for height, weight, spine curvature, but not muscle morphology (black), and models adjusted for height, weight, spine curvature, and muscle morphology.

CSA (cm^2)	T6		T7		T8		T9		T10		T11		T12	
Rectus Abdominis									4.29	3.76	2.66	1.80	3.67	2.40
Latissimus Dorsi	3.83	3.96	9.58	6.65	8.53	5.71	8.76	4.86	5.63	3.16	4.33	2.16	2.31	2.03
Trapezius	3.14	2.11	2.32	1.17	1.99	0.83	1.68	0.92	1.72	1.34	1.31	1.44		
External Oblique							2.56	0.66	2.91	1.18	3.08	1.63	5.55	2.76
Internal Oblique														
Erector Spinae	3.92	2.21	4.62	2.60	2.90	1.58	3.79	4.00	6.30	4.71	9.33	2.88	9.81	3.15
Mutlifidus	1.24	0.29	1.16	0.32	1.02	0.25	1.83	0.34	1.41	0.23	1.37	0.35	1.93	0.27
Psoas Major														
Quadratus Lumborum														

CSA (cm^2)	L1		L2		L3		L4	
Rectus Abdominis	3.66	2.33	3.22	2.12	3.24	2.14	3.16	1.65
Latissimus Dorsi	3.52	3.09	3.69	3.22	3.00	2.75		
Trapezius								
External Oblique	4.55	2.03	4.53	4.98	5.12	2.20	6.16	3.33
Internal Oblique			3.08	2.30	6.71	3.78	5.20	3.37
Erector Spinae	9.69	2.74	5.91	5.49	6.74	3.39	9.59	2.64
Mutlifidus	1.39	0.20	2.02	0.72	3.74	1.42	3.78	0.89
Psoas Major	2.01	1.22	4.26	2.36	5.54	1.10	7.45	3.27
Quadratus Lumborum	2.52	0.29	2.25	0.61	4.30	1.54	3.04	1.97

Supplemental Table 5.2: RMSEs comparing model-equivalent ML moment arms and CT-measured ML moment arms in models adjusted for height, weight, spine curvature, but not muscle morphology (black), and models adjusted for height, weight, spine curvature, and muscle morphology.

ML Moment Arm (cm)	T6		T7		T8		T9		T10		T11		T12	
Rectus Abdominis									0.89	0.23	0.93	0.72	0.90	0.84
Trapezius	1.10	0.31	1.22	0.41	1.20	0.39	0.97	0.34	0.80	0.33	0.56	0.38		
Erector Spinae	0.59	0.14	0.40	0.09	0.46	0.08	0.53	0.10	0.82	0.34	0.34	0.35	0.86	0.83
Mutlifidus	0.42	0.10	0.65	0.09	0.47	0.07	0.25	0.10	0.33	0.17	0.32	0.10	0.50	0.11
Psoas Major														
Quadratus Lumborum														

ML Moment Arm (cm)	L1		L2		L3		L4	
Rectus Abdominis	0.87	0.39	1.18	0.18	1.10	0.28	1.00	0.04
Trapezius								
Erector Spinae	0.54	0.47	0.31	0.06	0.29	0.11	0.66	0.17
Mutlifidus	0.50	0.12	0.29	0.07	0.30	0.12	0.31	0.15
Psoas Major	0.54	0.01	0.71	0.14	0.65	0.11	0.62	0.11
Quadratus Lumborum	1.33	0.17	1.39	0.42	1.14	0.43	1.53	0.10

Supplemental Table 5.3: RMSEs comparing model-equivalent AP moment arms and CT-measured AP moment arms in models adjusted for height, weight, spine curvature, but not muscle morphology (black), and models adjusted for height, weight, spine curvature, and muscle morphology.

AP Moment Arm (cm)	T6		T7		T8		T9		T10		T11		T12	
Rectus Abdominis									2.60	0.36	2.87	0.74	3.03	0.94
Trapezius	0.85	0.18	0.72	0.18	0.55	0.21	0.54	0.24	0.53	0.24	0.75	0.52		
Erector Spinae	0.28	0.03	0.28	0.02	0.31	0.03	0.36	0.05	0.51	0.19	0.46	0.26	0.66	0.66
Mutlifidus	0.22	0.09	0.35	0.06	0.30	0.03	0.29	0.06	0.34	0.12	0.34	0.07	0.41	0.07
Psoas Major														
Quadratus Lumborum														

AP Moment Arm (cm)	L1		L2		L3		L4	
Rectus Abdominis	2.89	0.64	2.66	0.16	2.59	0.36	2.52	0.08
Trapezius								
Erector Spinae	0.41	0.50	0.55	0.11	0.47	0.15	0.51	0.13
Mutlifidus	0.31	0.10	0.41	0.12	0.45	0.20	0.76	0.20
Psoas Major	0.64	0.03	0.58	0.25	0.84	0.26	0.89	0.24
Quadratus Lumborum	0.32	0.29	0.84	0.49	0.85	0.37	0.99	0.10

5.8 REFERENCES

1. Delp, S.L., et al., *OpenSim: open-source software to create and analyze dynamic simulations of movement.* IEEE Trans Biomed Eng, 2007. **54**(11): p. 1940-50.

2. Bouxsein, M.L., et al., *Age- and Sex-Specific Differences in the Factor of Risk for Vertebral Fracture: A Population-Based Study Using QCT.* Journal of Bone and Mineral Research, 2006. **21**(9): p. 1475-1482.

3. Christophy, M., et al., *A musculoskeletal model for the lumbar spine.* Biomech Model Mechanobiol, 2012. **11**(1-2): p. 19-34.

4. Han, K.S., et al., *An enhanced and validated generic thoraco-lumbar spine model for prediction of muscle forces.* Med Eng Phys, 2012. **34**(6): p. 709-16.

5. Bruno, A.G., et al., *The effect of thoracic kyphosis and sagittal plane alignment on vertebral compressive loading.* J Bone Miner Res, 2012. **27**(10): p. 2144-51.

6. Briggs, A., et al., *The effect of osteoporotic vertebral fracture on predicted spinal loads in vivo.* European Spine Journal, 2006. **15**(12): p. 1785-1795.

7. Briggs, A.M., et al., *Thoracic Kyphosis Affects Spinal Loads and Trunk Muscle Force.* Physical Therapy, 2007. **87**(5): p. 595-607.

8. Keller, T.S., et al., *Influence of spine morphology on intervertebral disc loads and stresses in asymptomatic adults: implications for the ideal spine.* The Spine Journal, 2005. **5**(3): p. 297-309.

9. Arnold, A.S., et al., *Accuracy of muscle moment arms estimated from MRI-based musculoskeletal models of the lower extremity.* Comput Aided Surg, 2000. **5**(2): p. 108-19.

10. Anderson, D.E., et al., *Regressions for estimating muscle parameters in the thoracic and lumbar trunk for use in musculoskeletal modeling.* Journal of Biomechanics, 2012. **45**: p. 66-75.

11. Bruno, A.G., et al., *Vertebral size, bone density, and strength in men and women matched for age and areal spine BMD.* J Bone Miner Res, 2014. **29**(3): p. 562-9.

12. Hajihosseinali, M., N. Arjmand, and A. Shirazi-Adl, *Effect of body weight on spinal loads in various activities: a personalized biomechanical modeling approach.* J Biomech, 2015. **48**(2): p. 276-82.

13. Bruno, A.G., M.L. Bouxsein, and D.E. Anderson, *Development and validation of a musculoskeletal model of the fully articulated thoracolumbar spine and rib cage.* Journal of Biomechanical Engineering, Accepted for publication March 24, 2015.

14. Gordon, C.C., et al., *Anthropometric survey of US army personnel: methods and summary statistics 1988*. 1989, DTIC Document.

15. Bernhardt, M. and K.H. Bridwell, *Segmental Analysis of the Sagittal Plane Alignment of the Normal Thoracic and Lumbar Spines and Thoracolumbar Junction.* Spine, 1989. **14**(7): p. 717-721.

16. Kuntz, C., et al., *Neutral upright sagittal spinal alignment from the occiput to the pelvis in asymptomatic adults: a review and resynthesis of the literature.* Journal of Neurosurgery: Spine, 2007. **6**(2): p. 104-112.

17. Gayzik, F.S., et al., *Quantification of age-related shape change of the human rib cage through geometric morphometrics.* J Biomech, 2008. **41**(7): p. 1545-54.

18. Thelen, D.G., *Adjustment of muscle mechanics model parameters to simulate dynamic contractions in older adults.* J Biomech Eng, 2003. **125**(1): p. 70-7.

19. Hoffmann, U., et al., *Defining normal distributions of coronary artery calcium in women and men (from the Framingham Heart Study).* Am J Cardiol, 2008. **102**(9): p. 1136-41, 1141 e1.

20. Kim, Y.M., et al., *Intra-and inter-reader reliability of semi-automated quantitative morphometry measurements and vertebral fracture assessment using lateral scout views from computed tomography.* Osteoporos Int, 2011. **22**(10): p. 2677-88.

21. Anderson, D.E., et al., *Variations of CT-based trunk muscle attenuation by age, sex, and specific muscle.* J Gerontol A Biol Sci Med Sci, 2013. **68**(3): p. 317-23.

22. Lee, J.-S., *Digital image smoothing and the sigma filter.* Computer Vision, Graphics, and Image Processing, 1983. **24**(2): p. 255-269.

23. Crowninshield, R.D. and R.A. Brand, *A physiologically based criterion of muscle force prediction in locomotion.* J Biomech, 1981. **14**(11): p. 793-801.

24. Hughes, R.E., *Effect of optimization criterion on spinal force estimates during asymmetric lifting.* J Biomech, 2000. **33**(2): p. 225-9.

Chapter 6: VARIATIONS IN SPINE LOADING MAY EXPLAIN THE SITE-SPECIFIC PREVALENCE OF VERTEBRAL FRACTURES

6.1 Abstract

Vertebral fractures occur most frequently in the mid-thoracic and thoracolumbar regions of the spine, yet the biomechanical mechanisms underlying this site-specific occurrence are not known. Our working hypothesis is that the locations of vertebral fracture may be explained by the pattern of spine loading, such that during daily activities the mid-thoracic and thoracolumbar regions experience preferentially higher mechanical loading compared to other spine regions. To test this hypothesis, we used a previously validated musculoskeletal model of the full thoracolumbar spine and rib cage to estimate vertebral compressive load and factor-of-risk (load-to-strength ratio) patterns across the spine for 125 quasi-static activities, while also parametrically varying spine curvature (high, average, low, and zero thoracic kyphosis models). We found that the majority of activities produced loading peaks in the thoracolumbar and lower lumbar regions of the spine, but that the highest factor-of-risks generally occurred in the thoracolumbar spine because these vertebral bodies had lower compressive strength. We did not find any activities that produced mid-thoracic peaks in compressive loading or factor-of-risk. The thoracolumbar peaks in compressive loading and factor-of-risk general persisted for the different curvature conditions, except for the case of a perfectly straight spine (zero thoracic kyphosis), in which the loading peaks were greatly diminished or completely eliminated. We found that strong activation of the multifidus muscle fascicles in the thoracolumbar region of the spine, but not in other spine regions, was the main contributor to the peaks in vertebral compressive loading in the thoracolumbar spine. In summary, this study provides a comprehensive data set of thoracic and lumbar spine loading and factor-of-risk for a large variety of daily activities, and provides a potential biomechanical mechanism for the high incidence of vertebral fractures in the thoracolumbar spine.

6.2 Introduction

Vertebral fractures are the most common complication of osteoporosis [1, 2], and occur most frequently in the mid-thoracic and thoracolumbar regions of the spine [3-6]. However, the mechanisms underlying this site-specific occurrence of vertebral fracture are not known. Our working hypothesis is that the locations of vertebral fracture may be explained by the pattern of spine loading, such that during daily activities the mid-thoracic and thoracolumbar

regions experience preferentially higher mechanical loading compared to other spine regions. Perhaps because it is difficult to measure spine loads *in vivo,* there are no prior studies that have systematically explored how both thoracic and lumbar spine loading vary with activities of daily living. Previous studies that have recorded intradiscal pressure *in vivo* have reported data from just a few vertebral levels, typically in the lumbar spine [7-10], with only one study that reported intradiscal pressure measurements in the thoracic spine [11]. Telemeterized vertebral implants have also been used to measure *in vivo* spine loads in a few patients for many different activities, but these implants were only at a single lumbar vertebral level, making it impossible to assess variations in loading across the entire thoracolumbar spine [12, 13].

Due to the difficulty in making *in vivo* measurements, many biomechanical models have been developed to predict spine loading *in silico*. Unfortunately, the majority of these models have focused on the lumbar spine only [8, 14, 15], and the few models which incorporate an articulated thoracic spine have only been used to predict loading for a neutral standing posture [16, 17]. Our laboratory recently developed a fully articulated model of the thoracolumbar spine and rib cage that can predict loading of the thoracic and lumbar vertebral bodies during different quasi-static activities [18][Chapter 4], thus allowing us to investigate how spine loading varies across the entire thoracolumbar spine, and to ultimately determine if these variations in loading explain the site-specific occurrence of vertebral fractures. The model's predictions of vertebral compressive loading and trunk muscle tension were previously validated by comparing the model's load predictions to *in vivo* measures of intradiscal pressure, vertebral loading from telemeterized implants, and trunk muscle myoelectric activity from EMG [18][Chapter 4].

Spine curvature varies significantly in the population, and it is an important determinant of vertebral loading magnitude [16, 17, 19]. The amount of curvature in the spine (thoracic kyphosis and lumbar lordosis angles) might also influence the pattern of thoracolumbar loading (ie: which vertebral bodies experience the highest loads) by altering factors such as trunk mass distribution and trunk muscle lever arms and muscle activation patterns. Yet, there has been limited investigation regarding the impact of spinal curvature on vertebral loading patterns throughout the spine.

Therefore, the objectives of this study were to use our fully articulated thoracolumbar spine model to: 1) describe how vertebral compressive load and the factor-of-risk (load-to-strength ratio) vary along the spine for a large number of activities and body positions; 2) identify activities for which the mid-thoracic and thoracolumbar regions of the spine have a higher factor-of-risk than other spine locations, 3) determine if the patterns of spine loading and factor-of-risk are affected by variations in spine curvature, and 4) determine the contribution of body weight loads, trunk muscle forces, and intervertebral joint moments to vertebral compressive loading patterns.

6.3 Materials and Methods

6.3.1 The Musculoskeletal Spine Model

We used a musculoskeletal model of the full thoracolumbar spine and rib cage to estimate vertebral compressive loading for a large variety of body positions and activities in a quasi-static fashion. The development and validation of the musculoskeletal model have been described in detail previously [18][Chapter 4]. In brief, the model was created using OpenSim musculoskeletal modeling software [20], and includes the individual thoracic and lumbar vertebrae, sacrum, pelvis, the individual ribs and sternum, a lumped head and neck body, and the upper extremities. The skeletal anatomy was based on computed tomography (CT) scans of a 25 year old 50^{th} percentile male (Height = 175 cm, Weight = 78 kg) taken from the OpenSim geometry file library. The positions and orientations of the vertebrae, which define the curvature of the spine, were based on measurements available in the literature [21, 22], and the anatomy of the rib cage was derived from previously published morphometric equations [23].

The connections between adjacent vertebrae, as well as the connection between the pelvis and the ground body, were modeled as ball joints to allow for flexion/extension, lateral bending, and axial rotation of the trunk. Trunk movement in the model was partitioned amongst the thoracic and lumbar intervertebral joints and the pelvis according to previously published *in vivo* studies, and described in detail previously [18][Chapter 4]. The shoulder joint was modeled as a ball joint, allowing for flexion/extension, abduction/adduction, and

internal/external rotation of the arm. The elbow was modeled as a pin joint allowing for flexion/extension of the forearm.

The major muscles that attach to the trunk were incorporated into the model using 552 individual Hill-Type muscle fascicles, thereby capturing the detailed anatomy and multi-level attachments of these muscle groups. To ensure that the musculoskeletal model was reflective of an older individual, the cross-sectional areas and positions of the muscle groups were then adjusted using CT-based measurements of trunk muscle cross-sectional area and position made in a sample of 682 men (average age = 58 ± 6 years) selected from the community-based Framingham Heart Study Multidetector CT Study cohort [18, 24] [Chapter 4].

For an activity, the muscle forces required to maintain static equilibrium of the body segments in the model were predicted using an optimization routine that minimized the sum of cubed muscle activations, which is equivalent to maximizing muscle endurance [25, 26]. We then calculated the compressive and shear force applied to each lumbar and thoracic vertebral body.

6.3.2 Varying Spine Curvature

To investigate how spine curvature influences vertebral loading and factor-of-risk patterns during different activities, we created several versions of the musculoskeletal model with different amounts of thoracic kyphosis (TK) and lumbar lordosis (LL). In addition to the baseline model that uses average TK and LL angles available from the literature (TK = 50°, LL = -43°) [21, 22], we created two additional models to capture ± 2 standard deviations in TK angle, and a third model with a straight thoracic spine (TK = 0°) to explore the extreme range of what exists in the population. We used a value of 12° to represent 1 standard deviation in TK angle [27]. Starting with the baseline model, we uniformly added or subtracted curvature from the thoracic intervertebral joints to create the desired spine curves. Similarly, we uniformly added or subtracted curvature from the lumbar intervertebral joints to maintain a congruent posture, which is when the lumbar curvature is proportional to and balances the thoracic curvature. Spinal congruency is necessary to maintain an upright posture, and is considered indicative of a healthy spine [19, 28]. The final spine curves for the four models used in this study were as

follows: high kyphosis (TK = 74°, LL = -51.7°), average kyphosis (TK = 50°, LL = -43°), low kyphosis (TK = 26°, -34.3°), and no kyphosis (TK = 0°, LL = -24.8°) (Fig. 6.1).

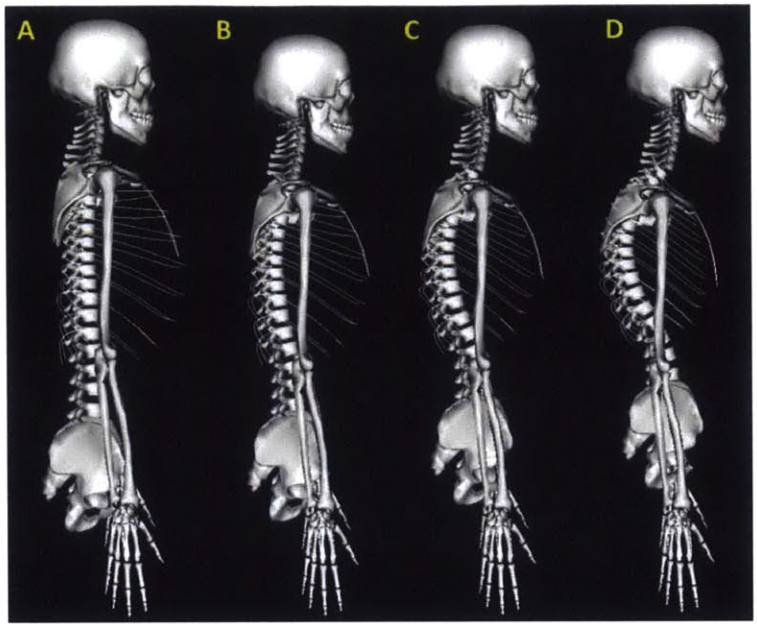

Figure 6.1: Image of the four spine models, each with a different spine curvature, used in this study. A) The model with no kyphosis (TK = 0°, LL = -24.8°), B) the low kyphosis model (TK = 26°, -34.3°), C) the average kyphosis model (TK = 50°, LL = -43°), and D) the high kyphosis model (TK = 74°, LL = -51.7°).

6.3.3 *Activities Simulated with the Spine Models*

Each spine model was used to compute vertebral compressive loading (T1 through L5) for 125 different activities. A list of these activities is provided in Supplemental Table 6.1. Some of the activities were chosen because prior studies had reported *in vivo* measurements of either spine loading or trunk muscle activity from patients performing these activities in a laboratory, and these were the activities used to validate our model previously [18][Chapter 4]. In selecting other activities, we attempted to cover a broad range of body positions and tasks that might be performed during daily activities. These included a variety of bending, lifting, carrying, and transferring activities with the trunk upright, flexed, laterally bent, axially rotated, or a combination of these. For example, we simulated lifting an object from the floor, lifting an object to a position above the head, transferring and object from left to right, and holding an object at the side. We varied shoulder flexion/extension and abduction/adduction, as well as elbow flexion, to cover a broad range of arm and forearm positioning. For the lifting, carrying, and transferring activities, we placed weights in either both hands or one hand. We also

simulated different pushing and pulling activities by applying forces to the hands that the model then had to resist. We simulated carrying a backpack or shoulder bag by applying forces downward on the shoulders. Finally, we simulated a sit-up (ie, trunk flexion while supine), which someone might perform as an exercise or while sitting up in bed. For each activity, we computed the compressive and shear loads at each vertebral level.

6.3.4 *Vertebral Strength and the Factor-of-Risk*

We estimated the average compressive strength of each vertebral body between T6 and L5 using previously acquired abdominal and thoracic QCT scans from a sample of 682 men aged 50 to 70 from the Framingham Heart Study Multidetector QCT cohort. This sample was chosen so that the vertebral strength estimates would be consistent with our musculoskeletal spine model, which uses muscle anatomy representative of an older male approximately 59 years of age. These men had a mean (± SD) age of 58.4 ± 6.3 years, height of 176.2 ± 6.7 cm, and weight of 90.1 ± 15.6 kg. Since the thoracic QCT scans did not extend above T6, we were unable to estimate compressive strength for T1 through T5. Additionally, because there is a gap between the thoracic and abdominal QCT scans, only a few subjects had T12 included in their scan (N=18) and only one subject had L1 included in their scan. Therefore, we used linear interpolation to estimate L1 vertebral strength from the other levels.

The compressive strength of each vertebral body was estimated as a linear combination of integral volumetric BMD (Int.vBMD, g/cm^3) and vertebral body cross-sectional (vCSA, cm^2), which were previously measured from the QCT scans [29]. This approach assumes the vertebral body is primarily loaded in compression and that the failure load of the vertebral body, or its strength, is proportional to its structural rigidity, which depends on bone size and bone elastic modulus. Previous studies have shown a strong association between QCT-based structural rigidity and compressive strength of human cadaveric vertebrae (r^2=0.65) [30]. In this case, the elastic modulus of vertebral bone was estimated using a previously published empirical relationship relating Int.vBMD to elastic modulus [31], which was then used in combination with vCSA to estimate vertebral strength according to the following equations [32]:

Elastic modulus = -34.7 + 3230 x Int.vBMD

Vertebral compressive strength (N) = 0.0068 x Elastic Modulus x vCSA

The factor-of-risk for vertebral fracture, defined here as the ratio of model-predicted compressive load to the average vertebral compressive strength, was computed for each vertebral body between T6 and L5 for each activity simulated with the model. Theoretically, when the applied force exceeds bone strength a fracture will occur, thus higher values of the factor-of-risk indicate greater risk of fracture.

6.3.5 *Intervertebral Joint Moments Due to Body Weight and Externally Applied Loads*

For the four spine models at each intervertebral joint we computed the flexion/extension moment required to balance the moment produced by body weight and any externally applied loads (such as forces or weights applied to the hands) for several activities (neutral standing, opening a window, and pushing forward against a load). Essentially, these flexion/extension moments are the moments that the trunk muscles must balance at the intervertebral joints to achieve static equilibrium. Understanding the patterns of these moments could provide insight as to why the trunk muscles might activate more strongly in one spine region compared to another.

6.3.6 *Contribution of Trunk Muscle Forces and Body Weight to Vertebral Loading*

We determined the contribution of body weight loads and trunk muscle forces to the net vertebral compression for a subset of activities: neutral standing, reaching forward to open a window (40 N of downward force applied to each hand), and pushing forward against a load (50 N applied to each hand). To compute trunk muscle forces, we summed the muscle tension of any fascicle that crossed the transverse mid-plane of a vertebra. Since the muscle fascicles run at different angles, we only summed the component of the muscle tension force vector that was parallel with the axial direction of the vertebral body, which was the same direction in which we computed vertebral compressive loading. We examined the muscle tension for all trunk muscles together, as well as by individual muscle group.

6.4 RESULTS

6.4.1 *VERTEBRAL STRENGTH*

The average vertebral strength of our older male sample increased monotonically from the thoracic to lumbar spine, increasing from 3116 ± 918 N at T6 to 5310 ± 1316 N at L5 (Fig. 6.2).

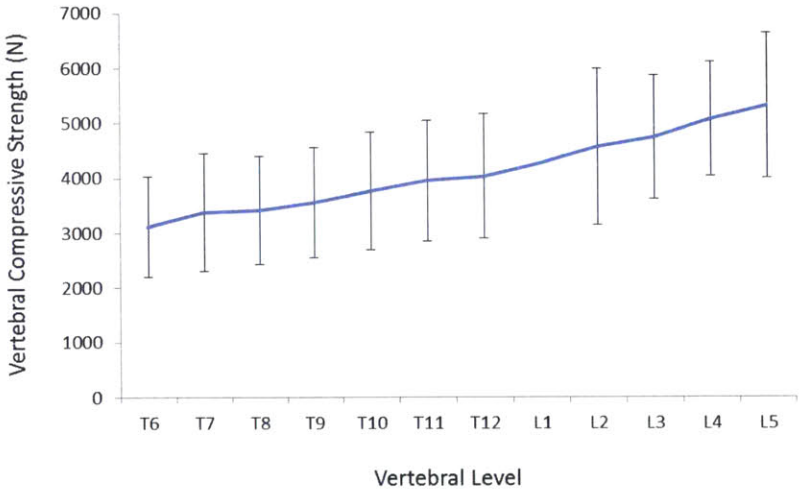

Figure 6.2: Variation in vertebral compressive strength across the spine for men between the ages of 50 and 70 in the Framingham cohort (N = 682). For each vertebral body, compressive strength was estimated from QCT-based measurements of vertebral cross-sectional area and integral volumetric BMD. Linear interpolation was used to estimate L1 vertebral compressive strength since the majority of subjects did not have L1 in either their abdominal or thoracic QCT scan. Error bars are ±1 standard deviation.

6.4.2 *VERTEBRAL COMPRESSIVE LOADING AND FACTOR-OF-RISK*

For the average kyphosis spine model, the majority of activities showed a peak in vertebral compressive loading in the thoracolumbar region, usually between T11 and L1, with the load then decreasing until the mid-lumbar spine, and increasing again in the lower lumbar spine (Fig. 6.3). We did not observe a loading peak in the mid-thoracic spine for any activity. The high kyphosis model exhibited the same general loading pattern, except that the peak in thoracolumbar loading was exaggerated. In comparison, reducing thoracic kyphosis reduced the peak in thoracolumbar loading, leading to a more linear pattern of loading along the spine. Since vertebral strength increased linearly along the spine, and was the same for all activities, variations in the factor-of-risk were determined by variations in vertebral compressive loading. Therefore, the peak in thoracolumbar compressive loading produced a peak in thoracolumbar factor-of-risk. A complete list of the activities simulated in this study, along with the resulting

vertebral compressive loads at a few levels of the spine (T8, T12, and L3), are included in Supplemental Table 6.1.

Vertebral compressive loading and factor-of-risk patterns are presented for several representative activities, including neutral standing (Fig. 6.3a), holding 10 kg weights in each hand with the trunk axially rotated 30° (Fig. 6.3b), reaching forward to open a window (40 N downward force applied to each hand) (Fig. 6.3c), and standing with the elbows flexed while the hands push forward against a load (50 N applied to each hand), such as what might be experienced while pushing a shopping cart (Fig. 6.3d). Shear loads in the anterior/posterior direction of the vertebral body are also presented for these activities in Supplemental Figure 6.1.

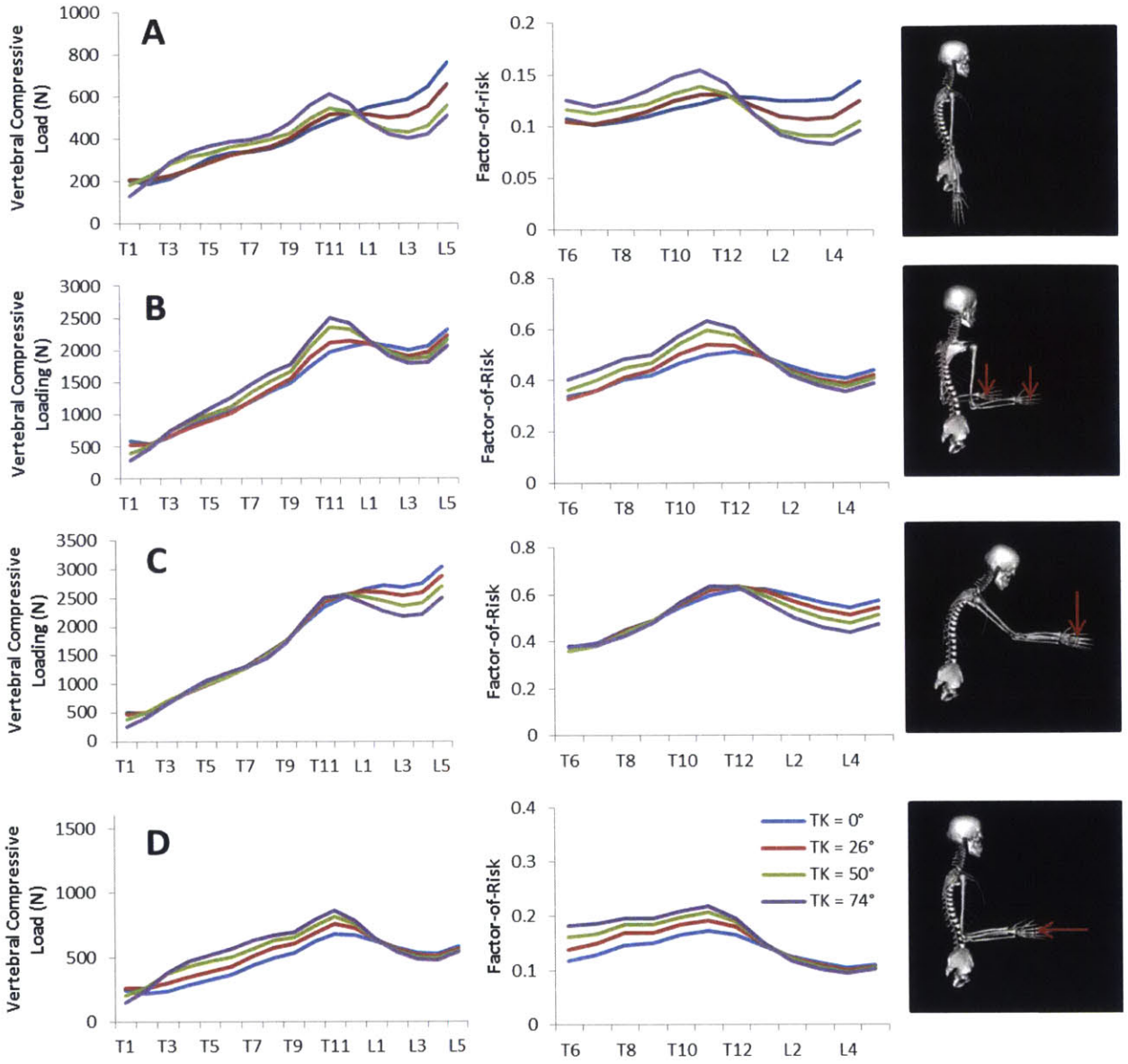

Figure 6.3: Variation in vertebral compressive loading and the factor-of-risk across the spine for A) neutral standing and B) holding weights in front of the body, with elbows flexed 90° and the trunk axially rotated 30° C) 30° of trunk flexion with the arms forward with 4 kg in each hand, and D) standing with the shoulders flexed 30° while pushing forward against 50 N of force applied to each hand. Each activity was simulated with the four spine models, demonstrating how the patterns of loading and factor-of-risk are affected by spine curvature.

For neutral standing (Fig. 6.3a), increasing TK resulted in higher loads and factor-of-risk in the thoracolumbar region but lower loads and factor-of-risk in the lumbar region. Specifically, the highest compressive loading occurred at T11 for the average kyphosis model and the high kyphosis model, whereas the highest loading occurred at L5 for the low kyphosis

model and no kyphosis models. However, there was a local peak in loading at T12 (528 N) in the low kyphosis model. The factor-of-risk was low for this activity, but the highest values occurred at the thoracolumbar region for the average, low, and high kyphosis models, but occurred at L5 for the no kyphosis model.

Holding weights in front of the body, with elbows flexed 90° and the trunk axially rotated 30°, produced some of the highest vertebral compressive loads among the activities simulated in this study (Fig. 6.3b). For the average and high kyphosis models, the highest loading occurred at the thoracolumbar region, whereas the highest loading occurred at L5 for the low and no kyphosis models, though local peaks in loading also occurred at T12 in the low kyphosis model and at L1 in the no kyphosis model. For this activity, the factor-of-risk was always highest in the thoracolumbar spine. Similar to neutral standing, increasing spine curvature generally resulted in higher loads and factor-of-risks in the thoracolumbar region but lower loads and factor-of-risks in the lumbar region for this activity.

For trunk flexion and reaching forward to open a window (Fig. 6.3c), the highest compressive loads generally occurred at L5, but local peaks in loading occurred in the thoracolumbar spine. Straightening of the spine produced higher loads and factor-of-risks in the thoracolumbar and lumbar regions of the spine, and diminished the local peaks in thoracolumbar loading. Factor-of-risk values were highest in the thoracolumbar spine except for the low and no kyphosis models during trunk flexion, where they were highest at L5.

For pushing against a load (Fig. 6.3d) the highest compressive loads and factor-of-risk values occurred at T11, and were higher for the models with greater thoracic kyphosis.

6.4.3 Intervertebral Joint Moments Due to Body Weight and Externally Applied Loads

To investigate the biomechanical basis for the observed vertebral loading patterns, we computed the moments produced by body weight and externally applied loads at each intervertebral joint. For standing, opening a window, and pushing forward against a load, we generally found that body weight and/or loads applied to the hands generated flexion moments at the intervertebral joints (Fig. 6.4). This makes sense considering that the mass of the trunk is always anterior to the spine, and during these activities the arms are anterior to the spine as well. For neutral standing, there were peaks in the flexion moment at the apex of the thoracic

kyphosis, and valleys in the flexion moment at the apex of the lumbar lordosis. These peaks and valleys became more exaggerated with increasing spine curvature, and disappeared in the case of a straight spine.

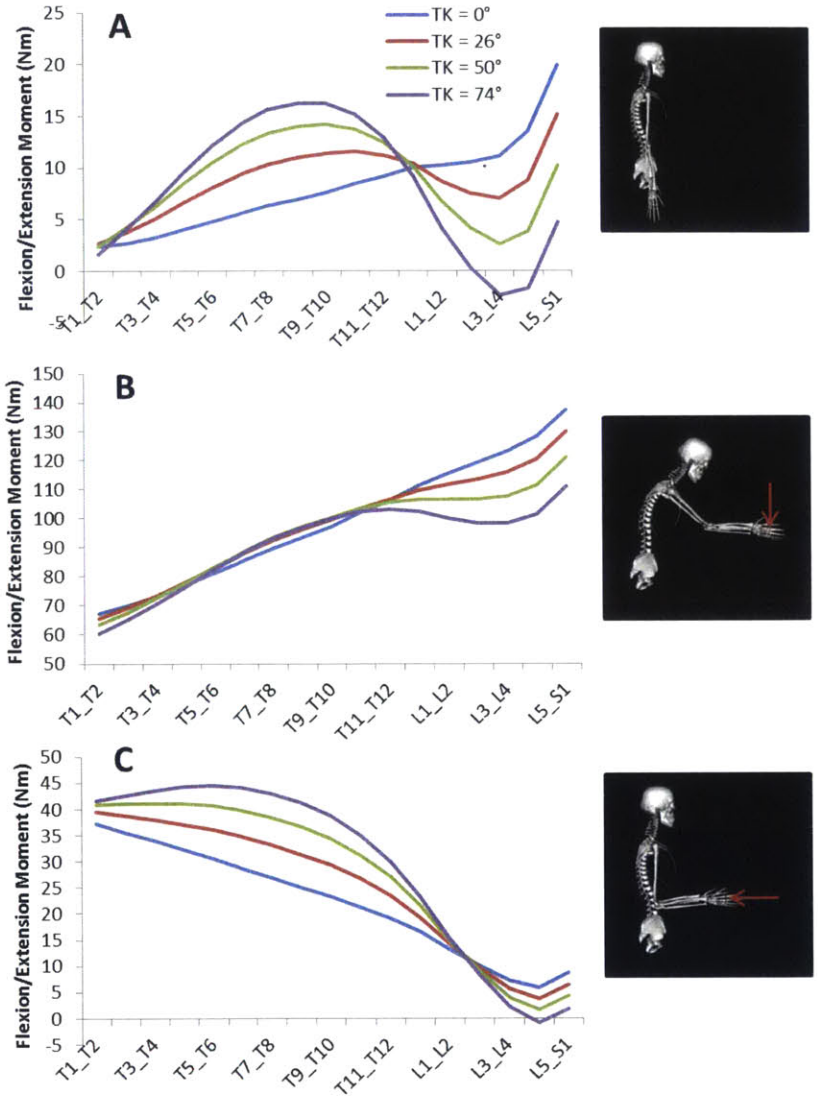

Figure 6.4: The flexion/extension moments applied to the intervertebral joints by body mass and any externally applied loads were computed for each curvature condition and during three different activities: A) neutral standing, B) opening a window, and C) pushing forward against a load. Flexion moments are positive, and extension moments are negative.

6.4.4 *Contribution of Trunk Muscle Forces vs Body Weight to Vertebral Compressive Loading*

To further delineate the biomechanical basis of the vertebral loading patterns, we used the average kyphosis model to compute the forces on each vertebral body due to body weight and trunk muscle forces for standing, opening a window, and pushing forward against a load

(Fig. 6.5). As expected, the forces on the vertebrae due to body weight increased linearly along the spine (147 N at T1 and 412 N at L5). For neutral standing, trunk muscle forces were generally low (Fig. 6.5a). In comparison, trunk muscle forces were much higher for opening a window (Fig. 6.5b) and pushing against a posteriorly directed force (Fig. 6.5c), and notably were highest in the thoracolumbar spine, specifically at T12. For instance, muscle forces were 2 to 3 fold higher at T12 than at L3 for standing and pushing forward. The largest contributors to the muscle force at each vertebra were the erector spinae and multifidus muscle groups, with all other muscle groups having minimal activation (generally less than 50 N). Activation of the multifidus muscle fascicles in the thoracolumbar region of the spine, but not in other spine regions, appears to be the main contributor to the peaks in vertebral compressive loading in the thoracolumbar spine.

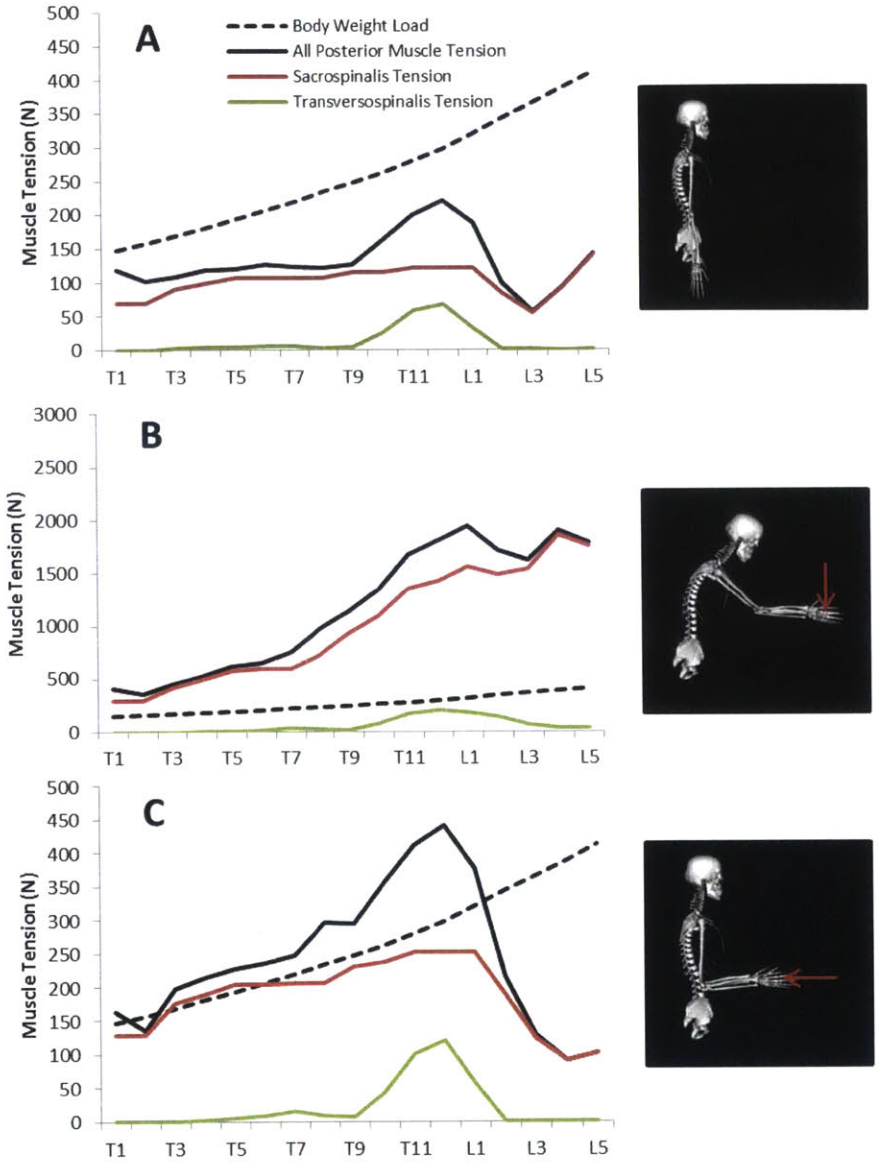

Figure 6.5: The contribution of body weight and muscle tension to the net compressive load on each vertebra was determined for the average kyphosis model during three activities: A) neutral standing, B) opening a window, and C) pushing forward against a load. The largest contributors to the muscle tension at each vertebra were the erector spinae and multifidus muscle groups, with all other muscle groups having minimal activation (generally less than 50 N). Strong activation of the multifidus was responsible for the thoracolumbar peak in loading observed during these activities.

6.5 Discussion

The first objective of this study was to use a previously validated musculoskeletal model of the spine to determine how vertebral compressive loading and factor-of-risk vary along the spine for a variety of activities and body positions. Prior *in vivo* and *in silico* studies of spine loading have been restricted to only one or a few spine levels, usually in the lumbar spine.

Therefore, this study is unique in that it presents the complete pattern of thoracic and lumbar spine compressive loading for a large number of activities. In general, we found that the highest compressive loads on the vertebrae occurred during activities in which body mass and/or externally applied weights were shifted anteriorly, such as during trunk flexion or carrying weights in front of the body. This finding is in line with basic mechanical principles, and was also demonstrated *in vivo* by Rohlmann and colleagues using telemeterized vertebral implants to record loads at L1 or L3 in five patients for 1000 different activities [13]. They found that the activities with the highest lumbar vertebral loads were those in which the upper body's center of mass was shifted anteriorly [13]. As body mass or externally held weights are shifted anteriorly, a flexion moment is generated about the intervertebral joints that must be balanced by the contraction of the posterior spinal muscles which generate equal and opposite extensor moments to maintain static equilibrium. In turn, the tension in these muscles generates large compressive forces on the vertebral bodies.

Our second objective was to determine if there are specific activities or body positions that might produce high spinal loads, and therefore high factor-of-risk, preferentially in the mid-thoracic (T7 to T8) or thoracolumbar (T11 to L1) regions of the spine, the two locations where vertebral fractures occur most frequently [3]. Interestingly, we found that almost all activities produced either local or global vertebral loading peaks in the thoracolumbar spine and the lower lumbar spine, but not in the mid-thoracic spine. The highest factor-of-risk generally occurred in the thoracolumbar spine because vertebral bodies in this region have a lower predicted strength than those in the lower lumbar spine, and therefore have a higher load-to-strength ratio. High thoracolumbar factor-of-risk across such a wide variety of activities could explain why this region of the spine has the highest prevalence and incidence of vertebral fractures.

Of interest, none of the 125 activities that we examined produced peaks in the factor-of-risk at the mid-thoracic region, the other common site for vertebral fracture. There are several possibilities for why we did not show this, including limitations in our spine loading or vertebral strength predictions, or simply not simulating the activities that actually cause mid-thoracic fractures *in vivo*. In terms of our strength predictions, there could be other important

determinants of thoracic vertebral body strength that are not accounted for in our strength model, which was derived empirically for lumbar vertebral bodies only [32]. Although we are confident in our vertebral loading predictions based on prior validation studies [18][Chapter 4], there could still be error in our thoracic loading predictions due to the complicated anatomy of the thorax. This is the first musculoskeletal model to realistically model the ribs, sternum, and thoracic musculature, but there are factors such as intra-thoracic pressure, intra-abdominal pressure, and intervertebral disc stiffness that are not yet accounted for in the model, and could influence loading patterns. When compared to a previous study that measured thoracic disc pressure *in vivo*, our musculoskeletal model slightly overestimated forces in the thoracic spine for very strenuous activities, such as lifting weights in front of the body. This observation indicates that our model is more likely to over-estimate rather than under-estimate thoracic vertebral loads, meaning that *in vivo* thoracic loads and factor-of-risk could be even lower than that observed in this study.

Another possibility for our observation of low mid-thoracic factor-of-risk could be that this does in fact reflect the *in vivo* reality, and perhaps mid-thoracic vertebral fractures are not as common as generally thought. Prior studies that have reported a high prevalence of mid-thoracic vertebral fractures have generally used quantitative or semi-quantitative methods to classify fractures based on short vertebral height and/or a wedged shape [5, 33, 34]. However, an alternative vertebral fracture assessment approach, known as algorithm-based qualitative assessment (ABQ), uses evidence of central endplate depression to classify fractures [35]. Unlike other methods of fracture assessment, the ABQ method shows a much lower prevalence of mid-thoracic vertebral fracture, but a similar prevalence of thoracolumbar fractures [35-37]. Ferrar and colleagues argue that short vertebral height is common in the mid-thoracic spine, and is a product of normal or developmental variation more often than osteoporotic vertebral fracture [36]. Furthermore, Ferrar and colleagues have shown that thoracic vertebrae with short height, which would be classified as fractures by other assessment methods, are not associated with low BMD [35]. In a cohort of 601 postmenopausal women followed for 6 years, the ABQ method showed that the prevalence of mid-thoracic fracture at baseline, as well as the incidence of new mid-thoracic fracture (T7 to T9), was less than 5%, which was on par or even

lower than that observed in the lower lumbar spine (L2 through L4) [37]. The prevalence and incidence of thoracolumbar vertebral fracture (T11 to L1) was generally much greater, ranging from 5 to 15%. Our model's predictions of relatively low mid-thoracic factor-of-risk but high thoracolumbar factor-of-risk support the epidemiological observations of Ferrar and colleagues, and call into question whether mid-thoracic fractures are as common as generally believed.

Another objective of this study was to determine if the patterns of spine loading, and therefore factor-of-risk, were influenced by variations in spine curvature. Although we found that straightening the spine (reducing thoracic kyphosis and lumbar lordosis) reduced the peaks in thoracolumbar loading, the peaks remained when thoracic kyphosis was within ±2 standard deviations of the population mean. It was only for the extreme case of zero thoracic kyphosis that the peak in thoracolumbar loading was completely eliminated for some activities, thus demonstrating that the natural curvature of the spine is associated with preferentially high thoracolumbar vertebral loading. Future studies should investigate further how variations in spine curvature influence loading patterns during different activities, by exploring for instance non-congruent spine curvatures and postures that become more common with ageing [19], as well as different strategies used to perform the same activity.

To investigate why our model predicts high thoracolumbar spinal loads, we analyzed the contribution of body weight loads and muscle forces to vertebral compression. As expected, the vertebral compressive loads attributable to body weight increased linearly down the spine. Thus, the peak in vertebral compressive loading in the thoracolumbar spine was due to high muscle forces in that region. Specifically, the multifidus muscle group, which contains short fascicles that connect adjacent or nearby vertebral bodies, was strongly activated in the thoracolumbar spine, but not in other spine regions. This pattern of muscle activation is not explained by the pattern of flexion moments at the intervertebral joints generated by body weight and/or externally applied loads, which ultimately have to be balanced to achieve static equilibrium. For standing, the greatest flexion moment from body weight loading occurred, as expected, at the apex of the thoracic kyphosis, however this did not lead to proportionally high posterior muscle forces in this region. Notably, muscles in the musculoskeletal model don't exclusively pull on the vertebral bodies to balance these joint moments. They also pull on other

structures, such as the ribs, which in turn can directly apply moments to the thoracic vertebral bodies via the costovertebral joints, for example. Further, as the muscles contract and pull on the spine, reaction forces are generated at the intervertebral joints, which in turn can also apply moments to the vertebral bodies. Therefore, the muscles in the model provide counter moments at each intervertebral joint (to balance the moments from body weight and external loads) both *directly*, by pulling on adjacent vertebrae that span those joints, and *indirectly*, by pulling on other structures that in turn can apply moments to the vertebral bodies that span the joint. Therefore, our results indicate that intuitively predicting where the highest vertebral loads and muscle forces will occur based on the pattern of body weight moments is inaccurate. This finding illustrates the necessity of modeling the complex anatomy of the spine and thorax as realistically as possible, which is a unique feature of the musculoskeletal model used in this study. High thoracolumbar spine and muscle loading is a phenomenon that emerges from the complex anatomy, and the fact that moments are being applied to the vertebrae both directly and indirectly by the trunk muscles. In a future study, we can use the model to determine the moments applied to each vertebral body from 1) the direct pull of muscles, 2) the reaction forces and moments of the left and right costovertebral joints, and 3) the reaction forces of the intervertebral joints. This will provide a more precise mechanical explanation for our finding of high thoracolumbar spine loads and multifidus muscle activation.

A limitation of this study was that we only investigated activities of daily living in a quasi-static fashion, despite the fact that highly dynamic activities, like falling or sneezing, may also be relevant to vertebral fracture [38]. Other limitations include lack of intervertebral joint stiffness, intra-abdominal and intra-thoracic pressures, which could affect the model's loading predictions. However, major strengths of this study include using a musculoskeletal model that accounts for the complex anatomy of the ribs, sternum, and trunk musculature. Furthermore, the model's trunk musculature anatomy was adjusted to match the *in vivo* muscle anatomy of men sampled from a population-based cohort, and the vertebral strength estimates used to compute factor-of-risk were derived from a large group of men sampled from the same cohort. An additional strength of this study was that we examined how spinal curvature, which varies significantly in the population, influences spine loading patterns.

In summary, this study provides a comprehensive data set of thoracic and lumbar spine loading and factor-of-risk for a large variety of daily activities, as well as for different spine curvatures. We showed that for a majority of activities and spinal curvature conditions, the highest factor-of-risk occurred in the thoracolumbar spine, and that this was driven by high multifidus muscle tension in that region, possibly explaining the high occurrence of vertebral fractures in the thoracolumbar region.

6.6 Acknowledgments

This work was supported by grants from the National Institutes of Health (R01AR053986, F31AG041629, and K99AG042458), and by the National Heart, Lung, and Blood Institute (NHLBI) Framingham Heart Study (NIH/NHLBI Contract N01-HC-25195). The contents are solely the responsibility of the authors, and do not necessarily represent the views of the NIH.

Authors' roles: Study design: AB, MB. Study conduct: AB. Data collection: AB. Data analysis: AB. Data interpretation: AB, DA, MB. Drafting manuscript: AB. Revising manuscript content: AB, DA, MB. Approving final version of manuscript: AB, DA, MB. All authors take responsibility for the integrity of the data analysis.

6.7 Supplemental Figures

Supplemental Figure 6.1: Variation in vertebral anterior/posterior shear forces across the spine for A) neutral standing and B) holding weights in front of the body, with elbows flexed 90° and the trunk axially rotated 30° C) 30° of trunk flexion with the arms forward with 4 kg in each hand, and D) standing with the shoulders flexed 30° while pushing forward against 50 N of force applied to each hand. Each activity was simulated with the four spine models, demonstrating how the patterns of loading and factor-of-risk are affected by spine curvature.

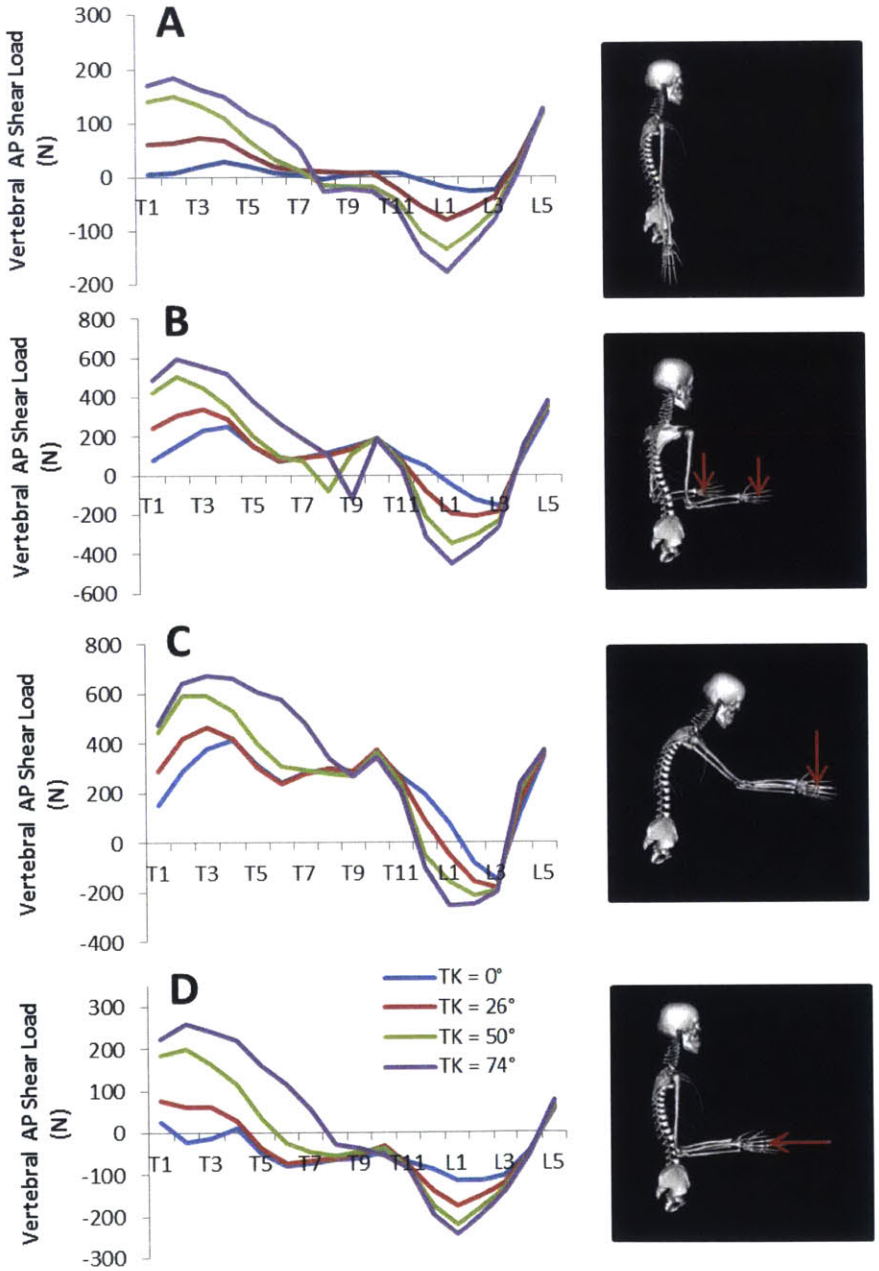

Supplemental Figure 6.2: Average vertebral compressive loads estimated for Framingham Heart Study participants (20 men and 20 women) using subject-specific spine models. These were the same individuals used in Chapter 5 to create subject-specific models using CT-based measurements of spine curvature and muscle morphology. The variation in spine curvature measurements in these individuals was representative of the variation in the whole Framingham cohort. Loading was estimated for four activities: a) neutral standing, B) standing with 10 kg weights in each hand and the elbows flexed 90°, C) 40° trunk flexion while holding 5 kg weights in each hand, and D) 10° lateral bending to the right while holding a 5 kg weight in the right hand. Error bars are ±1 standard deviation. We found peaks in thoracolumbar vertebral loading despite the large variations in the spine curvature and muscle morphology of these individuals. These results indicate that our finding of high thoracolumbar loading and factor-of-risk may be generalizable to the adult populations.

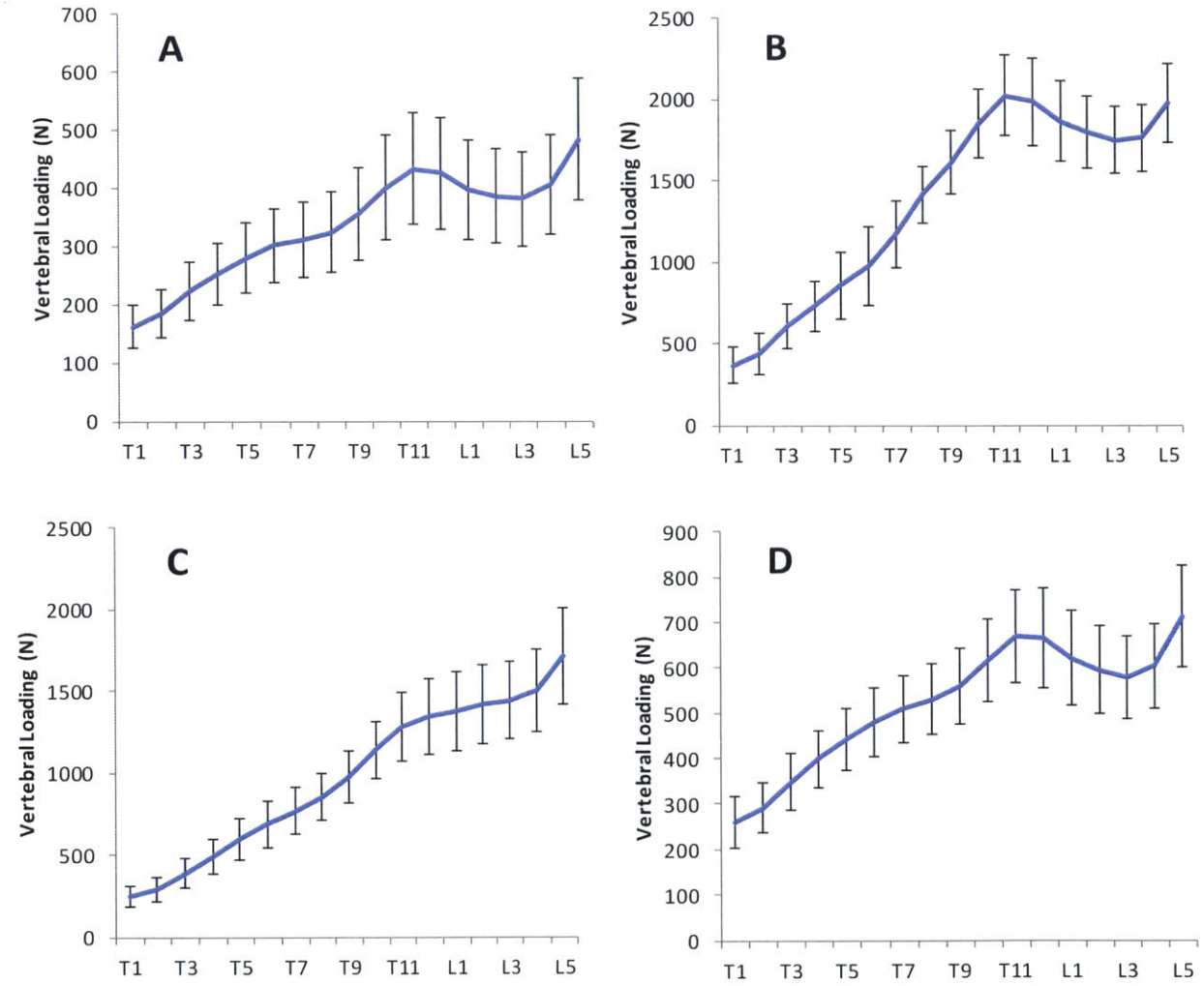

Supplemental Table 6.1: List of activities simulated in this study with associated vertebral compressive loads (N) at T8, T12, and L3 for the average kyphosis spine model (model height = 176 cm, weight = 90 kg). The model was too weak to achieve static equilibrium for some of the most strenuous activities, and these were left blank.

From Wilke et. al., Polga et. al., and Sato et. al. [7, 11, 39]	**T8 (N)**	**T12 (N)**	**L3 (N)**
1. 15° trunk extension	486	636	456
2. Neutral standing	398	533	433
3. 30° trunk flexion (arms hanging down)	636	1090	1079
4. 45° trunk flexion (arms hanging down)	729	1312	1367
5. 90° trunk flexion (arms hanging down)	798	1600	1960
6. Standing with 10 kg weights in each hand at the side	714	971	730
7. Standing with 20 kg weight in left hand at the side	1099	1411	1076
8. Standing with 20 kg weights in each hand at the side	1031	1409	1027
9. Standing with 10 kg weights in each hand, elbows flexed to 90°	1493	2283	1901
10. 30° trunk flexion with 10 kg weights in each hand	1109	1874	1769
11. 90° trunk flexion with 10 kg weights in each hand	-	-	-
12. 30° trunk axial twist to the left	466	606	473
13. 20° trunk lateral bend to the right	508	668	550
14. Trunk axial twist and trunk flexion, each at 30° with 10 kg weight	1136	1834	1738
15. 30° trunk axial twist, 10 Kg weight in each hand, elbows flexed to 90°	1524	2327	1864
16. 20° trunk lateral bend to the right, with 20 kg in right hand	1293	1614	1302
17. Standing with 20 kg weight in right hand	1099	1412	1076
18. 75° of trunk flexion	809	1572	1813
19. 75° of trunk flexion with 10 kg weights in each hand	1400	2664	2974
20. Opening window with both hands	1005	1642	1504
21. Opening window with one hand	898	1468	1353
22. Push shopping cart	538	757	581
23. Opening door, Pull	372	509	494
24. Opening door, Push	524	702	561
25. Tie shoes: 90° of flexion all in lumbar spine, pelvis upright	798	1600	1960
From Takahashi et. al. [9]			
26. Standing with 5 kg in each hand	556	752	581
27. 10° trunk flexion	465	727	659
28. 10° trunk flexion, 5 kg in each hand	647	1007	876
29. 20° trunk flexion	554	916	874
30. 20° trunk flexion, 5 kg in each hand	770	1254	1156
31. 30° trunk flexion, 5 kg in each hand	874	1483	1425
From Rohlmann et. al. [12]			
32. Shoulder flexion 90°, right arm	500	764	641
33. Shoulder flexion 90°, both arms	627	993	845
34. Shoulder abduction 90°, both arms	390	536	434
From Schultz et. al. [40]			
35. Standing with arms in, holding 4kg in each hand	729	1049	860
36. Standing with arms out	619	961	817
37. Standing with arms out, holding 4kg in each hand	1205	1992	1693
38. 30° of trunk flexion with arms out	857	1458	1401
39. 30° of trunk flexion with arms out, holding 4 kg in each hand	1493	2565	2367

Trunk Extension			
40. 5° trunk extension	390	518	398
41. 30° trunk extension	622	798	539
Both shoulders flexion range with weight			
42. 20° shoulder flexion 5 kg in each hand	871	1313	1088
43. 40° shoulder flexion 5 kg in each hand	1170	1799	1515
44. 60° shoulder flexion 5 kg in each hand	1374	2151	1825
45. 80° shoulder flexion 5 kg in each hand	1399	2325	1978
Right shoulder flexion range with weight			
46. 20° shoulder flexion 5 kg in right hand	666	969	789
47. 40° shoulder flexion 5 kg in right hand	761	1168	975
48. 60° shoulder flexion 5 kg in right hand	867	1344	1131
49. 80° shoulder flexion 5 kg in right hand	888	1436	1210
Both shoulders abduction range with weight			
50. 20° shoulder abduction 5 kg in each hand	550	753	581
51. 40° shoulder abduction 5 kg in each hand	549	754	582
52. 60° shoulder abduction 5 kg in each hand	549	755	583
53. 80° shoulder abduction 5 kg in each hand	550	756	584
Right shoulder abduction range with weight			
54. 20° shoulder abduction 5 kg in right hand	714	936	733
55. 40° shoulder abduction 5 kg in right hand	850	1091	864
56. 60° shoulder abduction 5 kg in right hand	961	1240	985
57. 80° shoulder abduction 5 kg in right hand	-	-	-
Lifting an object from floor with both hands			
58. 0° trunk flexion 5 kg in each hand	556	752	581
59. 20° trunk flexion 5 kg in each hand	770	1254	1156
60. 40° trunk flexion 5 kg in each hand	953	1682	1679
61. 60° trunk flexion 5 kg in each hand	1064	1984	2126
Lifting an object from floor with one hand			
62. 0° trunk flexion 5 kg in right hand	567	750	587
63. 20° trunk flexion 5 kg in right hand	613	991	936
64. 40° trunk flexion 5 kg in right hand	713	1287	1331
65. 60° trunk flexion 5 kg in right hand	770	1488	1665
Lifting an object from the side with one hand			
66. 0° trunk lateral bend 5 kg in right hand	567	750	587
67. 10° trunk lateral bend 5 kg in right hand	641	841	666
68. 20° trunk lateral bend 5 kg in right hand	698	903	737
69. 30° trunk lateral bend 5 kg in right hand	745	948	795
Lifting object that is on the floor and anterior-lateral to you, both hands			
70. 30° trunk axial twist, 0° flexion, 5 kg in each hand	660	855	634
71. 30° trunk axial twist, 20° flexion, 5 kg in each hand	779	1218	1116
72. 30° trunk axial twist, 40° flexion, 5 kg in each hand	906	1585	1629
73. 30° trunk axial twist, 60° flexion 5 kg in each hand	-	-	-

Lifting object that is on the floor and anterior-lateral to you, one hand			
74. 30° trunk axial twist, 0° flexion, 5 kg in right hand	646	844	630
75. 30° trunk axial twist, 20° flexion, 5 kg in right hand	648	987	910
76. 30° trunk axial twist, 40° flexion, 5 kg in right hand	703	1241	1304
77. 30° trunk axial twist, 60° flexion, 5 kg in right hand	678	1420	1661
Lifting an object above the head with both hands			
78. 0° shoulder flexion, 90° elbow flexion, 5 kg in each hand	975	1476	1232
79. 45° shoulder flexion, 90° elbow flexion, 5 kg in each hand	1204	1853	1562
80. 90° shoulder flexion, 90° elbow flexion, 5 kg in each hand	966	1552	1295
Lifting an object above the head with one hand			
81. 0° shoulder flexion, 90° elbow flexion, 5 kg in right hand	671	1009	834
82. 45° shoulder flexion, 90° elbow flexion, 5 kg in right hand	776	1192	997
83. 90° shoulder flexion, 90° elbow flexion, 5 kg in right hand	671	1043	862
Transferring an object right to left with both hands			
84. 0° trunk axial twist, 5 kg in each hand	975	1476	1232
85. 15° trunk axial twist, 5 kg in each hand	939	1450	1199
86. 30° trunk axial twist, 5 kg in each hand	1029	1528	1224
87. 45° trunk axial twist, 5 kg in each hand	1094	1552	1194
Transferring an object right to left with one hand			
88. 0° trunk axial twist, 5 kg in right hand	671	1009	834
89. 15° trunk axial twist, 5 kg in right hand	755	1073	864
90. 30° trunk axial twist, 5 kg in right hand	-	-	-
91. 45° trunk axial twist, 5 kg in right hand	841	1146	861
Transferring an object from the chest forward with both hands			
92. 0° shoulder flexion, 90° elbow flexion, 5 kg in each hand	975	1476	1232
93. 45° shoulder flexion, 45° elbow flexion, 5 kg in each hand	1351	2099	1779
94. 90° shoulder flexion, 0° elbow flexion, 5 kg in each hand	1407	2341	1992
Transferring an object from the chest forward with one hand			
95. 0° shoulder flexion, 90° elbow flexion, 5 kg in right hand	671	1009	834
96. 45° shoulder flexion, 45° elbow flexion, 5 kg in right hand	853	1317	1107
97. 90° shoulder flexion, 0° elbow flexion, 5 kg in right hand	-	-	-
Having a backpack or object on shoulders			
98. Wearing a backpack (standing)	413	553	445
99. Wearing a backpack (30° trunk flexion)	663	1135	1119
100. Wearing a backpack (20° trunk lateral bend)	531	696	569
101. Carrying something on one shoulder (standing)	408	545	440
Hands pushing forward, pulling back, or pushing down			
102. Pushing forward, elbows flexed 90°	627	761	503
103. Pulling back, elbows flexed 90°	324	554	634
104. Pushing down, elbows flexed 90°	430	622	483
105. Pushing forward, arms at side	666	879	906
106. Pulling back, arms at side	918	1276	932
107. Pushing down, arms at side	439	632	615
108. Pushing forward, shoulders flexed 30°	228	318	288

109. Pulling back, shoulders flexed 30°	751	975	768
110. Pushing down, shoulders flexed 30°	941	1322	977
111. Pushing forward, shoulders flexed 130°	314	407	469
112. Pulling back, shoulders flexed 130°	393	550	438
113. Pushing down, shoulders flexed 130°	793	1033	1048
114. Pushing forward, shoulders flexed 130°	1001	1290	829
115. Pulling back, shoulders flexed 130°	-	-	-
116. Pushing down, shoulders flexed 130°	448	636	494
117. Pushing to the side, shoulders flexed 130°	1387	1732	1494
Sit-up			
118. Sit-up: start by lying flat on floor	884	1000	1166
119. Sit-up: 25° flexion at pelvis	812	916	1218
120. Sit-up: 50° flexion at pelvis	561	571	1075
Shoveling			
121. Shoveling - Upright	-	-	-
122. Shoveling - 30° trunk flexion	-	-	-
123. Shoveling - 60° trunk flexion	-	-	-
124. Shoveling - Upright and 30° axial rotation	1181	1661	1286
125. Shoveling - 30° trunk flexion and 30° axial rotation	-	-	-

6.8 REFERENCES

1. *Bone Health and Osteoporosis: A Report of the Surgeon General.* 2004, US Department of Health and Human Services, Office of the Surgeon General: Rockville, MD, USA.

2. Riggs, B.L. and L.J. Melton, *The worldwide problem of osteoporosis: Insights afforded by epidemiology.* Bone, 1995. **17**(5): p. S505-S511.

3. Cooper, C., et al., *Incidence of clinically diagnosed vertebral fractures: A population-based study in rochester, minnesota, 1985-1989.* Journal of Bone and Mineral Research, 1992. **7**(2): p. 221-227.

4. Ismail, A.A., et al., *Number and Type of Vertebral Deformities: Epidemiological Characteristics and Relation to Back Pain and Height Loss.* Osteoporosis International, 1999. **9**(3): p. 206-213.

5. Melton, L.J., et al., *Prevalence and incidence of vertebral deformities.* Osteoporosis International, 1993. **3**(3): p. 113-119.

6. Siminoski, K., et al., *Anatomical distribution of vertebral fractures: comparison of pediatric and adult spines.* Osteoporos Int, 2012. **23**(7): p. 1999-2008.

7. Sato, K., S. Kikuchi, and T. Yonezawa, *In vivo intradiscal pressure measurement in healthy individuals and in patients with ongoing back problems.* Spine (Phila Pa 1976), 1999. **24**(23): p. 2468-74.

8. Schultz, A.B. and G.B.J. Andersson, *Analysis of Loads on the Lumbar Spine.* Spine, 1981. **6**(1): p. 76-82.

9. Takahashi, I., et al., *Mechanical load of the lumbar spine during forward bending motion of the trunk-a biomechanical study.* Spine (Phila Pa 1976), 2006. **31**(1): p. 18-23.

10. Wilke, H.J., et al., *New In Vivo Measurements of Pressures in the Intervertebral Disc in Daily Life.* Spine, 1999. **24**(8): p. 755-762.

11. Polga, D.J., et al., *Measurement of In Vivo Intradiscal Pressure in Healthy Thoracic Intervertebral Discs.* Spine, 2004. **29**(12): p. 1320-1324 10.1097/01.BRS.0000127179.13271.78.

12. Rohlmann, A., et al., *Loads on a telemeterized vertebral body replacement measured in two patients.* Spine (Phila Pa 1976), 2008. **33**(11): p. 1170-9.

13. Rohlmann, A., et al., *Activities of everyday life with high spinal loads.* PLoS One, 2014. **9**(5): p. e98510.

14. Christophy, M., et al., *A musculoskeletal model for the lumbar spine.* Biomech Model Mechanobiol, 2012. **11**(1-2): p. 19-34.

15. Han, K.S., et al., *An enhanced and validated generic thoraco-lumbar spine model for prediction of muscle forces.* Med Eng Phys, 2012. **34**(6): p. 709-16.

16. Briggs, A.M., et al., *Thoracic Kyphosis Affects Spinal Loads and Trunk Muscle Force.* Physical Therapy, 2007. **87**(5): p. 595-607.

17. Keller, T.S., et al., *Influence of spine morphology on intervertebral disc loads and stresses in asymptomatic adults: implications for the ideal spine.* The Spine Journal, 2005. **5**(3): p. 297-309.

18. Bruno, A.G., M.L. Bouxsein, and D.E. Anderson, *Development and validation of a musculoskeletal model of the fully articulated thoracolumbar spine and rib cage.* Journal of Biomechanical Engineering, Accepted for publication March 24, 2015.

19. Bruno, A.G., et al., *The effect of thoracic kyphosis and sagittal plane alignment on vertebral compressive loading.* J Bone Miner Res, 2012. **27**(10): p. 2144-51.

20. Delp, S.L., et al., *OpenSim: open-source software to create and analyze dynamic simulations of movement.* IEEE Trans Biomed Eng, 2007. **54**(11): p. 1940-50.

21. Bernhardt, M. and K.H. Bridwell, *Segmental Analysis of the Sagittal Plane Alignment of the Normal Thoracic and Lumbar Spines and Thoracolumbar Junction.* Spine, 1989. **14**(7): p. 717-721.

22. Kuntz, C., et al., *Neutral upright sagittal spinal alignment from the occiput to the pelvis in asymptomatic adults: a review and resynthesis of the literature.* Journal of Neurosurgery: Spine, 2007. **6**(2): p. 104-112.

23. Gayzik, F.S., et al., *Quantification of age-related shape change of the human rib cage through geometric morphometrics.* J Biomech, 2008. **41**(7): p. 1545-54.

24. Hoffmann, U., et al., *Defining normal distributions of coronary artery calcium in women and men (from the Framingham Heart Study).* Am J Cardiol, 2008. **102**(9): p. 1136-41, 1141 e1.

25. Crowninshield, R.D. and R.A. Brand, *A physiologically based criterion of muscle force prediction in locomotion.* J Biomech, 1981. **14**(11): p. 793-801.

26. Hughes, R.E., *Effect of optimization criterion on spinal force estimates during asymmetric lifting.* J Biomech, 2000. **33**(2): p. 225-9.

27. Hammerberg, E.M. and K.B. Wood, *Sagittal Profile of the Elderly.* Journal of Spinal Disorders & Techniques, 2003. **16**(1): p. 44-50.

28. Knight, R., et al., *White Paper on Sagittal Plane Alignment.* Scoliosis Research Society,, 2003. **accessed from SRS.org**.

29. Samelson, E.J., et al., *QCT measures of bone strength at the thoracic and lumbar spine: the Framingham Study.* J Bone Miner Res, 2012. **27**(3): p. 654-63.

30. Crawford, R.P., C.E. Cann, and T.M. Keaveny, *Finite element models predict in vitro vertebral body compressive strength better than quantitative computed tomography.* Bone, 2003. **33**(4): p. 744-750.

31. Kopperdahl, D.L., E.F. Morgan, and T.M. Keaveny, *Quantitative computed tomography estimates of the mechanical properties of human vertebral trabecular bone.* Journal of Orthopaedic Research, 2002. **20**(4): p. 801-805.

32. Bouxsein, M.L., et al., *Age- and Sex-Specific Differences in the Factor of Risk for Vertebral Fracture: A Population-Based Study Using QCT.* Journal of Bone and Mineral Research, 2006. **21**(9): p. 1475-1482.

33. Genant, H.K., et al., *Vertebral fracture assessment using a semiquantitative technique.* Journal of Bone and Mineral Research, 1993. **8**(9): p. 1137-1148.

34. Melton, L.J., et al., *Epidemiology of vertebral fractures in women.* American Journal of Epidemiology, 1989. **129**(5): p. 1000-1011.

35. Ferrar, L., et al., *Identification of vertebral fracture and non-osteoporotic short vertebral height in men: the MrOS study.* J Bone Miner Res, 2007. **22**(9): p. 1434-41.

36. Ferrar, L., et al., *Is short vertebral height always an osteoporotic fracture? The Osteoporosis and Ultrasound Study (OPUS).* Bone, 2007. **41**(1): p. 5-12.

37. Ferrar, L., et al., *Association between incident and baseline vertebral fractures in European women: vertebral fracture assessment in the Osteoporosis and Ultrasound Study (OPUS).* Osteoporos Int, 2012. **23**(1): p. 59-65.

38. Freitas, S.S., et al., *Rate and circumstances of clinical vertebral fractures in older men.* Osteoporos Int, 2008. **19**(5): p. 615-23.

39. Wilke, H.-J., et al., *Intradiscal pressure together with anthropometric data - a data set for the validation of models.* Clinical Biomechanics, 2001. **16**(Supplement 1): p. S111-S126.

40. Schultz, A., et al., *Loads on the lumbar spine. Validation of a biomechanical analysis by measurements of intradiscal pressures and myoelectric signals.* The Journal of Bone & Joint Surgery, 1982. **64**(5): p. 713-720.

Chapter 7: A BIOMECHANICAL MECHANISM FOR THORACOLUMBAR VERTEBRAL FRACTURE

7.1 Abstract

Vertebral fractures occur most frequently in the thoracolumbar region of the spine (T11-L1), but the mechanisms underlying this site-specific prevalence are not known. In Chapter 6, we found that our musculoskeletal spine model frequently predicted peaks in thoracolumbar vertebral compressive loading (via strong activation of the thoracolumbar multifidus), supporting the idea that the high prevalence of vertebral fracture in this region may be due to high compressive loads *in vivo*. The goal of this study was to examine the mechanics of spinal loading more closely to explain why the model predicts high loads in this region. For multiple activities and spine curvature conditions (zero, low, average, and high thoracic kyphosis), we calculated the flexion/extension moments applied to each vertebral body by 1) the body weight associated with that vertebra, 2) the adjacent intervertebral joint reaction forces, and 3) the adjacent left and right costovertebral joint reaction forces and moments (only in the thoracic spine). These moments must be balanced by the pull of muscles directly attached to that vertebra. We found that the multifidus muscle group applies large compressive forces to the thoracolumbar vertebrae (T11-L1) in an effort to balance competing moments applied by the intervertebral and costovertebral joint reactions. This phenomenon was consistent across activities, and was exaggerated with increasing thoracic kyphosis. Further, this analysis also showed that the moments from the costovertebral and intervertebral joint reaction forces largely balanced each other in the upper thoracic spine (T1 to T6), resulting in low muscle loads and spine compression, illustrating a unique mechanism for thoracic load sharing between the ribs and spine.

7.2 Introduction

Vertebral fractures occur most frequently in the thoracolumbar region of the spine (T11-L1) [1-4], but the mechanisms underlying this site-specific prevalence are not known. One possibility is that this region of the spine experiences relatively high loading, increasing the risk of fracture. To investigate this possibility, we previously developed an anatomically detailed and fully articulated musculoskeletal model of the full thoracolumbar spine and rib cage to estimate patterns of spine loading for a large variety of daily activities [5][Chapter4]. Loading estimates from this model frequently produced a peak in compressive loading around T11-L1,

supporting the idea that the high prevalence of vertebral fracture in this region may be due to high compressive loads *in vivo* [Chapter 6]. The goal of this study was to examine the mechanics of spinal loading more closely to explain why the model predicts high loads in this region.

7.3 Materials and Methods

We used an anatomically detailed model of the fully articulated thoracolumbar spine and rib cage (implemented in OpenSim) to predict trunk muscle forces and spine loading for three activities: 1) neutral standing, 2) trunk flexion at 70°, and 3) reaching forward to open a window (40 N downward force applied to each hand). In addition, we computed loading for four different spine curvature conditions during neutral standing: zero, low, average, and high thoracic kyphosis [Chapter 6]. The model was previously validated against *in vivo* measures of intradiscal pressure, vertebral loading from telemetrized implants, and trunk muscle activity from EMG [5][Chapter 4]. The model uses a static optimization routine to predict the pattern of muscle forces required to balance moments from body weight and any externally applied loads, while at the same time minimizing the sum of cubed muscle activations (equivalent to maximizing muscle endurance) [6, 7].

To investigate vertebral compressive loading patterns predicted by the model, and to understand why the model generally predicts high thoracolumbar spinal compression, we calculated the flexion/extension moments applied to each vertebral body by 1) the body weight (bm) associated with that vertebra, 2) the adjacent intervertebral joint (ivj) reaction forces, and 3) the adjacent left and right costovertebral joint (cv) reaction forces and moments (only in the thoracic spine) (Fig. 7.1). These moments must be balanced by the pull of muscles directly attached to that vertebra.

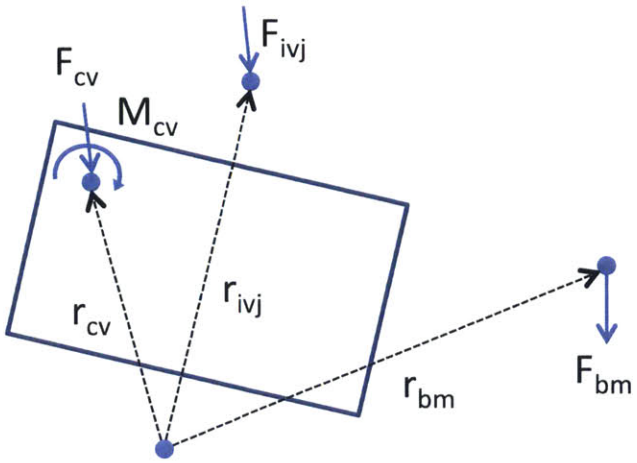

$$\Sigma M = M_{cv} + r_{cv} \, x \, F_{cv} + r_{ivj} \, x \, F_{ivj} + r_{bm} \, x \, F_{bm} = M_{muscles}$$

Figure 7.1: The intervertebral joints are modeled as ball joints and the costovertebral joints are modeled as pin joints. The sum of flexion/extension moments was computed about the inferior intervertebral joint of each vertebra.

7.4 Results and Discussion

7.4.1 Vertebral Compression and Trunk Muscle Tension

Patterns of spine loading and trunk muscle tension were the same as those found in Chapter 6, and therefore only standing load results are presented here (Fig. 7.2 and 7.3). For all three activities, our musculoskeletal spine model predicted a peak in thoracolumbar compressive loading (T11/T12) (Fig. 7.2). The erector spinae and multifidus were the primary muscle groups activated during these activities, with the other trunk muscle groups generally producing less than 50 N of tension (Fig. 7.3). The multifidus activated strongly in the thoracolumbar region of the spine, contributing to the peak in thoracolumbar vertebral compressive loading.

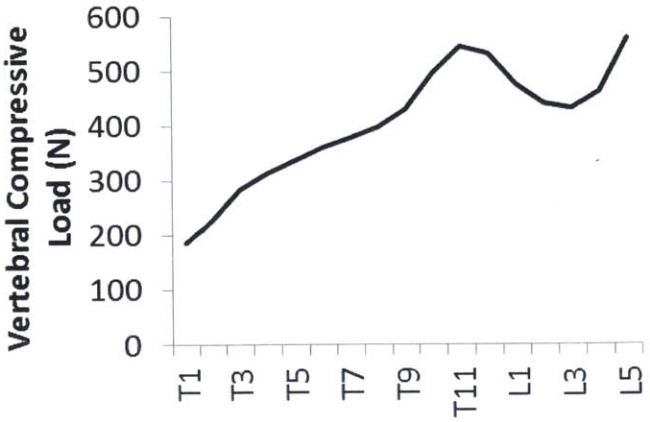

Figure 7.2: Vertebral compressive loading during neutral standing.

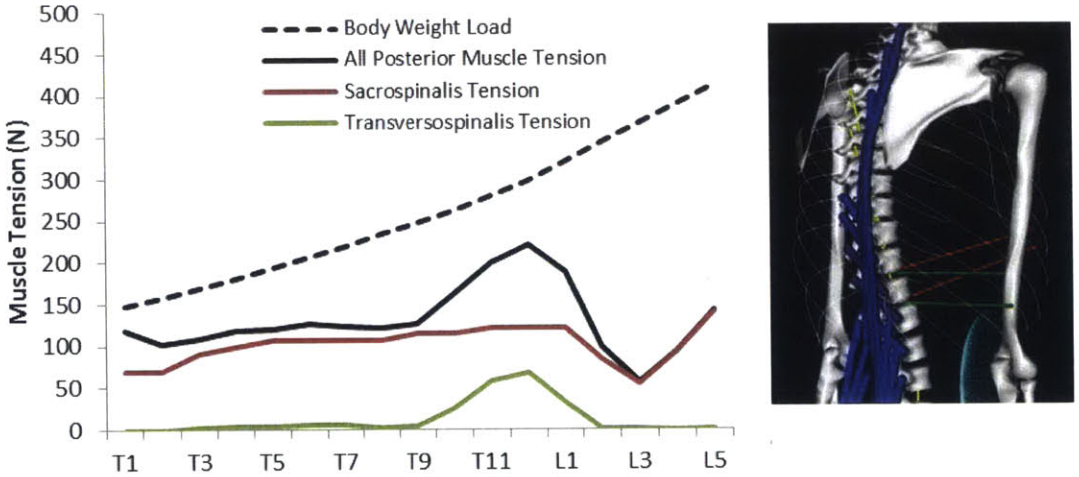

Figure 7.3: Left) The contribution of body weight and muscle tension to vertebral compression during neutral standing. Right) Activation patterns of the multifidus and a subset of erector spinae muscle fascicles, where blue = low activation and red = high activation. The multifidus fascicles connecting T11, T12, and L1 are activating more than the fascicles connected to other vertebral bodies

7.4.2 *Flexion/Extension Moments Applied to Each Vertebra - Activities*

The moments applied to each vertebra during each activity are shown in Figure 7.4. It appears that the reason for strong activation of the multifidus, and thus high thoracolumbar compressive loads, is the requirement that the muscles apply extension moments to T11, but flexion moments to T12 and L1 (dashed line in Fig. 7.4). The only way for this requirement to be met is for the multifidus muscle group to activate. The multifidus consists of short fascicles posterior to the spine that connect adjacent vertebrae. When contracting, the multifidus will

pull down and apply an extension moment to its superior vertebra (ie: T11), and pull up and apply a flexion moment to its inferior vertebra (ie: T12). The reason for this different requirement is that at T11 the muscles must balance flexion moments applied by the costovertebral joint reaction forces, whereas at T12 and L1 the dominant moments the muscles must balance are extension moments applied by the intervertebral joint reaction forces. The pattern of moments produced by the intervertebral joint reaction forces are likely driven by the curvature of the spine and the moment arms between adjacent intervertebral joints. Interestingly, this analysis also showed that the moments from the costovertebral and intervertebral joint reaction forces largely balanced each other in the upper thoracic spine (T1 to T6), resulting in low muscle loads and spine compression, illustrating a unique mechanism for thoracic load sharing between the ribs and spine. For the more strenuous activities, we also found an equal and opposite increase in the moments from the costovertebral and intervertebral joint reaction forces in parts of the thoracic spine (T4-T6), which kept muscle forces low in this region.

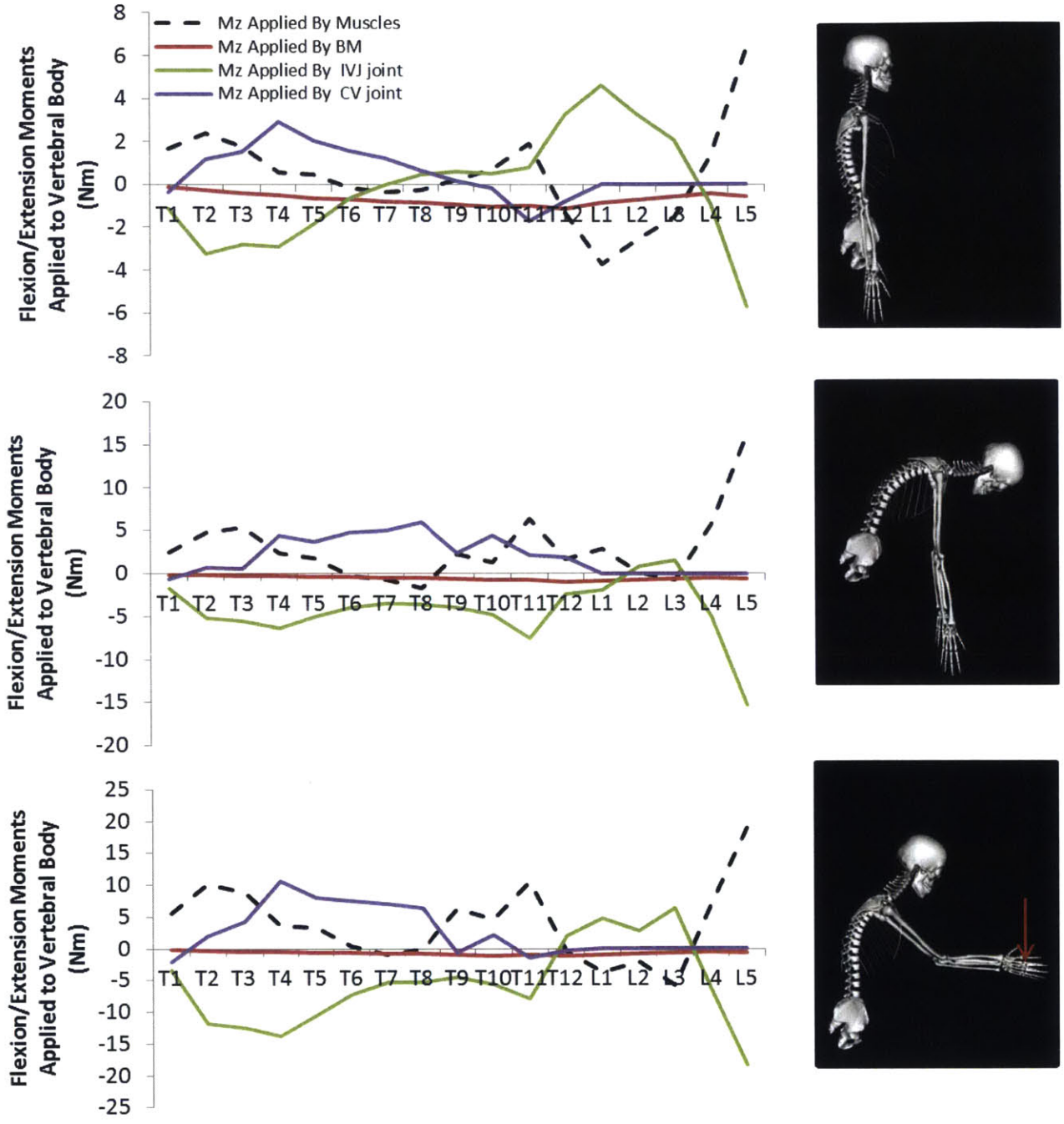

Figure 7.4: For each activity, we computed the moments applied to each vertebra by body mass, and the costovertebral (CV) and intervertebral joint (IVJ) reaction forces, all of which must be balanced by equal and opposite moments generated by the muscles (dashed line). Negative values are flexion moments.

7.4.3 *Flexion/Extension Moments Applied to Each Vertebra – Spine Curvature*

The moments applied to each vertebra for each spine curvature condition are shown in Figure 7.5 for neutral standing. For increasing thoracic kyphosis angle, we found that the

difference between the extension moment required at T11 and the flexion moments required at T12 and L1 became even greater, indicating that the thoracolumbar multifidus must activate more strongly with increasing thoracic kyphosis. This explains our finding from Chapter 6 that increasing thoracic kyphosis increases the peak in thoracolumbar vertebral compressive loading for standing activities (ie: neutral standing and standing while holding weights). For increasing thoracic kyphosis angle, we also found an equal and opposite increase in the moments from the costovertebral and intervertebral joint reaction forces in parts of the thoracic spine (T4-T6), which kept muscle forces low in this region.

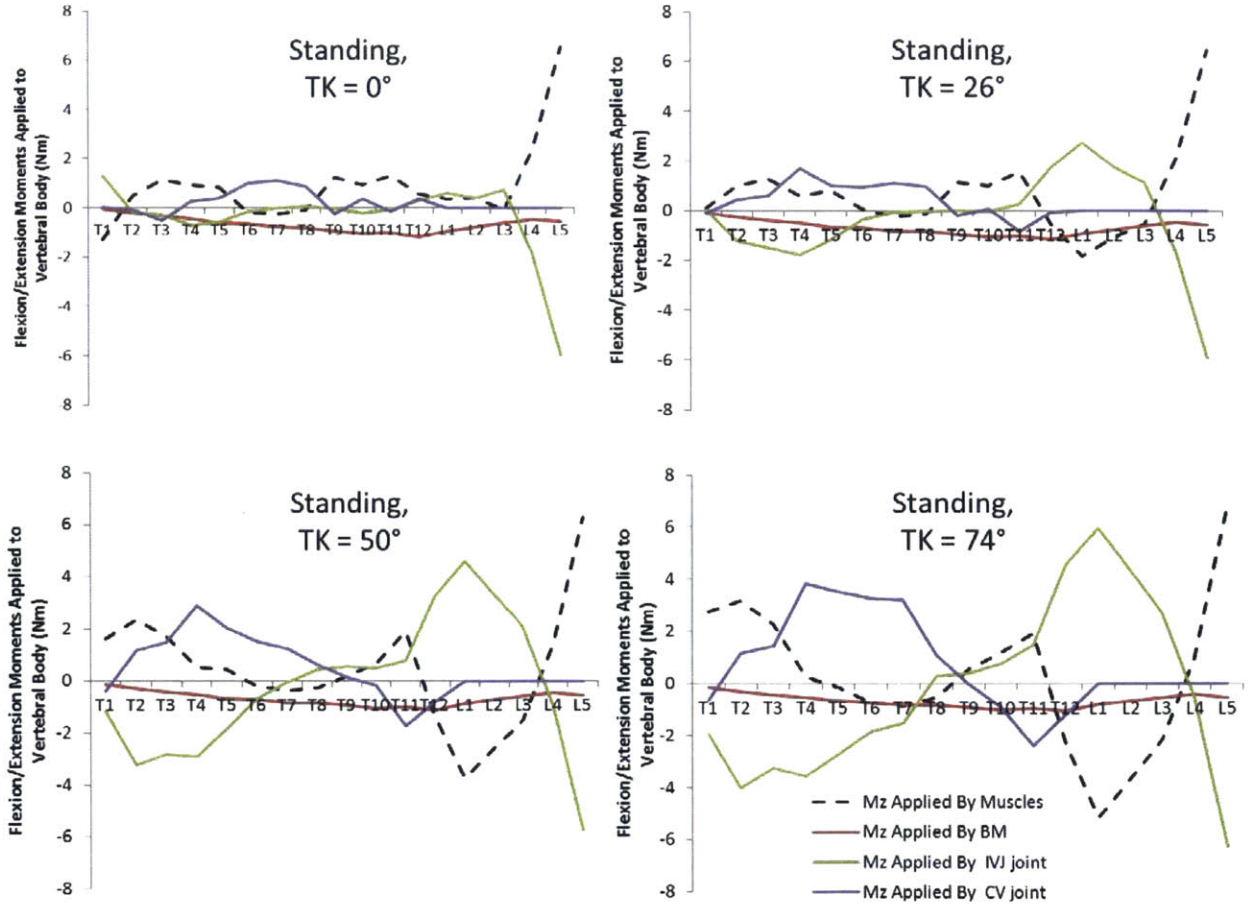

Figure 7.5: For each spine curvature condition, we computed the moments applied to each vertebra by body mass, and the costovertebral (CV) and intervertebral joint (IVJ) reaction forces, all of which must be balanced by equal and opposite moments generated by the muscles (dashed line). Negative values are flexion moments.

7.5 Conclusion

Using a unique model that accounts for the complex anatomy of the spine and rib cage, we demonstrated that the multifidus muscle group applies large compressive forces to the

thoracolumbar vertebrae (T11-L1) in an effort to balance competing moments applied by the intervertebral and costovertebral joint reactions. The resulting high loading could contribute to the high prevalence of vertebral fractures in this region.

7.6 REFERENCES

1. Cooper, C., et al., *Incidence of clinically diagnosed vertebral fractures: A population-based study in rochester, minnesota, 1985-1989.* Journal of Bone and Mineral Research, 1992. **7**(2): p. 221-227.

2. Ismail, A.A., et al., *Number and Type of Vertebral Deformities: Epidemiological Characteristics and Relation to Back Pain and Height Loss.* Osteoporosis International, 1999. **9**(3): p. 206-213.

3. Melton, L.J., et al., *Prevalence and incidence of vertebral deformities.* Osteoporosis International, 1993. **3**(3): p. 113-119.

4. Siminoski, K., et al., *Anatomical distribution of vertebral fractures: comparison of pediatric and adult spines.* Osteoporos Int, 2012. **23**(7): p. 1999-2008.

5. Bruno, A.G., M.L. Bouxsein, and D.E. Anderson, *Development and validation of a musculoskeletal model of the fully articulated thoracolumbar spine and rib cage.* Journal of Biomechanical Engineering, Accepted for publication March 24, 2015.

6. Crowninshield, R.D. and R.A. Brand, *A physiologically based criterion of muscle force prediction in locomotion.* J Biomech, 1981. **14**(11): p. 793-801.

7. Hughes, R.E., *Effect of optimization criterion on spinal force estimates during asymmetric lifting.* J Biomech, 2000. **33**(2): p. 225-9.

Chapter 8: Summary of Key Findings and Contributions

8.1 Review of Key Findings and Contributions

Whereas much is known about the determinants of vertebral strength, little is known about the *in vivo* loading of the spine that may contribute to vertebral fractures. Thus, the overall goal of this thesis was to improve the understanding of vertebral fractures through detailed analysis of spinal loading.

8.1.1 Sex-Specific Differences in Skeletal Fragility

In Chapter 2, we used the factor-of-risk concept together with estimates of spine loading to explore possible mechanisms underlying sex-specific differences in skeletal fragility that may be obscured by two-dimensional areal bone mineral density (aBMD) measures, the most commonly used clinical assessment of skeletal fragility and fracture risk. We found that when matched for both age and spine aBMD at L3, men have higher vertebral CSA, lower volumetric density, higher vertebral compressive strength, and higher factor-of-risk for vertebral fracture compared to women. This study provides new insights into the sex-specific structural and biomechanical differences that exist between the vertebra of men and women, and has important clinical implications concerning the use of aBMD to predict vertebral fracture and diagnose osteoporosis in both men and women. Taken together, the results of this study suggest that men and women do not have similar risk of vertebral fracture at the same absolute level of spine aBMD, and that the use of sex-specific spine aBMD reference values to predict fracture risk in men and women deserves further investigation.

8.1.2 Spine Curvature, Posture, and Loading

In Chapter 3, we parametrically investigated how spine curvature and overall sagittal plane posture influence spinal loading and risk of future vertebral fracture. We found evidence linking hyperkyphosis of the thoracic spine to vertebral fractures and other spinal degenerative diseases. It is thought that excessively stooped posture increases the forces applied to various spinal tissues to a level capable of causing pathology and degeneration. However, we suggest that the current theory ascribing increased spinal loading to greater amounts of thoracic kyphosis is overly simplistic as it does not take into account other postural adjustments that accompany age-related increases in thoracic kyphosis, and which act to modulate any increases

in loading. Our results indicate that in addition to measuring thoracic kyphosis angle, it is also necessary to evaluate overall posture and spino-pelvic alignment when assessing one's risk for degenerative spinal pathology due to altered spine biomechanics, such as vertebral fractures. Further, when treating spinal deformities, clinicians should strive to restore congruent posture because of its positive effects on spinal loading, balance, and eye gaze.

8.1.3 An Innovative Musculoskeletal Spine Model

In Chapter 4, we used OpenSim to create a novel musculoskeletal model of the full thoracolumbar spine and rib cage that accurately predicts *in vivo* vertebral compressive loading and trunk muscle tension, thereby addressing a crucial technical gap in the literature. Whereas numerous musculoskeletal models have been developed in the past to study the extremities, lumbar spine, and cervical spine, modeling of the thorax has been limited due to the anatomic complexity of this region. Our new model allows for the prediction of the *in vivo* skeletal and muscular loads that occur in the thorax during different activities, and will facilitate investigations into the biomechanical mechanisms underlying, and potential treatments for, multiple thoracic diseases and conditions, including vertebral fractures, hyperkyphosis, scoliosis, respiratory insufficiency, and back pain. The model will have broad applications in the fields of orthopedic biomechanics, physical and occupational therapy, ergonomics, surgical and clinical planning, ventilation and respiratory mechanics, and any other field in which detailed knowledge of spine and thoracic mechanics may be useful. Furthermore, the impact of this model will be enhanced by its open source nature. The model will be made available to the broader research and educational communities via the OpenSim website so that anyone in the world can use and/or build upon the model for their own purposes.

Also in Chapter 4, we created a unique approach for adjusting the size and position of muscle fascicles in the model using *in vivo* CT measurements of muscle morphology, a technique we built upon in Chapter 5 to create subject-specific musculoskeletal models and investigate how population variability in trunk anatomy (spine curvature and muscle morphology) influence *in vivo* spinal loads

8.1.4 Creating Patient-Specific Musculoskeletal Spine Models

In Chapter 5, we developed a set of methods to rapidly create subject-specific musculoskeletal models of the thoracolumbar spine using measurements of spine curvature and muscle morphology from clinical CT scans. This was the first study to our knowledge that incorporated both spine curvature and muscle morphology measurements into subject-specific spine models to make individualized estimates of spine loading. Using these models, we demonstrated that individual variations in both spine curvature and muscle morphology substantially influence predictions of vertebral loading compared to simple height and weight adjusted models. Furthermore, there was a trend for individuals with higher thoracic kyphosis and lower lumbar lordosis angles compared to the baseline generic model to have higher predicted vertebral loads compared to their baseline height and weight adjusted model. However, we only found weak to moderate associations relating differences in thoracic kyphosis and lumbar lordosis to differences in vertebral loading, indicating that other aspects of spine curvature not captured by the thoracic and lumbar Cobb angles have important effects on vertebral loading. This is in agreement with our main finding from Chapter 3 that the thoracic kyphosis Cobb angle is not a sufficient summary measure of spine loading. Rather, an individual's complete spine curvature and sagittal plane posture must be accounted for when trying to evaluate spine loading and risk of future fracture or injury. Variations in spine curvature, posture, and muscle morphology appear to have large effects on spine loading, and therefore accounting for these differences in musculoskeletal models will be essential for understanding the differential risk of spine injury and back pain among individuals.

8.1.5 The Contribution of Spine Loading to Thoracolumbar Vertebral Fracture

In Chapter 6, we provided a comprehensive data set of thoracic and lumbar spine loading and factor-of-risk for a large variety of daily activities, as well as for different spine curvatures. We showed that for a majority of activities and spinal curvature conditions, the highest factor-of-risk occurred in the thoracolumbar spine, and that this was driven by high multifidus muscle tension in that region, possibly explaining the high occurrence of vertebral fractures in the thoracolumbar region. In Chapter 7, we found that high thoracolumbar spine and muscle loading is a phenomenon that emerges from the complex anatomy of the trunk, and the fact that moments are being applied to the vertebrae both directly and indirectly by the trunk

muscles More specifically, the muscles in the model provide counter moments at each intervertebral joint (to balance the moments from body weight and external loads) both *directly*, by pulling on adjacent vertebrae that span those joints, and *indirectly*, by pulling on other structures that in turn can apply moments to the vertebral bodies that span the joint. Therefore, our results indicate that intuitively predicting where the highest vertebral loads and muscle forces will occur based on the pattern of body weight moments is inaccurate. This finding illustrates the necessity of modeling the complex anatomy of the spine and thorax as realistically as possible, which is a unique feature of the musculoskeletal model developed in this thesis. To our knowledge, we are the first to put forth a comprehensive biomechanical explanation for the high incidence of thoracolumbar vertebral fractures.